

# Evaluating Human Electromagnetic Exposure in a UAV-aided Network

Thomas Detemmerman

Student number: 01707806

Supervisors: Prof. dr. ir. Wout Joseph, Prof. dr. ir. Luc Martens

Counsellors: Dr. ir. Margot Deruyck, German Dario Castellanos Tache

Master's dissertation submitted in order to obtain the academic degree of  
Master of Science in Information Engineering Technology

Academic year 2019-2020



## Acknowledgement

I would like to thank Prof. dr. ir. Wout Joseph, Prof. dr. ir. Luc Martens and Dr. ir. Margot Deruyck for providing me access to their capacity based deployment tool which allowed me to complete my research regarding electromagnetic exposure but also for helping me map the road of my research. Further I would like to express my gratitude to MPhil German Dario Castellanos Tache who followed up my weekly progress by providing answers to questions or problems I had and gave me extensive feedback and suggestions to the results I booked. I would also like to show my deepest appreciation towards mrs. Carine Lambrecht and miss. Anke Blommaert for taking a second - and even a third - eye on the linguistic part of this document but also for the general mental support during this journey making this entire degree possible allowing me to stand where I am today.

*The author(s) gives (give) permission to make this master dissertation available for consultation and to copy parts of this master dissertation for personal use. In all cases of other use, the copyright terms have to be respected, in particular with regard to the obligation to state explicitly the source when quoting results from this master dissertation.*

# Evaluatie van de electromagnetische blootstelling van de mens in een netwerk van drones

door

Thomas Detemmerman

Masterproef ingediend tot het behalen van de academische graad van Master of Science in de  
industriële wetenschappen: informatica  
Academiejaar 2019-2020

Promotoren: Prof. dr. ir. Wout Joseph, Prof. dr. ir. Luc Martens

Begeleider: Dr. ir. Margot Deruyck, MPhil. German Dario Castellanos Tache

Faculteit Ingenieurswetenschappen en architectuur

Universiteit Gent

## Samenvatting

TODO: Ook updaten op plato TODO: Translate

## Trefwoorden

LTE, electromagnetische blootstelling, energieverbruik, drone, femtocell, microstrip patch antenna, stralingspatronen, specific absorption rate (SAR)

# Evaluating Human Electromagnetic Exposure in a UAV-aided Network

by Thomas Detemmerman

Master's dissertation submitted in order to obtain the academic degree of Master of Science in  
Information Engineering Technology industriële wetenschappen: informatica  
Academiejaar 2019-2020

Supervisors: Prof. dr. ir. Wout Joseph, Prof. dr. ir. Luc Martens  
Counsellors: Dr. ir. Margot Deruyck, MPhil. German Dario Castellanos Tache  
Faculty of engineering and architecture  
Ghent University

## Samenvatting

Society relies more than ever on the availability of wireless networks. Due to the mobility of a UAV, a UAV-aided network is able to provide this necessary access in case the existing terrestrial network gets damaged. However, the public is concerned about the potential health effects of the electromagnetic radiation caused by these networks. Therefore, mobile devices and base stations have to comply to strict legislation enforced by the government.

This research investigates how different scenarios influence power consumption, electromagnetic exposure and specific absorption rate. These different scenarios are defined by various flying heights, number of UAVs available and population densities. Further, also an analysis on the difference between a realistic microstrip patch antenna and a fictional equivalent isotropic radiator is performed. Thereafter, the network will be optimized towards goals like electromagnetic exposure of the average user or power consumption of the entire network which result in conflicting requirements.

To accomplish this goal, a capacity based deployment tool will be used which simulates an entire UAV-aided network. In this way, all important sources for electromagnetic radiation, like all user equipment and all flying base stations, will be considered.

It looks from the results that a power consumption optimized network with a fixed flying height of 80 metres is the recommended approach for the city centre of Ghent. A microstrip patch antenna with a sufficiently large aperture angle is a good starting point. However, different antenna array configurations still have to be investigated.

## Trefwoorden

LTE, microstrip patch antenna, radiation pattern, specific absorption rate (SAR), deployment tool, electromagnetic exposure, power consumption, UAV, unmanned aerial base stations

# Evaluatie van de electromagnetische blootstelling van de mens in een netwerk van drones

Thomas Detemmerman

Supervisor(s): Wout Joseph, Luc Martens, Luc Martens, German Dario Castellanos Tache

**Abstract**— De hedendaagse samenleving vertrouwt meer dan ooit op de aanwezigheid van draadloze netwerken. Tevens groeit ook de bezorgdheid bij de menigte over de electromagnetische straling die hiervoor gebruikt wordt. De overheid hanteert dan ook strenge richtlijnen waaraan mobiele toestellen en zendmasten moeten voldoen.

Dit onderzoek tracht de specifieke absorptie snelheid van elektromagnetische straling in kaart te brengen door rekening te houden met alle mobiele toestellen en zendmasten. Om dit te verwelijken wordt gebruik gemaakt van een tool ontwikkeld door de onderzoeksgroep WAVES aan de UGent. Deze tool simuleert een volledig netwerk waarbij zendmasten bevestigd worden aan drones. Dit onderzoek observeert verder hoe deze drones kunnen worden aangestuurd zodende dat bepaalde doelstellingen zoals het minimaliseren van energieverbruik of elektromagnetische straling bereikt kunnen worden.

Uit de resultaten blijkt dat...

**Keywords**— LTE, elektromagnetische blootstelling, energieverbruik, drone, femtocell, microstrip patch antenna, radiation pattern, specific absorption rate (SAR)

## I. Introductie

### THE Introduction in Dutch

## II. Section

### A. Gerelateerd werk

TODO

### B. Scenario's

todo

### C. Elektromagnetische blootstelling

todo

## III. Resultaten

todo

## IV. Conclusie

todo

### A. References

todo

## References

- [1] Bart Lannoo, Didier Colle, Mario Pickavet, Piet Demeester, Optical Switching Architecture to Implement Moveable Cells in a Multimedia Train Environment, Proc. of ECOC 2004, 30th European Conf. on Optical Communication, vol. 3, pp. 344-345, Stockholm, Sweden, 5-9 Sep. 2004.
- [2] Michael Neufeld, Ashish Jain, Dirk Grunwald, Nsclick:: bridging network simulation and deployment, <http://systems.cs.colorado.edu/Networking/nsclick/>
- [3] The Click Modular Router Project, <http://www.read.cs.ucla.edu/click/>

- [4] NS – Network Simulator, <http://nsnam.isi.edu/nsnam/>

# Evaluating Human Electromagnetic Exposure in a Unmanned Aerial Vehicle (UAV)-aided Network

Thomas Detemmerman

Supervisor(s): Prof. dr. ir. Wout Joseph, Prof. dr. ir. Luc Martens

**Abstract**—Society relies more than ever on the availability of wireless networks. Due to the mobility of a UAV, a UAV-aided network is able to provide this necessary access in case the existing terrestrial network gets damaged. However, the public is concerned about the potential health effects of the electromagnetic radiation caused by these networks. Therefore, mobile devices and base stations have to comply to strict legislation enforced by the government.

This research investigates how different scenarios influence power consumption, electromagnetic exposure and specific absorption rate. These different scenarios are defined by various flying heights, number of UAVs available and population densities. Further, also an analysis on the difference between a realistic microstrip patch antenna and a fictional equivalent isotropic radiator is performed. Thereafter, the network will be optimized towards goals like electromagnetic exposure of the average user or power consumption of the entire network; which results in conflicting requirements.

To accomplish this goal, a capacity based deployment tool will be used which simulates an entire UAV-aided network. In this way, all important sources for electromagnetic radiation, like all user equipment and all flying base stations, will be considered.

It looks from the results that a power consumption optimized network with a fixed flying height of 80 metres is the recommended approach for the city centre of Ghent. A microstrip patch antenna with a sufficiently large aperture angle is a good starting point. However, different antenna array configurations still have to be investigated.

**Keywords**—LTE, microstrip patch antenna, radiation pattern, specific absorption rate (SAR), deployment tool, electromagnetic exposure, power consumption, wireless access network, emergency network, UAV, unmanned aerial base stations

## I. Introduction

SOCIETY is constantly getting more and more dependent on wireless communication. On any given moment, in any given location, an electronic device can request to connect to the bigger network, starting from small Internet of Things (IoT) up to self-driving cars.

Also in exceptional and possibly life threatening situations, the public relies on the cellular network despite the fact that the network might be severely damaged and not properly functioning anymore. One solution for a fast temporarily deployable network is to use UAVs. A base station can be attached to these flying UAVs to support the network over a limited area. This approach is also useful in case of an unexpected increase in traffic. For example during the terrorist attacks at Brussels Airport, mobile network operators saw all telecommunications drastically increasing causing moments of contention. Some operators even decided to temporarily exceed the exposure limits in order to handle all connections [1]. Electromagnetic exposure caused by these networks can however not be neglected. Research shows how excessive electromagnetic radiation can cause diverse biological side effects [2], [3]. It becomes clear that electromagnetic exposure is a key value

when designing a UAV-aided network and should definitely not surpass the limits predefined by the government.

UAV-aided networks can, thanks to their mobility, easily be repositioned towards a certain goal. Several papers explain how a network can be optimized towards different goals like power consumption. However, very limited research has been done where a UAV-aided network is optimized towards electromagnetic exposure. While several publications exist, discussing how the electromagnetic exposure can be calculated, most of them only consider a limited number of sources; e.g. only base stations or only the user's mobile device. Papers who cover electromagnetic exposure from all the different sources and convert it into a single value are rather limited.

This research proposes a method to optimize the network towards electromagnetic exposure and power consumption when considering all four sources of radiation in a telecommunications network, being: the user's own phone, the base station that is serving this user, all devices from other users in the network and all other active base stations that are not serving this user. In this way, the contribution of each source towards the total electromagnetic exposure can easily be identified.

The behaviour of the electromagnetic exposure and power consumption of the network will be analysed by applying the tool in different scenarios by using different types of antennae, various flying height and population densities. Values like Specific Absorption Rate (SAR), electromagnetic exposure and power consumption will give insight in how the network behaves so the network could be optimized accordingly.

To make this research possible, an existing capacity based deployment tool developed by the WAVES research group at Ghent University is used. This planning tool describes a fully configured UAV-network which is a suitable starting point for this research.

## II. State of the Art

### A. Electromagnetic exposure

Users in a telecommunication network are exposed to various sources of electromagnetic radiation, expressed in  $V/m$ . Once the exposure is absorbed by the human body, we speak of the specific absorption rate (SAR) which is expressed in  $W/kg$ . All these values are subjected to limitations enforced by the government. This research is performed in Ghent, a Flemish city in Belgium where the 2.6 GHz frequency band, an individual antenna cannot exceed

4.5 V/m and the cumulative sum of all fixed sources has its maximum at 31 V/m [4], [5]. The maximum whole body SAR-values for a mobile device over a 10 g tissue ( $SAR_{10g}$ ) is defined at  $2W/kg$  [6].

Several papers calculate exposure originating from specific sources [7], [8], [9], [10] where some convert the up-link (UL) radiation into localized specific absorption rates [9], [10]. With the advent of 5G, paper [11] describes how the localized SAR-values are achieved from all different sources. Finally, [12] describes how the electronic radiation can be converted into whole body SAR values.

In a realistic network, some users are calling while others are using other types of telecommunication services like browsing the web. Therefore, all absorbed electromagnetic exposure should be expressed in whole body SAR while still covering all sources.

### B. Optimized UAV-aided networks

A UAV knows several applications. It was originally mainly used to support the military for surveillance and remote attacks without endangering pilots [13]. However, UAVs have recently become more accessible by the general public due to decreasing costs. This allowed UAVs to be researched for various applications.

A UAV equipped with a femtocell base station antenna will be called a Unmanned Arial Base Station (UABS) which brings several advantages like mobility and rapid deployment. However, it brings also challenges like limited weight of the payload and sparse power supply.

Kawamoto et al. introduced in [14] a WiFi network with the support of UAVs while considering resource allocation and antenna directivity. Gangula et al. illustrates in [15] how UAVs can be used as a relay for Long-Term Evolution (LTE) and Zeng et al. proposes in [13] a tutorial in 5G-and-beyond wireless systems where challenges like energy consumption, mobility and antenna direction are discussed. In [16], Deruyck et al. designed a capacity based deployment tool for UAV-aided emergency networks for large-scale disaster scenarios where an ideal flying height of 100 m is suggested. This was expanded in [17] with a performance evaluation of the direct-link backhaul of this tool where a slightly lower flying height of 80 metres is recommended.

Mozaffari et al. provides in [18] guidelines on how to optimize and analyse UAVs equipped for wireless communication equipment. One path that has been excessively researched are location optimization solutions where the network is designed in such a way that certain goals like minimal power consumption are achieved [19], [20], [21], [22]. These optimizations can be done through different implementation methods like exact algorithms or machine learning [18], [23].

Research where network is optimized towards electromagnetic exposure is rather limited. Deruyck et al. discusses in [8] how a terrestrial network can be optimized towards either a minimal exposure or minimal power consumption of the entire network. However, to the best of the author knowledge, no research has been done where a UABS-network has been optimized towards electromag-

netic exposure.

### C. Technologies

For the deployment of the network, the more robust UAVs from [16] will be used (details in table I) and will be operating in the 2.6 Ghz bandwidth. Since the users are assumed to experience a constant electromagnetic exposure without interruptions, frequency division duplex is used.

The onboard antenna of the UAV will act as the gateway between the UE and the backhaul network. However, determining which antenna to use and how to position it, can be challenging. The radiation pattern from the antenna can be influenced by the UAV [24]. Also the fact that the UAV will hover above the user makes traditional 2D modelling insufficient. A 3D-model which accounts for both elevation and azimuth directivity will be required [13].

The easiest radiation pattern is a hypothetical isotropic radiator which radiates equally in all directions. Antennae that radiate equal quantities for a certain plane are called omnidirectional antennae [13] and several types for UAV usage like monopoles, dipoles and wing antennae have been considered [25], [26], [27], [28]. Another type of antennae are directional antennae which save energy by focussing the electromagnetic energy there where it is needed. One type that has excessively been researched in various array-configurations are microstrip patch antennae [29], [30], [31]. They provide several advantages compared to traditional antennae [32], [33] like lightweightness, low in cost and thin causing them to be more aerodynamic.

A basic microstrip antenna consists of a ground plane and a radiating patch, both separated by a dielectric substrate. Several variations exist like microstrip patch antennae, microstrip slot antennae and printed dipole antennae which all have similar characteristics [32], [?]. They are all thin, support dual frequency operation and they all have the disadvantage that they will transmit at frequencies outside the aimed band which is also known as spurious radiation. The microstrip patch and slot antenna support both linear and circular polarization while the printed dipole only supports linear polarization. Further, the fabrication of a microstrip patch antenna is considered to be the easiest of the considered patch antennae [32].

## III. Scenarios

The default configuration is given in table I and is always applicable unless mentioned otherwise.

Three main scenarios will be investigated. The first one has only one user and one drone present in the network. SAR, electromagnetic exposure, power consumption and antenna transmission power are investigated at different flying heights.

In a second scenario, the network is expanded for multiple users still only one drone is available. The scenario is divided into two cases. One with a variable flying height but with a fixed number of 224 users as is average on an usual day at 5 p.m. in Ghent. In the other case, the number of users varies but the flying height is set to 100 metres

Broadband cellular network	
technology	LTE
frequency	2.6 GHz
Carrier	
carrier power	13.0 A
average carrier speed	12.0 m/s
average carrier power usage	17.33 Ah
carrier battery voltage	22.2 V
Femtocell antenna	
maximum $P_{tx}$	33 dBm
antenna direction	downwards (az: 0°; el: 90°)
gain	4 dBm
feeder loss	2 dBm
implementation loss	0 dBm
radiation pattern	EIRP or microstrip patch
height	100m
UE Antenna	
height	1.5m from the floor
gain	0 dBm
feeder loss	0 dBm
radiation pattern	EIRP
number present in the network	224

TABLE I

Overview of default configuration values.

[16]. The power consumption, electromagnetic exposure and specific absorption rate are investigated for each case.

The third scenario is quite similar to the previous scenario. The same two cases are investigated, but now an unlimited number of UABSs is available.

Each case from each scenario consists out of four possible configurations. There are two possible antennae, namely EIRP and microstrip patch antenna, which can both be applied in a power consumption optimized (PwrC. Opt.) network or an exposure optimized (Exp. Opt.) network. An overview is given in figure 1

#### IV. Methodology

##### A. Electromagnetic Exposure

The total whole body SAR ( $SAR_{10g}^{wb,total}$ ) of a user can be calculated by a simple sum of individual SAR values from the different sources and is based on [11] where SAR values are used that are induced into the head. Using  $SAR_{10g}^{head}$  would however result into incorrect conclusions since the position of the phone relative to the user is unknown. The position of the phone can be next to the head but also in front of the user. The induced electromagnetic radiation will therefore be expressed in function of the entire body.

$$SAR_{10g}^{wb,total} = SAR_{10g}^{wb,my\_UE} + SAR_{10g}^{wb,my\_UABS} + SAR_{10g}^{wb,other\_UE} + SAR_{10g}^{wb,other\_UABSs} \quad (1)$$

Optimization strategy			
	Exposure optimized	Power consumption optimized	
Antenna type	Equivalent isotropic radiator	EIRP, Exp Opt	EIRP, PwrC Opt
	Microstrip patch antenna	Microstrip, Exp Opt	Microstrip, PwrC Opt

Fig. 1  
Matrix with the four possible configurations

The first parameter,  $SAR_{10g}^{wb,my\_UE}$ , indicates the absorbed electromagnetic radiation by the whole body originating from the user's own device. However that the UL radiation is destined for the serving UABS, a portion of that radiation is directly absorbed by its user, due to the omnidirectional nature of the mobile's antenna. The second parameter,  $SAR_{10g}^{wb,my\_UABS}$ , represents the downlink (DL) radiation caused by the UABS that is serving the user. As the third parameter, we have the  $SAR_{10g}^{wb,other\_UE}$  which is radiation caused by other people's devices. The radiation of these devices is once again destined for a specific UABS but again, a portion of that UL radiation will also be absorbed by our user. Finally,  $SAR_{10g}^{wb,other\_UABSs}$  represents the DL radiation by the other UABSs to which our user is exposed to but not served by. An illustration is given in figure 2. The green arrow stands for near-field radiation, the others represent far-field radiation.

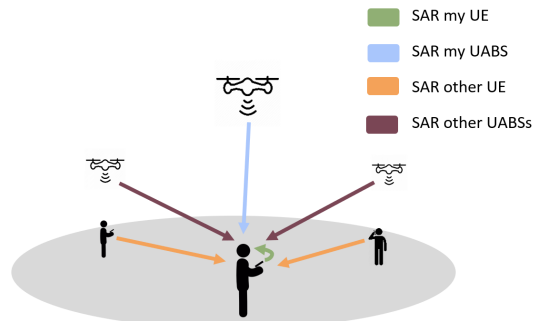


Fig. 2  
Illustration of the network that shows how the average user (here shown in the center) is influenced by different types of sources.

## B. Electromagnetic Exposure Caused by Far-Field Radiation

### B.1 Electromagnetic Radiation from a Single Source

Calculating far-field exposure needs to be done for all UABSSs and UE that do not belong to the user. The total exposure  $E$  of this single user  $u$  from a single radiator  $i$  can be calculated as follows.

$$E_i(u)[V/m] = 10^{\frac{RRP(u)[dBm] - 43.15 + 20 * \log(f[MHz]) - PL(u)[dB]}{20}} \quad (2)$$

Caculating the real radiation power (RRP) for a certain user  $u$ , requires first the EIRP-value to be calculated [7], [8]. This is achieved by adding the transmission power  $P_t$  to the transmitter gain  $G_t$  and thereafter subtracting the feeder loss  $L_t$ . This formula needs to be expanded to also account for attenuation. This value depends on the angle between this user and the antenna's main beam. This leads to the following formula.

$$RRP[dBm] = P_t[dBm] + G_t[dBi] - L_t[dB] - \text{attenuation}(u)[dB] \quad (3)$$

The used frequency in formula 2 is denoted as  $f$  and is expressed in MHz. Since LTE is used, this value will be 2600 MHz.

At last, formula 3 requires the path loss (in dB). In order to calculate this, an appropriate propagation model —of which several exist— is required . The Walfish-Ikegami model is used since it performs well for femtocell networks in urban areas [16].

### B.2 Combining Exposure

The electromagnetic exposure, in a certain spot, originating from different sources can be calculated with formula 4.  $E_i$  stands for the electromagnetic exposure from source  $i$  and  $n$  stands for all far-field radiators of a certain category which will either be UABSSs or UE from other people.  $E_{tot}$  will be calculated for each location where a user is positioned.

$$E_{tot}[V/m] = \sqrt{\sum_{i=1}^n (E_i[V/m])^2} \quad (4)$$

### B.3 Converting electromagnetic radiation into SAR-values

Formula 1 expects that the radiation is expressed in whole body SAR-values. To make this calculation possible, a distinction has to be made between near-field SAR ( $SAR^{wb,nf}$ ) and far-field SAR ( $SAR^{wb,ff}$ ).  $SAR_{10g}^{wb,my\_UABS}$  is a form of near-field radiation, all the other types are far-field radiation.

Converting the electromagnetic radiation is done with a conversion factor which is based on Duke of the Virtual Family. Duke is a 34-year old male with a weight of 72 kg, a height of 1.74 m and body mass index of 23.1 kg/m [12]. Research shows that the conversion factor for WiFi

in the far-field is  $0.0028 \frac{W/kg}{W/m^2}$  and for  $0.0070 \frac{W/kg}{W}$  [12] in the near-field.

Since WiFi, at a frequency of 2400 MHz, is very close to LTE, at 2600 MHz, it is assumed in [12] that this value is also applicable for LTE.

Calculating SAR from far-field radiation is done as follows.

$$S[W/m^2] = \frac{(E_{tot}[V/m])^2}{337} \quad (5)$$

$$SAR_{10g}^{wb,ff}[W/kg] = S[W/m^2] * 0.0028 \left[ \frac{W/kg}{W/m^2} \right] \quad (6)$$

The constant in 6 converts the power flux density  $S$  to the required  $SAR_{10g}^{ff,wb}$ . To make this possible, the electromagnetic radiation from formula 4 should first be converted to the power flux density with formula 5.

The SAR caused by near-field radiation is calculated by multiplying the constant with the used transmission power of the User Equipment (UE) which results to the following formula.

$$SAR_{10g}^{wb,nf} \left[ \frac{W}{kg} \right] = 0.0070 \left[ \frac{W/kg}{W} \right] * P_{tx}[W] \quad (7)$$

### C. Microstrip Patch antenna

A microstrip patch antenna is chosen because it allows easy production but more important, it has a low weight and has a thin profile causing it to be very aerodynamic which is useful when attaching it to a drone [32].

The dimensions of the antenna depend on the frequency it is operating at and the characteristics of the used substrate. The antenna will be radiating at a centre frequency  $f_0$  of 2.6 GHz. Each substrate has a dielectric constant  $\epsilon_r$  representing the permittivity of the substrate that depends on the used material. Substrates with a high dielectric constant and low height reduce the dimensions of the antenna while a lower dielectric constant with a high height improves the performance of the antenna [33], [34]. In this document, a substrate like glass is chosen because of the higher dielectric constant of  $\epsilon_r = 4.4$  compared to materials like teflon with only a dielectric constant of  $\epsilon_r = 2.2$  [33]. Doing this in combination with an antenna height of 2.87 mm will decrease the dimensions of the entire antenna surface. This comes in handy since drones only have limited space available.

description	symbol	value
centre frequency	$f_0$	2600 Hz
dielectric constant	$\epsilon_r$	4.4
height of the substrate	$h$	0.00287 m

TABLE II  
Overview of configuration parameters.

The dimensions of the radiating patch can be calculated with the formulas from [33], [34]. Doing so will result in a

radiating patch of 35.09 mm by 26.55 mm and a ground-plane of at least 52.40 mm by 43.80 mm. The microstrip patch antenna as illustrated in fig. 3 will result in the radiation pattern of fig. 4.

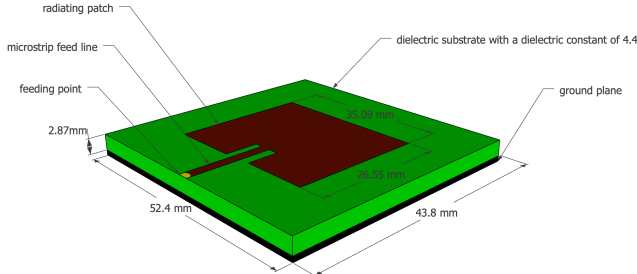


Fig. 3

Design of the microstrip patch antenna.

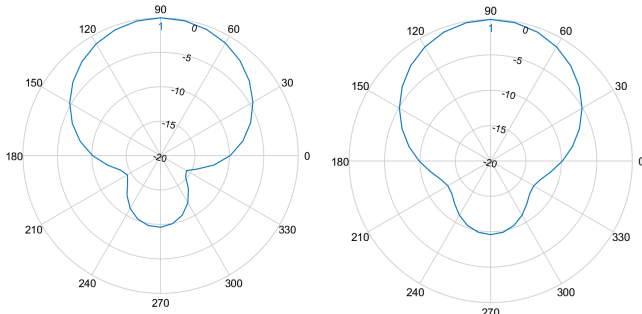


Fig. 4

Radiation pattern 1: On the left the radiation pattern of the E-plane and at the right for the H-plane.

#### D. Optimizing the network

Deruyck et al. discusses in [8] how a terrestrial telecommunication network either can be optimized towards electromagnetic exposure of an individual or towards power consumption of the entire network. However, an increasing transmission power of an antenna comes with an increasing electromagnetic exposure. This is not the case considering both values for an entire network. In fact, the authors from [8] prove that both become inversely equivalent. The reason the network behaves like this is because it is often cheaper to increase the exposure of an already active base station than activating a new one. This leads to the following fitness function which is based on [8].

$$f = w * \left(1 - \frac{E_m}{E_{max}}\right) + (1 - w) * \left(1 - \frac{P}{P_{max}}\right) * 100 \quad (8)$$

Formula 8 returns a fitness value which represents the performance of the entire network.  $w$  is the importance factor of electromagnetic exposure ranging from 0 to 1,

boundaries included. A  $w$  set to 0 means that electromagnetic exposure is not important. Such a network will therefore be called a PwrC. Opt. network. Likewise, a  $w$  set to 1 means that minimizing exposure is top priority and will result in an Exp. Opt. network.  $P_{max}$  is the power consumption of all UABSs, both active and inactive, when radiating at the highest level possible while  $P$  is the effective power used by the current designed network. This will be the power required for the flying drones themselves and their antennae.  $E_m$  will be the weighted exposure of the average user for the current designed network and  $E_{max}$  the weighted average of the electromagnetic exposure when all antennae are at their highest power level.

When optimizing the network, it is not only important to consider the average exposure of all users, but also to limit high extremes [8]. A weighted average will be used not only considering the median but also the 95 percentile from all users' DL exposure using formula 9. Since both values are considered to have equal importance, the weight factors  $w_1$  and  $w_2$  will both have an equal importance of 50%.

$$E_m = \frac{w_1 * E_{50} + w_2 * E_{95}}{w_1 + w_2} \quad (9)$$

## V. Results

### A. One User and One UAV

The results show that for a varying flying height, a logarithmic relationship exists between the  $P_{tx}$  and the flying height. This is mainly caused by the logarithmic scale in which the decibels of the  $P_{tx}$  are expressed. So while 10 dBm equals 10 mW, 20 dBm equals 100 mW. Each time the flying height becomes too large to cover, the  $P_{tx}$  increases with one dBm. When using the default configuration, with a maximum  $P_{tx}$  of 33 dBm, a UABS can fly up to 387 m before losing connection in a free line of sight (LOS) scenario.

This scenario is investigated with a microstrip patch antenna using power consumption optimization. However, the chosen optimization strategy doesn't really matter because the decision algorithm decides which user needs to be connected to which UABS. Since only one UABS is available, both optimization strategies will behave identical. Further, also the used antenna will not make any difference. The user is namely positioned in the perfect centre of the main beam where there is no attenuation experienced for both antennae.

When investigating this scenario at different flying heights, we notice that the UL radiation increases exponentially while the DL radiation remains constant during the entire time. The reason that the DL radiation remains constant is because of power control which makes sure that no more power is used than strictly necessary. So at lower flying altitudes, there is less path loss and the UABS will therefore reduce the  $P_{tx}$ . This results in formula 10 where the electromagnetic exposure is a constant fraction of power and distance. The UL radiation starts very low but surpasses the DL radiation around 80 metres.

$$\vec{E}(V/m) = \frac{\Delta U(V)}{\Delta x(m)} \quad (10)$$

## B. Increased Traffic with one UABS

### B.1 Variable Flying Height

A PwrC. Opt. network has higher exposure compared to an Exp. Opt. network; a behaviour that was already proven by [8]. However, for this scenario, a PwrC. Opt. network will also result in a higher power consumption. To understand this, the behaviour of the deployment tool needs to be understood first. A PwrC. Opt. network will result in a few high powered UABSs because increasing the input power of an antenna costs less than activating a new UAV. Likewise, an Exp. Opt. network generates a lot of low powered UABSs because the lower the power of the antenna, the lower the exposure. This has the consequence that the cover radius is less and therefore more UAVs, which cost more energy, are required. When only a limited amount of UABSs are available, like only one in this scenario, the tool will only keep UABSs which cover the most users. Therefore, the power consumption in a PwrC. Opt. network is much more higher.

Further, the results also show that the exposure increases with higher flying altitudes because there is less path loss by obstructing buildings. This has as consequence that more users become covered. The increasing electromagnetic radiation is however not unlimited. At even higher flying altitudes, the distance between a given UABS and some users further away becomes too large causing the coverage to decrease again. When this decrease occurs depends on the configuration. A PwrC. Opt. network tends to decline earlier than an Exp. Opt. network.

When replacing the fictional equivalent isotropic radiation power (EIRP) antenna by a microstrip patch antenna, the percentage of covered users drops for both optimization strategies. This is because users, who have a higher horizontal distance between themselves and the UABS, experience a higher attenuation.

The results further show that the radiation from the UABS is the main factor followed by the near-field radiation from the user's own device. The far-field radiation from other UE barely contributes anything.

### B.2 Variable Number of Users

Also the results from this case show how EIRP antennae designs are able to cover more users than microstrip patch antennae just like PwrC. Opt. networks will reach more users than Exp. Opt. networks. The contribution to the total SAR from each individual source is identical to the previous scenario.

There is still only one UABS available. When population grows, more users become uncovered and therefore the average electromagnetic exposure decreases. For example, an EIRP PwrC. Opt. network will have the highest exposure and therefore covers the most users as opposed to a microstrip patch antenna in an Exp. Opt. network which

will radiate the least and thus has the lowest number of covered users.

While the population grows, more and more users become uncovered causing the average SAR to drop. However, this does not conclude that by increasing the population, the SAR of a user who is directly beneath a UABS would be less. To investigate this, a user is positioned in the middle of the city centre of Ghent and a UAV is positioned above him. Initially, only 49 people are active around him. The SAR of our central user is monitored while the population around him is growing. Figure 5 shows with the black lines which users are connected. The left map is for only 50 users and shows that only one user is connected besides our central user. The map on the right considers 600 users and shows much more connected users. The results show that the UL SAR remains constant; a normal behaviour since the flying altitude does not change. The SAR from the UABS experiences a slight increase. When the population grows, more users become available and some will spawn near the central user. The UABS will likely decide to cover these users as well as visible in figure 5. These users might have a slightly worse path loss because of obstructing buildings or a somewhat bigger distance. The UABS reacts to this by increasing its power consumption causing an increase in the DL SAR for the central user. The results further also show that the SAR from other UE increases when the population increases. But as mentioned before, it is much less compared to the other sources.

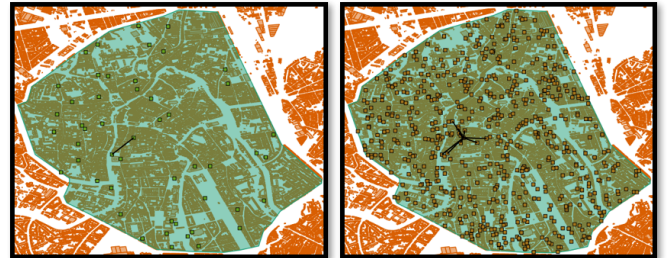


Fig. 5

Overview of which users are connected to the UABS. The map on the left is for 50 active users while the map on the right considers 600 active users.

## C. Unlimited Number of UABSs

### C.1 Variable Flying Height

The same cases as in the previous scenario are investigated. Only now, an unlimited number of UABSs is available. The results prove that the different optimization strategies work as intended. PwrC. Opt. networks have indeed a lower power consumption but therefore result in higher electromagnetic radiation. On the other hand, an Exp. Opt. network will reduce the electromagnetic exposure by using more UAVs and thence also increase the network's power consumption. This conclusion was already made in [8] and is supported by these results.

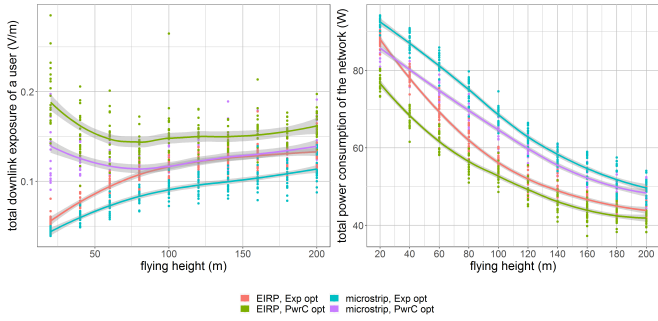


Fig. 6

These two figures show how the flying height influences the downlink electromagnetic radiation of the average user (left) and power consumption of the entire network (right) for an unlimited number of drones.

The exposure in figure 6 shows that an Exp. Opt. network increases logarithmically while the PwrC. Opt. network rather has a concave relationship with the flying height, and has its lowest point at around 70 metres.

At a flying height of 20 m, the Exp. Opt. network has on average 220 to 224 UABSSs. That is (almost) one UABS for each user so it is logical that the electromagnetic exposure is very low. The number of UAVs in a PwrC. Opt. network is much less in order to save energy but it is still able to achieve the same percentage of coverage. This is done by increasing the radiation so the cover radius would become larger. The results further show that the network profits from increasing the flying altitude. Not only less UAVs are needed but also the power consumption is lower. Both can be explained by the lower path loss when UABSSs fly higher.

Figure 7 shows how each source contributes to the total SAR. A first consequence of higher flying altitudes is the increase in electromagnetic radiation from the user's own device; a behaviour also explained in the first scenario. A second consequence is that also the exposure from 'other UABSSs' increases, caused by lower path loss from less obstructing buildings. The figures from 7 further also clearly show that this increase in electromagnetic radiation will be less for a microstrip patch antenna. The reason behind this is that energy will be more focussed towards the ground and there is less sideways radiation because of attenuation.

## C.2 Variable Number of Users

When the flying height of the UABSSs is fixed to 100 metres and the density of the population increases, also the number of required UAVs increases in order to reach a 100 % coverage. Figure 8 shows that when the number of UABSSs and users increases, also the electromagnetic exposure and power consumption increases. Once again, the EIRP antenna in a power consumption network has the highest exposure for the lowest power consumption and a microstrip patch antenna in an Exp. Opt. network the lowest exposure for the highest power consumption. The two other combinations are in the middle and behave very

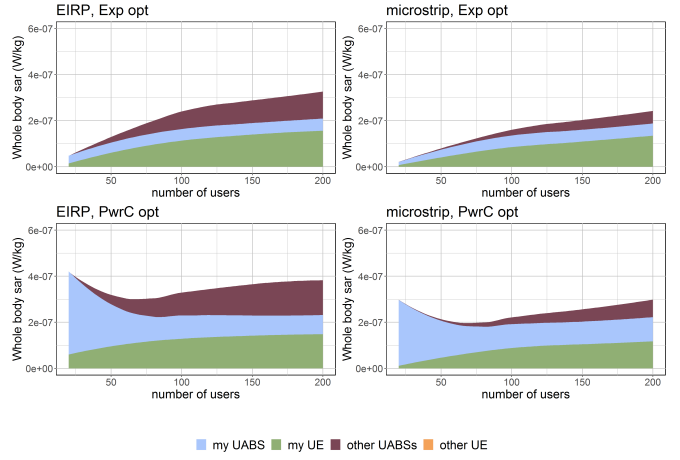


Fig. 7

Each chart corresponds with one of the four possible configurations. The contribution of each source towards the total SAR for a varying flying height is shown.

similar.

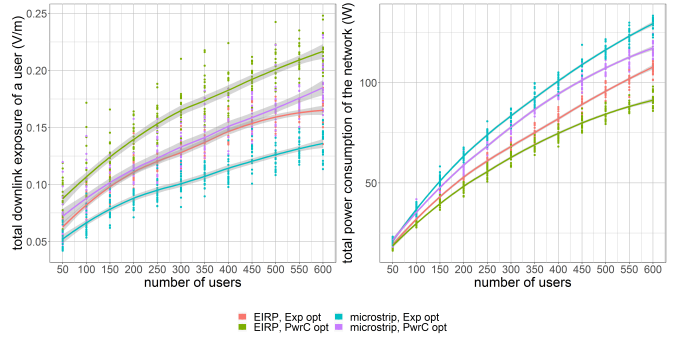


Fig. 8

These two figures show how the number of users influences the downlink electromagnetic radiation of the average user (left) and power consumption of the entire network (right) for an unlimited number of drones.

When looking at the different contributions to the total SAR in figure 9, we see that the weighted average SAR from the users' own device and from the serving UABS remains constant. The flying altitude is always the same so also the required energy to cover that distance will remain the same. The only SAR values that increase are the DL SAR from other UABSSs and the UL SAR from other UE. When more users come online, also more UAVs will be radiating. The electromagnetic radiation will thus increase for both types of sources. Moreover, there is very little path loss at this flying altitude since it is higher than the average building.

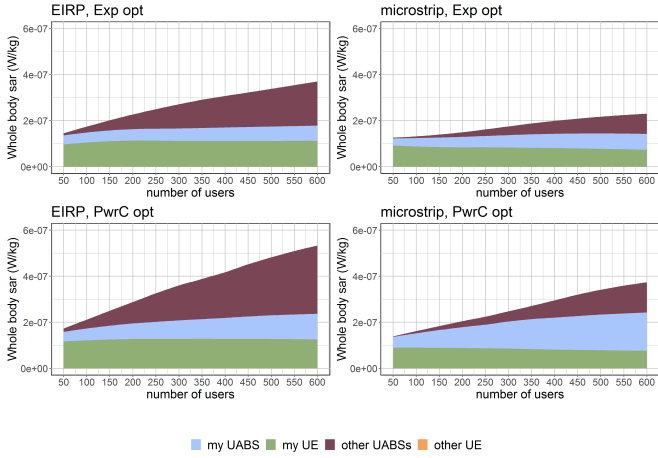


Fig. 9

Each chart corresponds with one of the four possible configurations. The contribution of each source towards the total SAR for a varying number of users shown.

## VI. Conclusion

Literature showed that a network can be optimized towards either the power consumption of the entire network or the electromagnetic exposure of the average user using a fitness function [8]. However, the fitness function should be used with care considering that UABSs can be placed anywhere as opposed to the transmission towers from [8] who have a predetermined position. In an Exp. Opt. network, this causes a lot of users to get a UABS all by themselves because this is the best approach to minimize exposure. A PwrC. Opt. network on the other hand will try to limit the number of drones in order to save energy. So as a rule of thumb: an Exp. Opt. network will result in a lot of low powered devices (increasing the overall power consumption) while a PwrC. Opt. network results in a few high powered devices (increasing the exposure of the average user). If the goal is to remain in the air for a longer period of time, an Exp. Opt. network is recommended because the power consumption of an individual UABS is lower. On the other hand, a PwrC. Opt. network is cheaper because less drones are involved. Moreover, the results show that the electromagnetic radiation in a PwrC. Opt. network (with high powered UABSs) is far below the thresholds enforced by the Flemish government.

The user's main sources of exposure are the user's own device and the UABS who is serving him, followed by all other UABSs in the network. When the population increases, there is not only more radiation from UE but also from more UABSs that are serving the other users. The exposure from other people's UE is so low that it can be neglected. An Exp. Opt. network will limit the total exposure mainly by trying to reduce the exposure from other UABSs.

A directional microstrip patch antenna is introduced be-

cause it gives several advantages compared to omnidirectional antennae. Directional antennae are able to focus their energy there where it is needed, namely towards the ground. Microstrip patch antennae further benefit from their thin and lightweight design. The performance of this directional microstrip patch antenna has been compared to a fictional equivalent isotropic radiator. This equivalent isotropic radiator has higher exposure and coverage for less power, compared to realistic antennae like microstrip patch antennae because of the absence of attenuation, and can hypothetically be compared with an antenna with a very big aperture angle. This type of antenna can achieve the same coverage with less resources like power and number of drones. A microstrip patch antenna with a more limited aperture angle of  $90^\circ$  requires more resources but causes less sideways radiation. So the exposure from other UABSs will be way less.

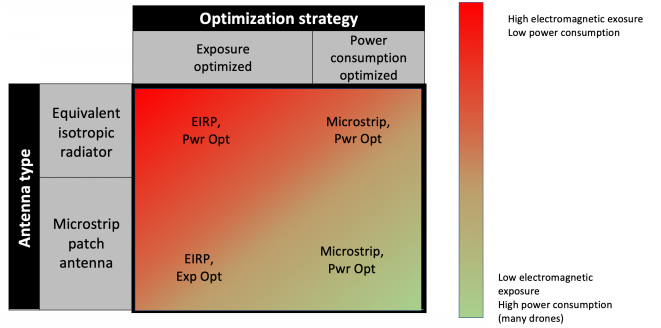


Fig. 10

Matrix with the four possible configurations, colour-coded based on the results.

Remarkable is that an EIRP Exp. Opt. network behaves very similar to a microstrip PwrC. Opt. network as shown in figure 10. This results in the best of both worlds. The microstrip patch antenna will generate less electromagnetic radiation by design and the power consumption optimization reduces the number of required drones and power. A microstrip patch antenna with an aperture angle of  $90^\circ$  is considered as a good solution but if budget is limited, an antenna with a larger aperture angle would further reduce cost without interfering with the Flemish legislation regarding electromagnetic exposure.

The electromagnetic radiation of an Exp. Opt. network increases with higher flying altitudes. Around 80 metres, the exposure from the user's device surpasses the exposure from the serving UABS. On the other hand, a PwrC. Opt. network shows that the lowest exposure is measured around 70 to 80 metres. Further, the results also show that the number of required drones decreases when the flying height becomes larger; a conclusion that was also made in [16]. When also considering the results from [17] where a flying altitude from 80 metres is suggested for an optimal access and backhaul connectivity, a flying height of 80 metres is also here proposed for the city centre of Ghent.

In short, a PwrC. Opt. network is proposed with a fixed flying height of 80 metres. A microstrip patch antenna with a sufficiently large aperture angle is a good starting point. However, different antenna configurations should be investigated.

### Acknowledgement

Special thanks to the WAVES research group at Ghent University for providing access to their capacity based deployment tool and therefore making this research possible.

### References

- [1] “Base overschred stralingsnormen na aanslagen,” De standaard, 2019.
- [2] L. Hardell and C. Sage, “Biological effects from electromagnetic field exposure and public exposure standards,” *Biomedicine and Pharmacotherapy*, vol. 62, no. 2, pp. 104 – 109, 2008.
- [3] “What are electromagnetic fields.” <https://www.who.int/peh-emf/about/WhatisEMF/en/index1.html>. Accessed: 15-10-2019.
- [4] “Elektromagnetische velden en gezondheid: Uw wegwijzer in het elektromagnetische landschap,” Federale overheidsdienst: volksgezondheid, veiligheid van de voedselketen en leefmilieu, vol. 5, 2014.
- [5] “Normen zendantennes.” <https://omgeving.vlaanderen.be/normen-zendantennes>. Accessed: 19-03-2020.
- [6] E. Commission, “Council recommendation of 12 july 1999 on the limitation of exposure of the general public to electromagnetic fields (0 hz to 300 ghz),” *Official Journal of the European Communities*, vol. 59, 1999.
- [7] D. Plets, W. Joseph, K. Vanhecke, and L. Martens, “Exposure optimization in indoor wireless networks by heuristic network planning,” *Progress In Electromagnetics Research*, vol. 139, pp. 445–478, 01 2013.
- [8] M. Deruyck, E. Tanghe, D. Plets, L. Martens, and W. Joseph, “Optimizing lte wireless access networks towards power consumption and electromagnetic exposure of human beings,” *Computer Networks*, vol. 94, 12 2015.
- [9] D. Plets, W. Joseph, S. Aerts, K. Vanhecke, G. Vermeeren, and L. Martens, “Prediction and comparison of downlink electric-field and uplink localised sar values for realistic indoor wireless planning,” *Radiation Protection Dosimetry*, vol. 162, no. 4, pp. 487–498, 2014.
- [10] D. Plets, W. Joseph, K. Vanhecke, and L. Martens, “Downlink electric-field and uplink sar prediction algorithm in indoor wireless network planner,” in *The 8th European Conference on Antennas and Propagation (EuCAP 2014)*, pp. 2457–2461, IEEE, 2014.
- [11] S. Kuehn, S. Pfeifer, B. Kochali, and N. Kuster, “Modelling of total exposure in hypothetical 5g mobile networks for varied topologies and user scenarios,” Final Report of Project CRR-816, Available on line at: <https://tinyurl.com/r6z2gqn>, 2019.
- [12] D. Plets, W. Joseph, K. Vanhecke, G. Vermeeren, J. Wiart, S. Aerts, N. Varsier, and L. Martens, “Joint minimization of uplink and downlink whole-body exposure dose in indoor wireless networks,” *BioMed research international*, vol. 2015, 2015.
- [13] Y. Zeng, Q. Wu, and R. Zhang, “Accessing from the sky: A tutorial on uav communications for 5g and beyond,” *Proceedings of the IEEE*, vol. 107, no. 12, pp. 2327–2375, 2019.
- [14] Y. Kawamoto, H. Nishiyama, N. Kato, F. Ono, and R. Miura, “Toward future unmanned aerial vehicle networks: Architecture, resource allocation and field experiments,” *IEEE Wireless Communications*, vol. 26, no. 1, pp. 94–99, 2018.
- [15] R. Gangula, O. Esrafilian, D. Gesbert, C. Roux, F. Kaltenberger, and R. Knopp, “Flying robots: First results on an autonomous uav-based lte relay using open airinterface,” in *2018 IEEE 19th International Workshop on Signal Processing Advances in Wireless Communications (SPAWC)*, pp. 1–5, IEEE, 2018.
- [16] M. Deruyck, J. Wyckmans, W. Joseph, and L. Martens, “Designing uav-aided emergency networks for large-scale disaster scenarios,” *EURASIP Journal on Wireless Communications and Networking*, vol. 2018, 12 2018.
- [17] G. Castellanos, M. Deruyck, L. Martens, and W. Joseph, “Performance evaluation of direct-link backhaul for uav-aided emergency networks,” *Sensors*, vol. 19, no. 15, p. 3342, 2019.
- [18] M. Mozaffari, W. Saad, M. Bennis, Y.-H. Nam, and M. Debbah, “A tutorial on uavs for wireless networks: Applications, challenges, and open problems,” *IEEE Communications surveys & tutorials*, vol. 21, no. 3, pp. 2334–2360, 2019.
- [19] Q. Wu, L. Liu, and R. Zhang, “Fundamental trade-offs in communication and trajectory design for uav-enabled wireless network,” *IEEE Wireless Communications*, vol. 26, no. 1, pp. 36–44, 2019.
- [20] M. Deruyck, A. Marri, S. Mignardi, L. Martens, W. Joseph, and R. Verdone, “Performance evaluation of the dynamic trajectory design for an unmanned aerial base station in a single frequency network,” in *2017 IEEE 28th Annual International Symposium on Personal, Indoor, and Mobile Radio Communications (PIMRC)*, pp. 1–7, IEEE, 2017.
- [21] A. V. Savkin and H. Huang, “Deployment of unmanned aerial vehicle base stations for optimal quality of coverage,” *IEEE Wireless Communications Letters*, vol. 8, no. 1, pp. 321–324, 2018.
- [22] H. Huang and A. V. Savkin, “A method for optimized deployment of unmanned aerial vehicles for maximum coverage and minimum interference in cellular networks,” *IEEE Transactions on Industrial Informatics*, vol. 15, no. 5, pp. 2638–2647, 2018.
- [23] C. T. Cicek, H. Gultekin, B. Tavli, and H. Yanikomeroglu, “Uav base station location optimization for next generation wireless networks: Overview and future research directions,” in *2019 1st International Conference on Unmanned Vehicle Systems-Oman (UVS)*, pp. 1–6, IEEE, 2019.
- [24] A. Rizwan, D. Biswas, and V. Ramachandra, “Impact of uav structure on antenna radiation patterns at different frequencies,” in *2017 IEEE International Conference on Antenna Innovations & Modern Technologies for Ground, Aircraft and Satellite Applications (iAIM)*, pp. 1–5, IEEE, 2017.
- [25] M. Nosrati, A. Jafargholi, and N. Tavassolian, “A broadband blade dipole antenna for uav applications,” in *2016 IEEE International Symposium on Antennas and Propagation (APSURSI)*, pp. 1777–1778, IEEE, 2016.
- [26] M. Nosrati, A. Jafargholi, R. Pazoki, and N. Tavassolian, “Broadband slotted blade dipole antenna for airborne uav applications,” *IEEE Transactions on Antennas and Propagation*, vol. 66, no. 8, pp. 3857–3864, 2018.
- [27] B. A. Arand, R. Shamsaei, and B. Yektakhah, “Design and fabrication of a broadband blade monopole antenna operating in 30 mhz–600 mhz frequency band,” in *2013 21st Iranian Conference on Electrical Engineering (ICEE)*, pp. 1–3, IEEE, 2013.
- [28] L. Akhoondzadeh-Asl, J. Hill, J.-J. Laurin, and M. Riel, “Novel low profile wideband monopole antenna for avionics applications,” *IEEE transactions on antennas and propagation*, vol. 61, no. 11, pp. 5766–5770, 2013.
- [29] S. S. Siddiq, G. Karthikeya, T. Tanjavur, and N. Agnihotri, “Microstrip dual band millimeter-wave antenna array for uav applications,” in *2016 21st International Conference on Microwave, Radar and Wireless Communications (MIKON)*, pp. 1–4, IEEE, 2016.
- [30] Y. Zheng, J. Zhou, W. Wang, and M. Chen, “A low-profile broadband circularly polarized antenna array for uav ground-to-air communication,” in *2018 IEEE Asia-Pacific Conference on Antennas and Propagation (APCAP)*, pp. 219–220, IEEE, 2018.
- [31] X. Sun, R. Blázquez-García, A. García-Tejero, J. M. Fernández-González, M. Burgos-García, and M. Sierra-Castañer, “Circular array antenna for uav-uav communications,” in *2017 11th European Conference on Antennas and Propagation (EUCAP)*, pp. 2025–2028, IEEE, 2017.
- [32] I. Singh and V. Tripathi, “Micro strip patch antenna and its applications: a survey,” *Int. J. Comp. Tech. Appl.*, vol. 2, no. 5, pp. 1595–1599, 2011.
- [33] K. Kashwan, V. Rajeshkumar, T. Gunasekaran, and K. S. Kumar, “Design and characterization of pin fed microstrip patch antennae,” in *2011 Eighth International Conference on Fuzzy Systems and Knowledge Discovery (FSKD)*, vol. 4, pp. 2258–2262, IEEE, 2011.
- [34] A. Sudarsan and A. Prabhu, “Design and development of microstrip patch antenna,” *International Journal of Antennas (JANT)* Vol. vol. 3, 2017.

# Contents

<b>List of Figures</b>	<b>xxi</b>
<b>List of Tables</b>	<b>xxii</b>
<b>List of Listings</b>	<b>xxiii</b>
<b>Glossary</b>	<b>xxiv</b>
<b>Acronyms</b>	<b>xxv</b>
<b>1 Introduction</b>	<b>1</b>
1.1 Outline of the Issue . . . . .	1
1.2 Objective . . . . .	2
1.3 Structure . . . . .	3
<b>2 State of the Art</b>	<b>4</b>
2.1 Electromagnetic Exposure . . . . .	4
2.1.1 Electromagnetic Field Radiation . . . . .	4
2.1.2 Specific Absorption Rate . . . . .	5
2.1.3 Related Work . . . . .	5
2.2 Optimized UAV-aided networks . . . . .	6

2.3 Technologies . . . . .	7
2.3.1 Type of Drone . . . . .	7
2.3.2 Long Term Evolution . . . . .	8
2.3.3 Type of Antennae . . . . .	8
<b>3 Scenarios</b>	<b>11</b>
3.1 A Single User . . . . .	12
3.2 Increasing Traffic with only one Drone available . . . . .	13
3.3 Increasing Traffic with an Undefined Amount of Drones . . . . .	14
3.4 Overview . . . . .	15
<b>4 Methodology</b>	<b>16</b>
4.1 Electromagnetic Exposure . . . . .	16
4.1.1 Calculation of the Total Specific Absorption Rate . . . . .	16
4.1.2 Electromagnetic Exposure Caused by Far-Field Radiation . . . . .	17
4.1.3 Electromagnetic Exposure Caused by Near-Field Radiation . . . . .	19
4.2 Microstrip Patch Antenna . . . . .	21
4.2.1 Design of a Microstrip Patch Antenna . . . . .	21
4.2.2 Radiation Pattern . . . . .	24
4.3 Optimizing the Network . . . . .	25
4.4 Implementation . . . . .	27
4.4.1 Network Planning, Bringing It All Together . . . . .	27
4.4.2 Implementation of the Radiation Pattern . . . . .	30
4.4.3 Performance Improvement . . . . .	32

<b>5 Results and Discussion</b>	<b>34</b>
5.1 Scenario 1: One User and One Unmanned Aerial Vehicle (UAV) . . . . .	34
5.1.1 The Influence of the Maximum Transmission Power . . . . .	34
5.1.2 Influence of the Flying Height . . . . .	36
5.2 Scenario 2: Increased Traffic . . . . .	38
5.2.1 Influence of the Flying Altitude . . . . .	39
5.2.2 Influence of the Number of Users . . . . .	43
5.3 Scenario 3: Unlimited UAVs . . . . .	47
5.3.1 Influence of the Flying Altitude . . . . .	47
5.3.2 Influence of the Number of Users . . . . .	51
<b>6 Conclusions</b>	<b>54</b>
6.1 Conclusion . . . . .	54
6.2 Future work . . . . .	56
<b>Appendices</b>	<b>62</b>
<b>A Radiation Patterns: Datasheet</b>	<b>63</b>
<b>B Radiation patterns: Example Configuration</b>	<b>65</b>

## List of Figures

2.1	Resource allocation scheme for Time Division Duplex (TDD). . . . .	8
2.2	Resource allocation scheme for Frequency Division Duplex (FDD). . . . .	8
2.3	General design of a microstrip antenna. . . . .	10
3.1	Matrix with the four possible configurations . . . . .	15
4.1	Illustration of the network that shows how the average user (here shown in the center) is influenced by different types of sources. . . . .	17
4.2	Distribution of how many phones belong to a certain SAR interval. Upper boundary not included. . . . .	21
4.3	Design of the microstrip patch antenna. . . . .	23
4.4	Radiation pattern 1: On the left a 3D model of the entire pattern with the configuration as described above. In the middle a 2D radiation pattern of the E-plane and at the right a 2D model of the H-plane. . . . .	25
4.5	Radiation pattern 2: Generated with a groundplane of 0.06m by 0.06m. On the left is the 3D model of the entire pattern plotted. In the middle a 2D radiation pattern of the E-plane and at the right a 2D model of the H-plane. . . . .	25
4.6	Flowchart of the main algorithm. . . . .	28
4.7	Flowchart of the decision algorithm. . . . .	29
4.8	Schematic example of slices in a radiation pattern. . . . .	30
4.9	Schematic example of how bilinear interpolation works. . . . .	31

4.10	Example of a KD-tree in two dimensions.	33
4.11	Distribution of how many connections belong to a certain interval of distance. Upper boundaries are not included.	33
5.1	Minimal required transmission power by the antenna to reach the ground just below it. The red line shows the default maximum transmission power.	35
5.2	This figure shows how SAR values from different sources are influenced by different flying altitudes.	37
5.3	This figure shows the behaviour of the power consumption over the entire network at different flying heights. For this scenario, the power is used by only one Unmanned Arial Base Station (UABS).	38
5.4	These two figures show how the flying height influences the downlink electromagnetic radiation of the average user (left) and power consumption of the entire network (right) for one UABS available in the network.	39
5.5	Scenario 2 with only 2 users. The coloured areas are only applicable for the red user. The blue user is connected during the entire time.	40
5.6	Schematic overview of scenario 2 with only 2 users.	40
5.7	This graph shows the percentage of covered users for only one UABS at different flying heights.	41
5.8	Each figure corresponds with a certain configuration and shows how the Specific Absorption Rate (SAR) from different sources are influenced by an increasing flying height.	42
5.9	The influence of increasing traffic on the user coverage.	44
5.10	These two figures show how various sizes of population influence the downlink electromagnetic radiation of the average user (left) and power consumption of the entire network (rights) for one UABS available in the network.	44
5.11	This figure shows how different sources are influenced by an increasing number of users.	45
5.12	SAR-values for the user who is directly beneath the only UABS available.	46

5.13 Overview of which users are connected to the UABS. The map on the left is for 50 active users while the map on the right has 600 active users. . . . .	47
5.14 These two figures show how the flying height influences the downlink electromagnetic radiation of the average user (left) and power consumption of the entire network (right) for an unlimited number of drones. . . . .	48
5.15 This graph shows how much UAVs are required at different flying heights while trying to achieve a 100% coverage. . . . .	49
5.16 Each figure corresponds with a certain configuration and shows how the SAR from different sources are influenced by an increasing flying height. . . . .	50
5.17 This graph shows how much UAVs are required for different flying heights while trying to achieve a 100% coverage. . . . .	51
5.18 The influence of the population density on the downlink electromagnetic radiation (left) and power consumption (right). . . . .	52
5.19 Each figure corresponds with a certain configuration and shows how the SAR from different sources are influenced by an increasing population density. An unlimited number of UABSs is available. . . . .	53
6.1 Matrix with the four possible configurations, colour-coded based on the results. .	55

## List of Tables

2.1	Overview of the different SAR limitations. . . . .	5
2.2	Specifications of the used drone. . . . .	7
3.1	Overview of default configuration values. . . . .	12
3.2	Overview of the configuration. . . . .	13
3.3	Overview of the configuration. . . . .	14
3.4	Overview of the configuration. . . . .	14
4.1	Overview of configuration parameters. . . . .	22
A.1	Overview of attenuation in dBm. . . . .	64

## List of Listings

1	Mathlab code to generate the radiation patterns for the microstrip patch antenna.	24
2	Example configuration of a radiation pattern.	66

## Glossary

<b>equivalent isotropic radiator</b>	A theoretical source of electromagnetic waves which radiates the same intensity for all directions. , 9, 14, 15, 19, 31, 37, 44, 45, 56
<b>exact algorithm</b>	An exact algorithm solves an optimization problem optimally. , 7, 57
<b>power flux density</b>	Magnitude of power ( $W$ ) that travels through a curtain area ( $m^2$ ). , 20
<b>RRP</b>	RRP is an abbreviation used in this paper to indicate an extension on EIRP and stands for Real Radiation Pattern. An RRP value indicates the power (in dBm) for a certain location unlike an EIRP where the power (in dBm) is independent of the location. , 19
<b>spurious radiation</b>	According to the thefreedictionary.com: Any emission from a radio transmitter at frequencies outside its frequency band. Also known as spurious emission. , 10
<b>thermoregulatory capacity</b>	The capacity of an organism to regulate body temperature. , 5



## Acronyms

<b>DL</b>	downlink. , 6, 8, 18, 37, 41, 43, 46, 47, 49, 53
<b>EIRP</b>	equivalent isotropic radiation power. , 13, 19, 40, 43, 57
<b>EU</b>	European Union. , 4, 5
<b>Exp Opt</b>	exposure optimized network. , 27
<b>FCC</b>	Federal Communications Commission. , 5, 21
<b>FDD</b>	Frequency Division Duplex. , 8
<b>ICNIRP</b>	International Commission on Non-Ionizing Radiation Protection. , 4, 5
<b>IEC</b>	International Electrotechnical Commission. , 21
<b>IoT</b>	Internet of Things. , 1
<b>LOS</b>	line of sight. , 19, 36, 37, 41, 49
<b>LTE</b>	Long-Term Evolution. , 6, 8, 13, 20, 21, 35, 36
<b>NLOS</b>	non line of sight. , 6, 41
<b>PwrC Opt</b>	power consuption optimized network. , 27
<b>SAR</b>	Specific Absorption Rate. , 5, 17, 18, 21, 37, 43, 44, 46, 47, 49–51, 53, 54
<b>TDD</b>	Time Division Duplex. , 8
<b>UABS</b>	Unmanned Arial Base Station. , 2, 3, 6, 7, 13–15, 18–20, 27–37, 39–50, 52–57

<b>UAV</b>	Unmanned Aerial Vehicle. , 1, 2, 6, 7, 9, 26, 31, 35, 37, 39, 40, 42, 46, 48–53
<b>UE</b>	User Equipment. , 4–7, 9, 13, 14, 19–21, 37, 44, 46, 47, 49, 53, 56
<b>UL</b>	uplink. , 6, 8, 18, 20, 22, 37, 43, 46, 47, 49, 50, 53
<b>USA</b>	United States of America. , 5
<b>WHIPP</b>	WiCa Heuristic Indoor Propagation Prediction.
<b>WHO</b>	World Health Organization. , 2



# 1

## Introduction

### 1.1 Outline of the Issue

Society is constantly getting more and more dependent on wireless communication. On any given moment, in any given location, an electronic device can request to connect to the bigger network. Devices need more than ever to be connected, starting from small Internet of Things (IoT) up to self-driving cars which all need to be supported by the existing infrastructure. It is not surprising that the city centre of Ghent has an average coverage of 97% of 4G over all telecom operators [1]. Once again it becomes clear why we're on the eve of a new generation of cellular communication named 5G.

Also in exceptional and possibly life-threatening situations, the public relies on the cellular network. In 2011, Pukkelpop, a yearly festival in Belgium, got struck by a severe storm. However the storm was quite short, the damage was done, including the mobile network which remained defective for the rest of the evening [2]. One solution for a fast temporarily deployable network is with the usage of UAVs. Base stations can be attached to these flying UAVs to support the damaged network over a limited area. This approach does not only come in handy for damaged networks but also in case of an unexpected increase of traffic. For example during the terrorist attacks at Brussels Airport, mobile network operators saw all telecommunications drastically increasing causing moments of contention. Some operators even decided to temporarily exceed

the exposure limits in order to handle all connections [3]. Electromagnetic exposure can however not be neglected. Research shows how excessive electromagnetic radiation can cause diverse biological side effects [?]. Because of increasing public concern [4], the World Health Organization (WHO) had launched a large, multidisciplinary research effort which eventually concluded that there was no sufficient evidence that confirmed that exposure to low level electromagnetic fields is harmful [5]. A large part of the population remains nevertheless very concerned about potential health risks. It becomes clear that electromagnetic exposure is a key value when designing a UAV-aided network and should definitely not surpass the predefined limits.

## 1.2 Objective

UAV-aided networks can, thanks to their mobility, easily be repositioned towards a certain goal. Several papers in literature exist, explaining how a network can be optimized towards different goals like power consumption. However, very limited research has been done where a UAV-aided network is optimized towards electromagnetic exposure. While several publications exist, discussing how the electromagnetic exposure can be calculated, most of them only consider a limited number of sources like only base stations or only mobile phones. Papers who cover electromagnetic exposure from all the different sources and convert it into a single value are rather limited.

This master dissertation proposes a method to optimize the network towards electromagnetic exposure and power consumption when considering all four sources of radiation in a telecommunications network, being: the user's own phone, the base station that is serving this user, all devices from other users in the network and all other active base stations that are not serving this user. In this way, the contribution of each source towards the total electromagnetic exposure can easily be identified.

The behaviour of the electromagnetic exposure and power consumption of the network will be analysed by applying the tool in different scenarios to give insight into which variables influence the exposure and how the network can be optimized accordingly. Further, also the difference between omnidirectional and directional antennae will be considered. This leads to the following research questions:

**Research question 1:** How can a UABS network be optimized to minimize global exposure and overall power consumption? What are the effects on the network?

**Research question 2:** How does the network behave differently after the introduction of a realistic antenna?

**Research question 3:** How does the UABS flying height and population density influence electromagnetic exposure and power consumption?

**Research question 4:** What is the contribution of each source towards the total electromagnetic exposure?

To make this research possible, an existing planning tool is used which gives insight in user and base station distributions. The tool also provides information about path loss between radiators, power usage of the different electrical devices and which base station serves which user. In other words, the tool describes a fully configured network. In this way, all needed parameters will be known.

### 1.3 Structure

This section briefly describes the structure of this document. Related research to the subject is discussed in chapter 2: State of the Art, explaining electromagnetic exposure and its absorption into the body. Also the used technology such as type of antenna, type of base station and which infrastructure will be examined. The chapter also discusses why this master dissertation differs from other papers. Thereafter, chapter 3 talks about the different scenarios that will be investigated. Eventually, the methodology covers in chapter 4 the calculations and implementation of the different aspects excerpted in State of the Art. Chapter 5 shows the results of this implementation for the scenarios described in chapter 3. Finally, a conclusion of these results is formed in chapter 6.

# 2

## State of the Art

This chapter gives an overview of related research that has been done in the field of work and aims to familiarize the reader with the subject. First, an overview of the legislation related to electromagnetic exposure and specific absorption rate is given after which the related work about electromagnetic exposure is discussed. The second section describes how UAV-networks are designed and how they can be optimized. Finally, the used technologies are summed up including the type of drone, which generation of telecommunication and the type of antennae that are often used for this type of applications.

### 2.1 Electromagnetic Exposure

#### 2.1.1 Electromagnetic Field Radiation

People in a telecommunication network are exposed to far-field electromagnetic radiation originating from base stations and other User Equipment (UE). Network planners need to make sure that the electromagnetic fields (expressed in V/m) do not exceed limitations enforced by the government. These limits are location dependent. The European Union (EU) recommends the guidelines as defined by the International Commission on Non-Ionizing Radiation Protection (ICNIRP) which limit electromagnetic exposure to 61 V/m. Each European country needs to

decide for themselves which limitations to enforce. Belgium for example delegated this responsibility to Flanders, Brussels and Wallonia [6]. Since the considered area is the city center of Ghent, the standards will be defined by the Flemish government. They state that in the 2.6 GHz frequency band, an individual antenna cannot exceed 4.5 V/m and the cumulative sum of all fixed sources has its maximum at 31 V/m [6, 7].

### 2.1.2 Specific Absorption Rate

The Specific Absorption Rate (SAR) represents the rate at which electromagnetic energy is absorbed by human tissue with the thermal effect as its most important health consequence. The volume of this tissue is typically 1 g or 10 g. The Federal Communications Commission (FCC) of the United States of America (USA) defines regulations based on 1 g tissue (indicated as  $SAR_{1g}$ ) while the EU handles the 10 g model ( $SAR_{10g}$ ). SAR values can further be categorized based on the area it covers, as an example, the whole body SAR ( $SAR^{wb}$ ) is defined as the average radiation over the entire body. Another example are localized SAR-values that only cover a certain part of the human body like the head. The ICNIRP has concluded that the threshold effect for  $SAR_{10g}^{wb}$  is at 4 W/kg meaning that any higher absorption rate would overwhelm the thermoregulatory capacity of the human body. Whole body SAR-values between 1 and 4 W/kg increase the temperature of human body less than 1°C, which is proven not to be harmful for a healthy human being [8]. Thereafter, a safety margin is introduced to tackle unknown variables like experimental errors, increased sensitivity for certain population groups and so on. The EU follows the recommendation from the ICNIRP [6] and suggests for an individual mobile device a whole body  $SAR_{10g}$  of 0.8 W/kg and 2 W/kg for localized  $SAR_{10g}$  at head and torso area [4, 9]. Belgium follows this recommendation [6, 7]. An overview is given in table 2.1.

Description	Value	Units
Max $SAR_{10g}^{wb}$ as defined by ICNIRP	4	W/kg
Max $SAR_{10g}^{wb}$ for UE as defined by the Belgian government	0.8	W/kg
Max $SAR_{10g}$ for UE for head and torso as defined by the Belgian government	2	W/kg

Table 2.1: Overview of the different SAR limitations.

### 2.1.3 Related Work

The goal of this master dissertation is the investigation of electromagnetic exposure considering all sources. Four types of sources are considered: the user's own phone, the base station that is serving this user, all devices from other users in the network and all other active base stations that are not serving this user. This electromagnetic radiation is thereafter absorbed by the human body and will be expressed in SAR values.

Several papers calculate exposure originating from certain sources, but very limited research has been done covering the whole picture. In [10] is described how electromagnetic radiation of several WiFi access points is being calculated. The authors of [11] used this knowledge to investigate electromagnetic exposure originating from base stations in a more outdoor environment. [12, 13] addresses the fact that also uplink (UL) traffic from the user's device should be considered. They therefore investigated indoor exposure. They did not only consider the electromagnetic radiation but also how much is absorbed by the body, which will be expressed as specific absorption rate. Since the authors only covered voice calls, uplink SAR was expressed in localized SAR values while the downlink traffic is expressed in whole body SAR. With the advent of 5G, paper [14] has been published, describing how localized SAR values are achieved from different sources including all mobile phones and all base stations. Finally, [15] describes how both UL and downlink (DL) traffic can be converted in whole body SAR values making it possible to achieve an overall picture. They applied this formula however only for the user's own device.

In a realistic network, some users are calling while others are using other types of telecommunication services like browsing the web. Therefore, all absorbed electromagnetic exposure should be expressed in whole body SAR while still covering all sources.

## 2.2 Optimized UAV-aided networks

A UAV knows several applications. It was originally mainly used to support the military for surveillance and remote attacks without endangering pilots [16]. However, UAVs have recently become more accessible by the general public due to decreasing costs. This allowed UAVs to be researched for various applications.

When attaching an antenna to a UAV, it can be used as a gateway for cellular communication for UE on the ground. Such a flying base station will be called a UABS. This has several advantages like mobility and rapid deployment which is ideal for emergency situations or temporary events. Thanks to this mobility, UABSs can easily be repositioned to satisfy certain requirements. A UAV-aided network also brings some challenges with it like the limited weight of the payload and sparse power supply.

Kawamoto et al. introduced in [17] a WiFi network with the support of UAVs while considering resource allocation and antenna directivity. Gangula et al. illustrates in [18] how UAVs can be used as a relay for Long-Term Evolution (LTE). If a terrestrial base station is in non line of sight (NLOS) with a user, a UABS can be used as a relay. Zeng et al. proposes in [16] a tutorial in 5G-and-beyond wireless systems where challenges like energy consumption, mobility and antenna direction are discussed. Deruyck et al. designed in [19] a capacity based deployment tool for

UAV-aided emergency networks for large-scale disaster scenarios where an ideal flying height of 100 m is suggested. This was expanded in [20] with a performance evaluation of the direct-link backhaul of this tool where a slightly lower flying height of 80 metres is recommended.

These UAV-aided networks can be optimized towards certain goals. Mozaffari et al. provides in [21] guidelines on how to optimize and analyse UAVs equipped for wireless communication equipment. Issues like deployment, performance and power consumption are addressed. One path that has been excessively researched are location optimization solutions. For instance, [22] provides an algorithm that minimizes latency, [23, 24] minimizes interference between UABS and [25] minimizes the distance between UABS and UE. Other papers investigate trajectory optimization like in [23, 26]. Further, [21, 27] discuss several implementation approaches on how optimization algorithms should be tackled by discussing options like heuristic algorithms, exact algorithms and machine learning.

Optimizing the network towards electromagnetic exposure is rather limited. For a terrestrial network, using traditional base stations, Deruyck et al. discusses in [11] how the network can be optimized towards either a minimal exposure or minimal power consumption of the entire network. However, to the best of the author knowledge, no research has been done where a UABS-network has been optimized towards electromagnetic exposure.

## 2.3 Technologies

### 2.3.1 Type of Drone

The type of UAV will have a major impact on the network performance. Two types of drones are considered in [19]: an off-the-shelf drone affordable by the general public and a more robust one. The results in [19] show that the second type will require less drones to cover the same number of users and will last longer in the air. The research in this paper will therefore be done with the usage of the second type. A technical overview of this drone is given in table 2.2.

Parameter	Value	Units
Carrier power	13.0	A
Average carrier speed	12.0	m/s
Average carrier power usage	17.33	Ah
Carrier battery voltage	22.2	V

Table 2.2: Specifications of the used drone.

### 2.3.2 Long Term Evolution

The tool makes use of LTE, by the general public better known as 4G. LTE allows better UL and DL data speeds compared to its predecessors and is based on an all IP architecture. This technology can cover macrocells supporting cell sizes ranging from 5 km up to 100 km. Macrocell antennae are usually used by transmission towers along highways or on top of buildings. LTE supports however also smaller cells like femtocells covering only a few hundred meters. These femtocell antennae are therefore more portable, require less energy and will not require a telecommunication operator because of their simplicity. Femtocell base stations are therefore used by the deployment tool. Further, LTE also supports both FDD and TDD.

FDD makes simultaneous UL and DL traffic possible by assigning different frequencies within the same frequency range to both data streams. A small guard band is used between the UL and DL direction in order to prevent interference. An illustration is given in fig 2.2.

TDD allows UL and DL traffic by splitting the time domain. Meaning that both traffic directions use the same frequency and therefore alternately (in time) use the same frequency. A small time interval is used to prevent interference in case of a slightly bad timed synchronization as illustrated in fig. 2.1

Since it is assumed in this master dissertation that the user is continuously exposed without interruption, FDD will be used throughout this document.

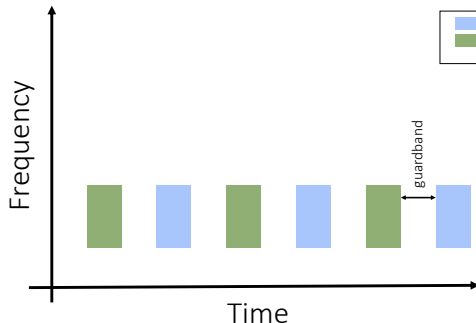


Figure 2.1: Resource allocation scheme for TDD.

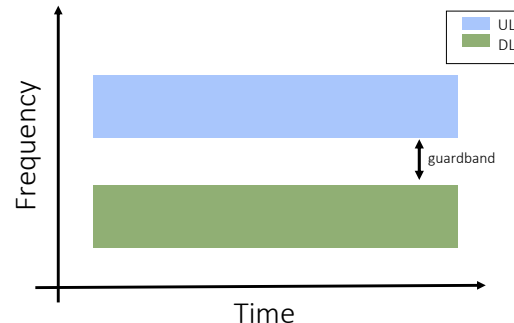


Figure 2.2: Resource allocation scheme for FDD.

### 2.3.3 Type of Antennae

The onboard antenna of the UAV will act as the gateway between the UE and the backhaul network. However, determining which antenna to use and how to position it, can be challenging.

Attaching an antenna to a UAV brings some additional challenges with it as explained by Rizwan et al. in [28]. Namely, the structure of the UAV can influence the radiation pattern. This can either have a constructive or destructive impact and depends on the relative position between the UAV and the antenna. When the antenna is too close to the UAV, the UAV can behave as a parasitic radiator, also emitting radiation. When using a directional antenna, the influence of the UAV will be much less but still existing, even when the UAV is not positioned in the direction of the mean beam. [28] suggest that this side-effect can be reduced by introducing a little offset between the antenna and the UAV. Another challenge that comes with attaching an antenna to a UAV is the need for 3D modelling of radiation patterns. In traditional terrestrial networks, the waves mainly propagated horizontally. When using UAVs, waves will have to travel rather downwards causing 2D antenna modelling to become insufficient. A 3D-model which accounts for both elevation and azimuth directivity will be required [16].

The easiest radiation pattern is a hypothetical equivalent isotropic radiator which radiates equally in all directions. Antennae that radiate equal quantities for a certain plane are called omnidirectional antennae [16] and several types exist. Attaching a conventional dipole antenna array might be low-cost, yet they are too high in profile and weight [29]. The authors of [30] and [31] both propose a broadband monopole blade antenna for UAV applications but this type suffers from a large surface which is a big disadvantage for the limited space available on the used UAVs in 2.3.1. [32, 33] propose a broadband blade dipole antenna which is much smaller. Their wing-shaped design allows good aerodynamics when flying. [34] proposes an alternative to blade antennae by presenting a wideband low profile monopole. The radiation pattern behaves similar to a traditional monopole but has a reduced height.

Another type of antennae are directional antennae that take advantage of throughput, lower interference and battery life [35]. This is done by focussing the electromagnetic energy there where it is needed. One type of directional antennae that has been investigated excessively for UAV-usage are microstrip antennae since they provide several advantages compared to traditional antennae [36, 37]. Microstrip antennae are lightweight, low in cost and thin causing them to be more aerodynamic which is a useful feature since the antennae will be attached to UAVs. Zeng et al. proposes in [29] the use of such an antenna in a sunflower-shaped array configuration. Also the authors from [38] attach star-shaped millimetre wave antennae to the wings of a UAV and [39] uses circular patch antennae in a circular array configuration for communication between UAVs.

A basic microstrip antenna like figure 2.3 consists of a ground plane and a radiating patch, both separated by a dielectric substrate. Several variations exist like microstrip patch antennae, microstrip slot antennae and printed dipole antennae which all have similar characteristics [36, 37]. They are all thin, support dual frequency operation and they all have the disadvantage that they will transmit at frequencies outside the aimed band. This is also known as spurious

radiation. The microstrip patch and slot antenna support both linear and circular polarization while the printed dipole only supports linear polarization. Further, the fabrication of a microstrip patch antenna is considered to be the easiest of the considered patch antennae [36].

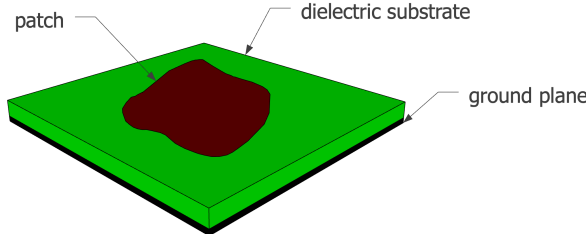


Figure 2.3: General design of a microstrip antenna.

The microstrip antenna requires besides the groundplane, dielectric substrate and the radiation patch also a feed line. Several feeding techniques exist of which the most popular are: coaxial probe feeding, microstrip line and aperture coupling.

A first feeding method is the usage of a coaxial cable where the outer conductor is attached to the ground plane and the inner conductor to the radiating patch. Modelling is however difficult, especially for thick substrates as will be used in this master dissertation. A second option is the usage of a microstrip line. This type of feeding is much easier to model since the microstrip line can be seen as an extension of the radiating patch. A disadvantage is the increased spurious radiation which limits bandwidth. A third is proximity coupling which has the largest bandwidth and low spurious radiation. It consists however of two dielectric substrates causing the overall thickness of the antenna to increase as well as its fabrication difficulty [36].

The increasing usage of the microstrip patch antennae can be explained by its easy fabrication and lightweightness and therefore knows a widespread application in the military, global positioning systems, telemedicine, WiMAX applications and so on. The authors of [36] also state that some of the disadvantages like lower gain and power handling can be solved by using an array configuration.

The radiating patch is usually made of a thin layer of either gold or copper [37, 40] and can have any form. However, shapes other than circles or rectangles would require large numerical computation [37]. Thus, a simple rectangular shape will be used. Further, also the dielectric constant of the substrate is important. It typically varies between 2.2 and 12. Finding a good dielectric depends on how the antenna will be used. A lower dielectric constant with a thick substrate will result in better performance, better efficiency and larger bandwidths [40]. On the other hand, a larger dielectric constant reduces the dimensions of the antenna [37] which is also useful when attaching the antenna to a limited surface. Glass as a dielectric substrate with a constant of 4.4 will be used.

# 3

## Scenarios

The tool supports multiple configurations and the behaviour will be different for most of these configurations. Three main scenarios will be investigated, order based on the network complexity. Within each scenario, different cases will be investigated. First, only one user with one drone will be present in the network. The network will thereafter be expanded for multiple users but with still only one drone available. Eventually, also that last restriction will be dropped meaning that multiple users with unlimited number of drones are examined. Table 3.1 shows the default values that are always applicable unless mentioned otherwise.

<b>Broadband cellular network</b>	
technology	LTE
frequency	2.6 GHz
<b>Carrier</b>	
carrier power	13.0 A
average carrier speed	12.0 m/s
average carrier power usage	17.33 Ah
carrier battery voltage	22.2 V
<b>Femtocell antenna</b>	
maximum $P_{tx}$	33 dBm
antenna direction	downwards (az: 0°; el: 90°)
gain	4 dBm
feeder loss	2 dBm
implementation loss	0 dBm
radiation pattern	EIRP or microstrip patch antenna
height	100m
<b>UE Antenna</b>	
height	1.5m from the floor
gain	0 dBm
feeder loss	0 dBm
radiation pattern	EIRP
number present in the network	224

Table 3.1: Overview of default configuration values.

### 3.1 A Single User

This first scenario will investigate how  $SAR_{10g}$  and power consumption behave in an isolated environment meaning there is no influence from other base stations or other UE. The tool will provision one single drone and position it directly above the user. These results will however depend on the position of the user. If the randomly generated location of the user is indoor, the flying height of the drone might be obstructed by the building where the user resides, causing the user to become uncovered. If this is not the case, the expected altitude of the user is half of the height of the building meaning that the user would be closer to the UABS as if he would have been outdoors. For more consistent results, the user will be positioned outdoor while systematically increasing the flying height.

Another considered variable will be the transmission power of the antenna. LTE makes use of power control meaning that no more power will be used than strictly necessary. The actual

transmission power therefore ranges between 0 and the maximum input power. This power is zero when either no user is present or the user is so far away that the actual transmitted power would exceed the maximum allowed transmission power. Increasing the maximum transmission power will not influence the actual power consumption or  $SAR_{10g}$  because the UABS will not use more than strictly required. It is therefore more useful to match the actual transmission power against a variable flying height.

This scenario investigates  $SAR_{10g}$ , power consumption and minimal transmission power for two different types of antennae: a fictional equivalent isotropic radiator and a realistic antenna. The used optimization strategy is not important for this scenario. This is because the decision algorithm decides which user needs to be connected to which drone. Since only one user and one UABS are available, both optimization strategies will behave identical.

The user gets a fixed position. The exact location doesn't matter as long as it is outside. For this experiment is chosen for the 'Koningin Maria Hendrikaplein', a square just next to the train station of Ghent. Doing so will force the UE to always be at the same height of 1.5 meters. An overview can be found in table 3.2

Parameter	Value	Input variables	Output variables
x position user	3.711198	type of antenna	$SAR_{10g}$
y position user	51.036747	flying height	power consumption
shadow margin user	-3.0398193		minimal $P_{tx}$
number of users	1		

Table 3.2: Overview of the configuration.

Note that there is no explicit restriction on the number of drones in table 3.2. The deployment tool initially places UABSs above each user and it is the optimization strategy that decides which of these potential positions will remain in the end solution. Since there is only one user, there can also be only one drone.

## 3.2 Increasing Traffic with only one Drone available

This scenario investigates the same behaviour as the previous one. Still with only one drone but for a higher number of users. The scenario can be divided into two cases. The first case has a variable flying height with a fixed number of 224 users. This is the number of active users on an average day at 5 p.m. implying rush hour and therefore resulting in the highest number of simultaneous users for the day [19]. The other case has a fixed flying height of 100 m as recommended by [19] but with a variable number of users. To force the tool to only use one drone, a facility capacity is set to one indicating that there is only one spot available in the

facility where the UABSs are stored. The tool will still consider as much potential places as there are users in the network. But when the optimization algorithm is done, only one drone will remain.

Parameter	Value	Input variables	Output variables
facility capacity	1	type of antenna flying height number of users optimization strategy	$SAR_{10g}$ power consumption user coverage

Table 3.3: Overview of the configuration.

For both cases, four configurations are possible because there are two antennae available (equivalent isotropic radiator and a realistic antenna) which can both operate in a power consumption optimized network or an exposure optimized network. The  $SAR_{10g}$ , power consumption and user coverage will be investigated for all four configurations.

### 3.3 Increasing Traffic with an Undefined Amount of Drones

Input variables	Output variables
type of antenna flying height number of users optimization strategy	$SAR_{10g}$ power consumption user coverage

Table 3.4: Overview of the configuration.

The third scenario implies no budget limitations. The tool can use as much UABSs as desired while trying to maximize coverage. A UABS will be considered above each user as was also the case in scenario 2. However, the last step where the capacity of the facility was checked and drones got eliminated is omitted here. It is expected that the optimization strategies will perform best for this scenario since the decision algorithm has been written with multiple drones in mind. The scenario can once again be divided into two cases: one with a fixed flying height of 100 m and a variable number of users and a second one with a variable flying height and a fixed number of 224 users. The influence that these input parameters have on the network will be based on the electromagnetic exposure, power consumption, number of drones required and user coverage.

### 3.4 Overview

Three different scenarios will be investigated where the second and third one, each consist out of two cases. The first case considers a fixed flying height while the second one has a fixed population size. Each case consists out of four configurations. An overview of these configurations is given in table 3.1.

		Optimization strategy	
		Exposure optimized	Power consumption optimized
Antenna type	Equivalent isotropic radiator	EIRP, Exp Opt	EIRP, PwrC Opt
	Microstrip patch antenna	Microstrip, Exp Opt	Microstrip, PwrC Opt

Figure 3.1: Matrix with the four possible configurations

# 4

## Methodology

The content of this chapter gives an answer to which steps that have to be taken to be able to answer the research questions. The first section explains how electromagnetic radiation is calculated for each source and how to convert these values to specific absorption rates. The second section gives a detailed overview of how a microstrip patch antenna can be designed and how its radiation pattern is achieved. The third section discusses how the network can be optimized towards either electromagnetic exposure or power consumption. The final section explains how these algorithms are implemented and how to further improve performance.

### 4.1 Electromagnetic Exposure

#### 4.1.1 Calculation of the Total Specific Absorption Rate

The total whole body SAR ( $SAR_{10g}^{wb,total}$ ) (expressed in  $W/kg$ ) of a user can be calculated by a simple sum of individual SAR values from the different sources. Formula 4.1 was originally described in [14] for SAR values induced into the head. Using  $SAR_{10g}^{head}$  would however result into incorrect conclusions since the position of the phone relative to the user is unknown. The position of the phone can be next to the head but also in front of the user. The induced

electromagnetic radiation will therefore be expressed in function of the entire body.

$$SAR_{10g}^{wb,total} = SAR_{10g}^{wb,my\_UE} + SAR_{10g}^{wb,my\_UABS} + SAR_{10g}^{wb,other\_UE} + SAR_{10g}^{wb,other\_UABSs} \quad (4.1)$$

The first parameter,  $SAR_{10g}^{wb,my\_UE}$ , indicates the absorbed electromagnetic radiation by the whole body originating from the user's own device. However that the UL radiation is destined for the serving UABS, a portion of that radiation is directly absorbed by its user, due to the omnidirectional nature of the mobile's antenna. The second parameter,  $SAR_{10g}^{wb,my\_UABS}$ , represents the DL radiation caused by the UABS that is serving the user. As the third parameter, we have the  $SAR_{10g}^{wb,other\_UE}$  which is radiation caused by other people's devices. The radiation of these devices is once again destined for a specific UABS but again, a portion of that UL radiation will also be absorbed by our user. Finally,  $SAR_{10g}^{wb,other\_UABSs}$  represents the DL radiation by the other UABSs to which our user is exposed to but not served by. An illustration is given in figure 4.1. The green arrow stands for near-field radiation, the others represent far-field radiation. This is further explained in subsequent chapters along with how each value in this formula can be calculated. We can only speak in terms of SAR when the electromagnetic radiation is absorbed by the user. This last step is however not shown in the illustration.

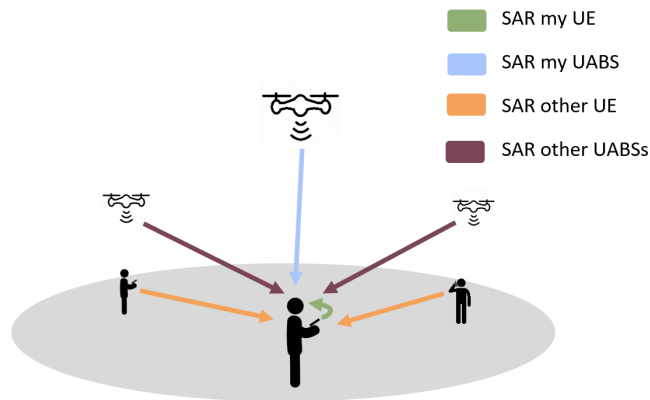


Figure 4.1: Illustration of the network that shows how the average user (here shown in the center) is influenced by different types of sources.

#### 4.1.2 Electromagnetic Exposure Caused by Far-Field Radiation

The electromagnetic exposure to which people are exposed can be categorized in two groups. One of them is near-field radiation which is caused by the user's own device and will be discussed in 4.1.3. The other type is far-field radiation and will be explained in this section. This kind of

radiation is caused by radiators ‘far away’. Examples of these types of radiators are UE which belong to other people and UABSs.

### Electromagnetic Radiation from a Single Source

To determine the total exposure of a single human being or even of the entire network, the electric-field  $\vec{E}$  from a single radiator  $i$  should be calculated. The formula to determine this electromagnetic value  $E$  (expressed in V/m) for a specific location  $u$  is given in equation 4.2.

$$E_i(u)[V/m] = 10^{\frac{RRP(u)[dBm] - 43.15 + 20 * \log(f[MHz]) - PL(u)[dB]}{20}} \quad (4.2)$$

**real radiation power and EIRP** In formula 4.2, as it was described in [10, 11], RRP was defined as equivalent isotropic radiation power (EIRP). EIRP is the radiation generated by an equivalent isotropic radiator which is a theoretical source of electromagnetic waves that radiate with the same intensity in all directions. The formula to find this EIRP value (in dBm) is described in 4.3 where  $P_t$  stands for the input power of the antenna,  $G_t$  for the gain of the transmitter and  $L_t$  being its feeder loss.

$$EIRP[dBm] = P_t[dBm] + G_t[dBi] - L_t[dB] \quad (4.3)$$

This formula, which is constructed out of different gains and losses, misses a factor when accounting for real life radiation patterns. Formula 4.2 solves this by using RRP instead of EIRP and can be defined as follows:

$$RRP(u)[dBm] = EIRP[dBm] - attenuation(u)[dB] \quad (4.4)$$

The attenuation for a user  $u$  is given based on the angle between the main beam and the user. More details on how this can be implemented are described in 4.4.2. When assuming that  $attenuation(u)$  returns positive values, the attenuation can simply be subtracted from the EIRP-value.

**frequency** The used frequency in the formula above is denoted as  $f$  and is expressed in MHz. Since LTE is used, this value will be 2600 MHz.

**path loss** At last, formula 4.3 requires the path loss (in dB). In order to calculate this, an appropriate propagation model —of which several exist— is required . The Walfish-Ikegami model is used since it performs well for femtocell networks in urban areas [19]. It consists of two formulas depending on whether a free line of sight (LOS) between the user and the base station exists or not. Both formulas expect a distance in kilometre.

### Combining Exposure

The electromagnetic exposure for a given location originating from different sources can be calculated with formula 4.5 (in V/m).  $E_i$  stands for the electromagnetic exposure from source  $i$  and  $n$  stands for all far-field radiators of a certain category; they can either be UABSs or UE from other people.  $E_{tot}$  will be calculated for each location where a user is positioned.

$$E_{tot}[V/m] = \sqrt{\sum_{i=1}^n (E_i[V/m])^2} \quad (4.5)$$

### Converting Far-Field Electromagnetic Exposure to $SAR_{10g}^{wb}$

Formula 4.1 expects that the radiation from each far-field source is expressed in  $SAR_{10g}^{wb,my\_UABS}$ ,  $SAR_{10g}^{wb,other\_UE}$  and  $SAR_{10g}^{wb,other\_UABSs}$ . The calculation for all these values is in fact identical since the only difference is the source. Physically seen, they all are whole body SAR values induced by far-field radiation ( $SAR_{10g}^{ff,wb}$ ).

The electromagnetic radiation needs to be converted into  $SAR_{10g}^{ff,wb}$ . The conversion factor is based on Duke from the Virtual Family. Duke is a 34-year old male with a weight of 72 kg, a height of 1.74 m and body mass index of 23.1 kg/m [15]. Research shows that the conversion factor for WiFi is  $0.0028 \frac{W/kg}{W/m^2}$ . Since WiFi, at a frequency of 2400 MHz, is very close to LTE, at 2600 MHz, it is assumed in [15] that this value is also applicable for LTE. The constant in 4.7 converts the power flux density  $S$  (in units  $\frac{W}{m^2}$ ) to the required  $SAR_{10g}^{ff,wb}$ . To make this possible, the electromagnetic radiation from formula 4.5 (expressed in V/m) should first be converted to the power flux density with formula 4.6 before formula 4.7 can be applied.

$$S[W/m^2] = \frac{(E_{tot}[V/m])^2}{337} \quad (4.6)$$

$$SAR_{10g}^{wb,ff}[W/kg] = S[W/m^2] * 0.0028 \left[ \frac{W/kg}{W/m^2} \right] \quad (4.7)$$

#### 4.1.3 Electromagnetic Exposure Caused by Near-Field Radiation

Up till now, only sources that cause far-field radiation have been considered. However, when a user is operating his device, a part of the UL radiation will enter his body despite the fact that the data traffic is destined for the serving UABS. This device is very close to the user and the emitted radiation is therefore considered to be near-field radiation.

## Localized Specific Absorption Rate

When assuming that all users hold their device next to their ear, a localized SAR-value for the head  $SAR_{10g}^{head}$  can be calculated. Various governments have defined different legislations. The European Union uses the directions of the IEC who define in IEC:62209-2 a maximum for a 10g tissue  $SAR_{10g}^{head}$  at 2 W/kg [6]. The FCC limits the maximum in the United States for a 1g tissue  $SAR_{1g}^{head}$  at 1.6 W/kg [41]. Most countries, including Belgium, enforce the 10g model and this will, therefore, be the point of reference for this master dissertation. The  $SAR_{10g}^{head}$  values are phone dependent. The values reported by mobile manufacturers are worst-case scenarios meaning that the values are measured when the phone is transmitting at maximum power. This is an understandable decision but will not result in a realistic scenario since modern cellular networks use power control mechanisms to prevent unnecessary high radiation of a nearby device. UE will therefore never use more energy than required to maintain a connection. To compensate for this overestimation, the actual  $SAR_{10g}^{head}$  of each user will be predicted. These will, however, remain an estimation since the position of the phone relative to the head differs from user to user. For example, by holding the phone differently, a hand can absorb more or less electromagnetic radiation. The SAR values will also depend on the age of the user, especially children who experience on average higher exposure in the brain regions because of different anatomical proportions [42, 12].

$$SAR_{10g}[W/kg] = \frac{P_{tx}[W]}{P_{tx}^{max}[W]} * SAR_{10g}^{max}[W/kg] \quad (4.8)$$

Equation 4.8 will be used to predict the actual  $SAR_{10g}^{head}$  of a certain user with  $P_{Tx}^{max}$  being the maximum transmission power for a phone which is in LTE and UMTS 23 dBm [43, 12]. The actual transmitted power ( $P_{tx}$ ) is calculated with equation 4.9 where  $P_{sens}$  stands for the receiver sensitivity and  $PL$  the path loss between sender and receiver.

$$P_{tx} = P_{sens}[W] + PL[dB] \quad (4.9)$$

However the legal  $SAR_{10g}^{max}$  for Belgium is set to 2 W/kg, the actual  $SAR_{10g}^{max}$  value is usually lower and different for each mobile device. An average is calculated based on 3516 different phones from various brands using a German database [44]. An overview can be found in fig. 4.2. When the phone is positioned at the ear, an average  $SAR_{10g}^{max}$  of 0.7 W/kg is found with a standard deviation of 0.25 W/kg which are very similar results as in ref. [45]. The median of 0.67 W/kg is used as  $SAR_{10g}^{max}$  in formula 4.8.

## Whole Body Specific Absorption Rate

The position of the phone relative to the user's body is however unknown. Some users will be calling and therefore probably holding their phone next to their ear while others are using other

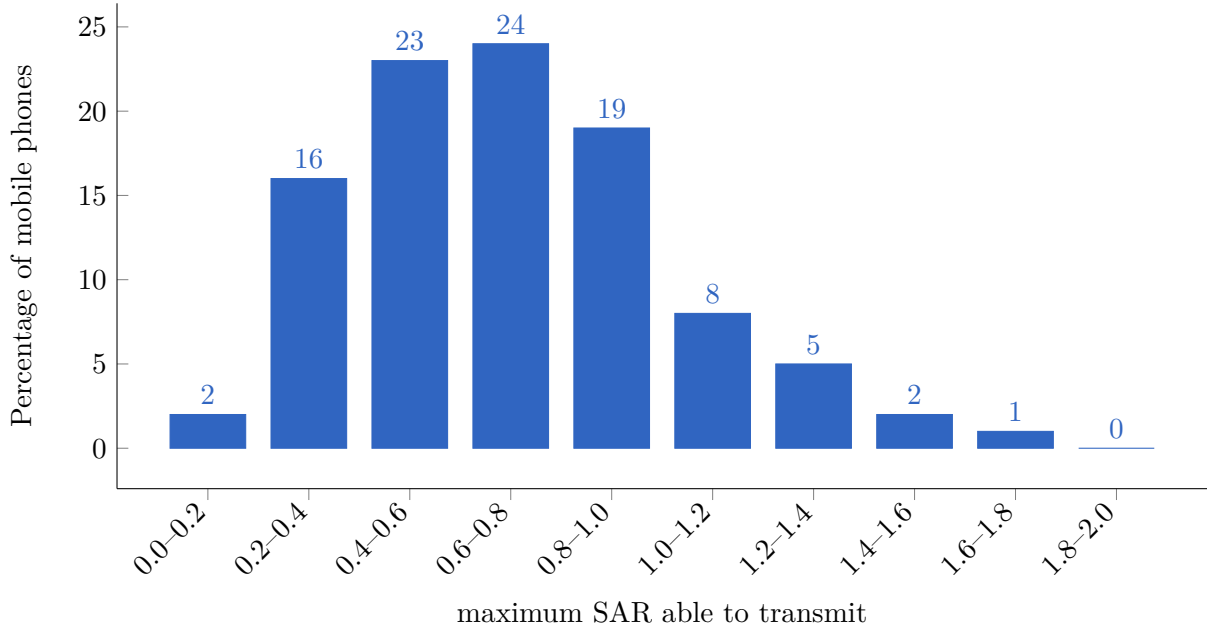


Figure 4.2: Distribution of how many phones belong to a certain SAR interval. Upper boundary not included.

services like browsing the web. This would result in different types of localized values. To be able to give an average SAR based on all active users, the whole body SAR will be used. For this reason formula 4.1 expects that the specific absorption rate is expressed for the entire body instead of localized  $SAR_{10g}^{head}$ . The conversion factors for Duke from the Virtual Family will be used again as it was already the case in 4.1.2. The constant to convert UL exposure to  $SAR_{10g}^{wb,ul}$  for WiFi is defined to be  $0.0070 \frac{W/kg}{W}$  [15] which leads to eq. 4.10.

$$SAR_{10g}^{wb,ul} \left[ \frac{W}{kg} \right] = 0.0070 \left[ \frac{W/kg}{W} \right] * P_{tx}[W] \quad (4.10)$$

## 4.2 Microstrip Patch Antenna

### 4.2.1 Design of a Microstrip Patch Antenna

A microstrip patch antenna is chosen because it allows easy production but more important, it has a low weight and has a thin profile causing it to be very aerodynamic which is useful when attaching it to a drone [36].

The dimensions of the antenna depend on the frequency it is operating at and the characteristics of the used substrate. The antenna will be radiating at a center frequency  $f_0$  of 2.6 GHz. Each

substrate has a dielectric constant  $\epsilon_r$  representing the permittivity of the substrate that depends on the used material. Substrates with a high dielectric constant and low height reduce the dimensions of the antenna while a lower dielectric constant with a high height improves antenna performance [37, 40]. In this document, a substrate like glass is chosen because of the higher dielectric constant of  $\epsilon_r = 4.4$  compared to materials like teflon with only a dielectric constant of  $\epsilon_r = 2.2$  [37]. Doing this in combination with an antenna height of 2.87 mm will decrease the dimensions of the entire antenna surface. This comes in handy since drones only have limited space available.

description	symbol	value
center frequency	$f_0$	2600 Hz
dielectric constant	$\epsilon_r$	4.4
height of the substrate	$h$	0.00287 m

Table 4.1: Overview of configuration parameters.

The dimensions of the radiating patch can be calculated with the formulas from [37] and [40] using the defined values from table 4.1. In that way, the width of the patch  $W_p$  is calculated using formula 4.11.

$$W_p[m] = \frac{C[m/s]}{2 * f_0[Hz]} * \sqrt{\frac{\epsilon_r + 1}{2}} \quad (4.11)$$

With  $C$  being the speed of light,  $f_0$  the center frequency of 2600 MHz and a dielectric constant  $\epsilon_r$  of 4.4, the width of the patch becomes 35.09 mm.

In order to find the length of the radiating patch, some other values need to be determined first. Formula 4.12 will calculate the effective dielectric constant ( $\epsilon_{ref}$ ).

$$\epsilon_{ref} = \frac{\epsilon_r + 1}{2} + \frac{\epsilon_r - 1}{2} * \left(1 + 12 * \frac{h[m]}{W_p[m]}\right)^{-\frac{1}{2}} \quad (4.12)$$

This formula requires the width found in the previous formula along with the dielectric constant and substrate height from table 4.1. This will result in a  $\epsilon_{ref}$  of 3.91.

$$L_{eff}[m] = \frac{C[m/s]}{2 * f_0[Hz]} * \sqrt{\epsilon_{ref}} \quad (4.13)$$

Now formula 4.13 can be used to calculate the effective length ( $L_{eff}$ ), resulting in 29.16 mm.

$$\Delta L[m] = 0.412 * h * \frac{(\epsilon_{ref} + 0.3) \left( \frac{W_p[m]}{h[m]} + 0.264 \right)}{(\epsilon_{ref} - 0.258) \left( \frac{W_p[m]}{h[m]} + 0.8 \right)} \quad (4.14)$$

Eventually, the length extension is found with formula 4.14 by substituting the values from above. Doing so determines that the  $\Delta L$  equals 1.3071 mm.

Finally, the length of the patch can be calculated using the expression 4.15

$$L_p[m] = L_{eff}[m] - 2 * \Delta L[m] \quad (4.15)$$

The length  $L_p$  results in 26.55 mm.

The dimensions of the radiation patch are now known. The only remaining questions are the dimensions of the ground plane and dielectric substrate to which the radiation patch is attached. The transmission line model is in fact only applicable for an infinite ground plane but it has been proven that similar results can be achieved if the ground plane's dimensions are bigger than the patch by approximately 6 times the height of the dielectric substrate [37, 40].

$$L_g[m] = 6 * h[m] + L_p[m] \quad (4.16)$$

$$W_g[m] = 6 * h[m] + W_p[m] \quad (4.17)$$

Therefore, the length of the ground plane  $L_g$  should be at least 0.0438 m and the width  $W_g$  at least 0.0524 m. A schematic overview of how the antenna will look like is given in figure 4.3.

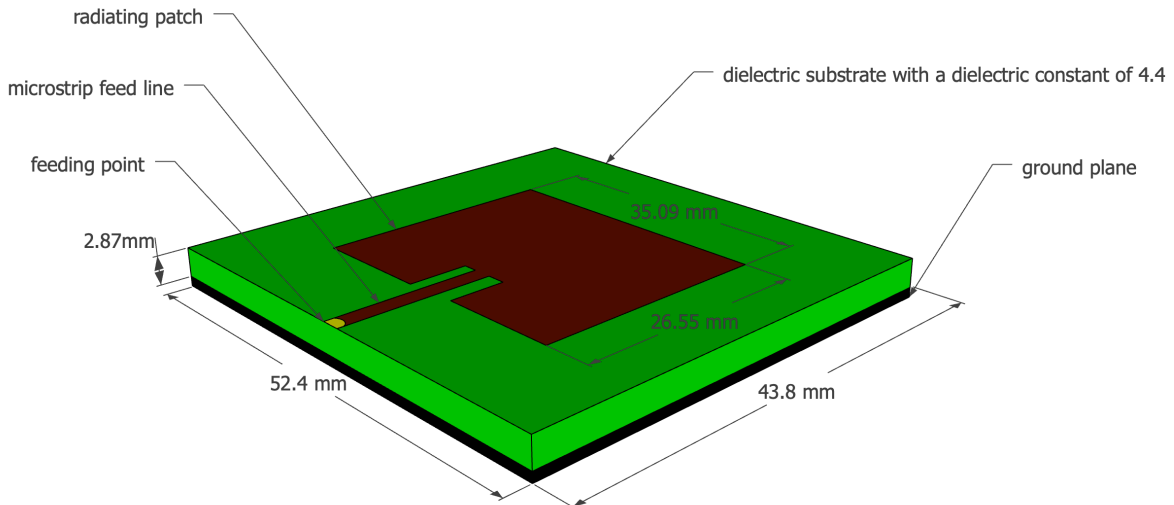


Figure 4.3: Design of the microstrip patch antenna.

### 4.2.2 Radiation Pattern

Mathlab is able to generate the radiation pattern for this microstrip patch antenna. The code in listing 1 starts by defining the dielectric substrate which will be glass with a dielectric constant of 4.4 and a height of 0.00287 m. Thereafter, the microstrip patch antenna is generated with the `width` and `length` being the dimensions of the radiation patch and the `GroundPlaneLength` and `GroundPlaneWidth` the dimensions of the ground plane and dielectric substrate. The `FeedOffset` is the relative offset from the center where the radio frequency power is fed to the radiating patch which will here be at the edge. This is in figure 4.3 indicated with a yellow dot. At last, the `dielectric`-object is substituted into the `patchMicrostripInsetfed`-object.

Generating the pattern is done with the `pattern`-command. The first value is the `patchMicrostripInsetfed`-object followed by the frequency at which the antenna will be operating. Optionally, an azimuth value can be parsed like in line 7 and 8 where 90 and 0 relatively stand for the H-plane and E-plane.

```

1 d = dielectric("Name",'glass',"Thickness",0.00287,"EpsilonR",4.4)
2 p = patchMicrostripInsetfed("Width",0.0351,"Length",0.02655,
3 "GroundPlaneLength",0.0438,"GroundPlaneWidth",0.0524,
4 "FeedOffset",[-0.021885 0],"Substrate", d)
5
6 pattern(p,2.6e9, "CoordinateSystem", 'polar', "Normalize",true)
7 pattern(p,2.6e9, 90, "CoordinateSystem", 'polar', "Normalize",true)
8 pattern(p,2.6e9, 0, "CoordinateSystem", 'polar', "Normalize",true)
```

Listing 1: Mathlab code to generate the radiation patterns for the microstrip patch antenna.

Running the configuration from listing 1 will generate the radiation pattern from figure 4.4. When running the same configuration for a slightly bigger square ground plane with an edge of 0.060 m, the radiation pattern from 4.5 is achieved. Both radiation patterns show an aperture angle of approximately 90°. It becomes clear that the radiation pattern from figure 4.4 has a higher attenuation in the direction it is not facing compared to the radiation pattern of figure 4.5. If it is assumed that drones fly lower than some users are positioned in some buildings, the pattern of 4.5 would be a better approach. However, for the continuation of this master dissertation, the radiation pattern from figure 4.4 will be used since this antenna is the smallest and therefore most suitable to attach to the limited space available under a drone. A data sheet of the exact values from both radiation patterns can be found in appendix A.

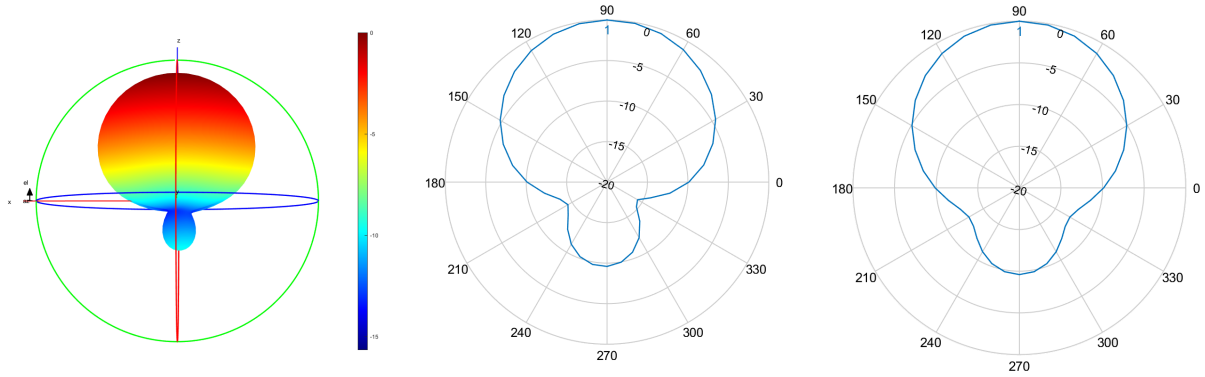


Figure 4.4: Radiation pattern 1: On the left a 3D model of the entire pattern with the configuration as described above. In the middle a 2D radiation pattern of the E-plane and at the right a 2D model of the H-plane.

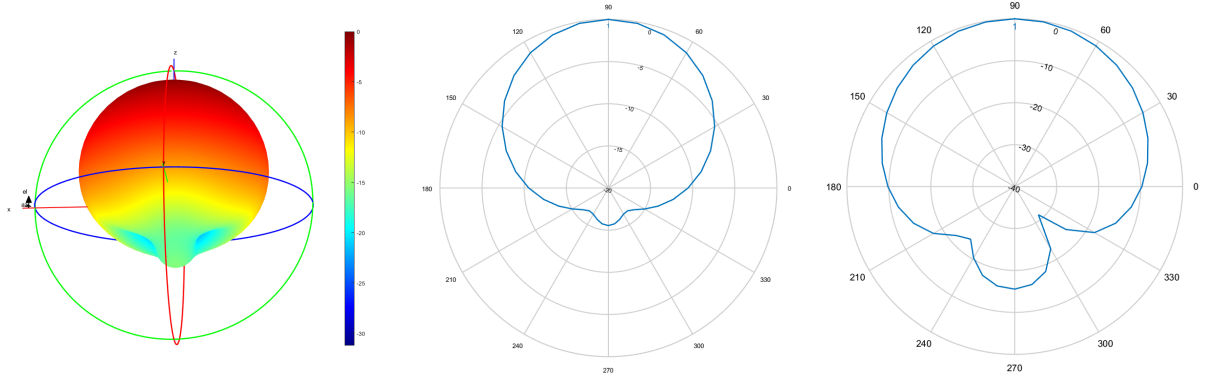


Figure 4.5: Radiation pattern 2: Generated with a groundplane of 0.06m by 0.06m. On the left is the 3D model of the entire pattern plotted. In the middle a 2D radiation pattern of the E-plane and at the right a 2D model of the H-plane.

### 4.3 Optimizing the Network

UAVs can remain in the air for only a limited time, which is certainly the case when also an antenna needs to be connected to the battery of his carrier. It is therefore interesting to not only consider electromagnetic exposure of the user but also the power consumption that comes with it. However an increasing transmission power of an antenna comes with an increasing electromagnetic exposure. This is not the case considering both values for an entire network. In fact, the authors from [11] prove that both become inversely equivalent.

The reason the network behaves like this is because it is often cheaper to increase the exposure of an already active base station than activating a new one. As an example, imagine there is a new user who can either be covered by activating a nearby base station or by an already

active base station a little further away. When this user is in a power consumption optimized network, the already active base station will increase its power level because that will be cheaper than activating a new base station. Users close by will thus experience a higher electromagnetic exposure. On the other hand, if the user would have been in an exposure optimized network, the nearby base station which was offline would be activated at a lower power level. So the electromagnetic exposure will also be lower but by activating a new base station, the overall power consumption increases.

This results in conflicting requirements. An optimization strategy that optimizes towards either electromagnetic exposure or total power consumption is given in 4.18 and is based on the fitness function described in [11].

$$f = w * \left(1 - \frac{E_m}{E_{max}}\right) + (1 - w) * \left(1 - \frac{P}{P_{max}}\right) * 100 \quad (4.18)$$

Formula 4.18 returns a fitness value which represents the performance of the entire network. Users are connected to different UABSs and each time a fitness value is calculated. The user will eventually be connected to the drone that results in the highest fitness value. This is repeated for each user. This process is explained in detail in section 4.4.1.  $w$  is the importance factor of electromagnetic exposure ranging from 0 to 1, boundaries included. A  $w$  set to zero means that electromagnetic exposure is not important. Such a network will therefore be called a power consumption optimized network (PwrC Opt). Likewise, a  $w$  set to one means that minimizing exposure is top priority and will result in an exposure optimized network (Exp Opt).  $P_{max}$  is the power consumption of all UABSs, both active and inactive, when radiating at the highest possible level while  $P$  is the effective power used by the current designed network. This will be the power required for the flying drones themselves and their antenna.  $E_m$  will be the weighted exposure of the average user for the current designed network and  $E_{max}$  the weighted average of electromagnetic exposure when all antennae are at their highest power level.

When optimizing the network, it is not only important to consider the average exposure of all users, but also to limit high extremes [11]. In formula 4.19 a weighted average of exposure will be found by not only considering the median but also the 95 percentile of all users' DL exposure. Since both values are considered to have equal importance, the weight factors  $w_1$  and  $w_2$  will both have an equal importance of 50%.

$$E_m = \frac{w_1 * E_{50} + w_2 * E_{95}}{w_1 + w_2} \quad (4.19)$$

## 4.4 Implementation

### 4.4.1 Network Planning, Bringing It All Together

#### Deployment Tool for an UAV Network

Calculating electromagnetic exposure requires knowledge about the area. For instance, the position of UABSs needs to be known but also other variables like the used transmission power and the distances between antennae.

The WAVES research group at Ghent University has developed a capacity based deployment tool for disaster scenarios with the aid of UAVs [19]. The idea of this UAV-aided emergency network is that in case of a disaster, the existing network might be damaged and will not be able to handle all users who are trying to reconnect to the backbone network. The tool makes a fast deployable network possible by attaching femtocells to UAVs, so-called UABSs. The tool will orchestrate the UABSs over the disaster area by describing a fully configured network. This tool is thus a suitable starting point and works as follows:

The deployment tool will try to calculate the optimal placement for each UABS and requires therefore a description of the area where the UAV-aided network needs to be deployed. This is done with the use of so-called shape files. These files contain three dimensional descriptions of the buildings present in the area and are key values in approaching results as realistic as possible. Furthermore, the tool also requires a configuration file containing technical specifications of the type of UABS that is being used. The tool will thereafter randomly distribute users over the area and assigns a certain bitrate to them.

In a second phase, the optimal position for each UABS is calculated. This is done by trying to locate a UABS above each active user. Two options are possible. If a fixed flying height is defined, a UABS is placed above each user at the given height, unless a building is obstructing its location. Then, no base station will be located above that user. Alternatively to the fixed flying height, a flying margin can be defined which represents the distance between the outdoor user and the drone. If the user is inside, this margin will be measured between the drone and the rooftop of that building. The latter is only allowed if the suggested height remains below the given maximum allowed height.

Thereafter, the decision algorithm calculates which users should be connected to which UABSs. These decisions are based on the specified optimization strategy. For this master dissertation, this will either be power consumption optimized or exposure optimized.

In the final state, unused UABSs are removed and the capacity of the facility is checked. If the

number of active drones would exceed this capacity, UABSs will be sorted based on the number of users they cover. Thereafter, drones with too few users are removed so that all the active drones could be stored in the facility. The flowchart of the main algorithm is given in figure 4.6.

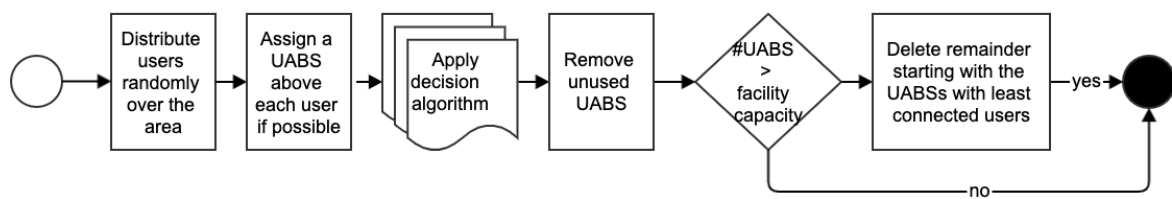
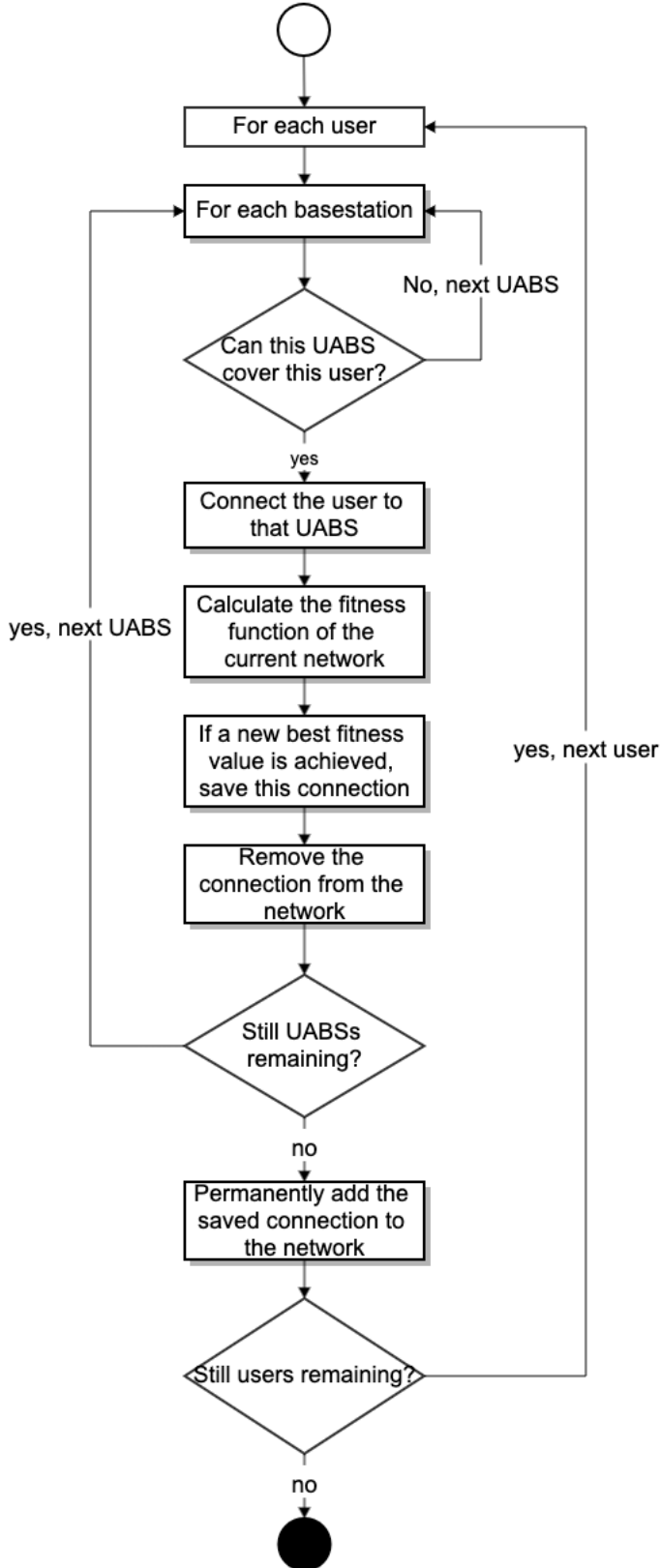


Figure 4.6: Flowchart of the main algorithm.

### Decision algorithm



Solving the network is done by the decision algorithm and starts by calculating the path loss between all users and between users and UABSSs. Thereafter, the tool iterates over each user and tries to connect that user to each UABS. This connection is not always possible. A UABS might be saturated with users and will not be able to cover yet another one or maybe the user is so far away that in order to cover that user, the UABS would have to exceed its maximum allowed input power. If however a connection is possible, the user will be connected to that UABS and the fitness function from section 4.3 is applied. This is repeated for each UABS. Only the connection which results in the best fitness value for the entire network will be used. Thereafter, the tool shifts to the next user. When the last user has been processed, the network is fully designed for an unlimited number of drones and the result is returned to the main algorithm for further processing. The flowchart of this algorithm is given in figure 4.7.

Figure 4.7: Flowchart of the decision algorithm.

#### 4.4.2 Implementation of the Radiation Pattern

Originally, the deployment tool did not consider attenuation. Therefore, the radiation from the antenna attached to the UAV was equal in each direction. Such a fictional antenna is called an equivalent isotropic radiator. Thus the tool has been extended in order to support several types of antennae by introducing new parameters like attenuation and direction. Doing so allows any type of antennae which is fully configurable in any given orientation. This configuration is done with the usage of an XML-file which will apply to all UABSs in the network. An equivalent isotropic radiator is still supported by returning a zero value when the attenuation is requested.

The orientation is done using two values called ‘downtilt’ and ‘north offset’. The first value defines the downtilt angle under which the antenna is pointing. A downtilt angle of zero degrees is perfectly horizontal and an antenna with a downtilt angle of 90° will be pointing straight to the ground. This parameter only supports positive values ranging from 0° to 360° (upper boundary not included). An antenna pointing to the sky would therefore require a value of 270°. The second value, the north offset, defines the azimuth orientation of the drone. The value given to this parameter indicates the offset between the north and the horizontal direction to which the antenna should be pointing at. The value once again ranges from 0° to 360° with the upper boundary not included. The angle is calculated in counterclockwise orientation. For instance, a north offset of 270° will let the UABS point to the east.

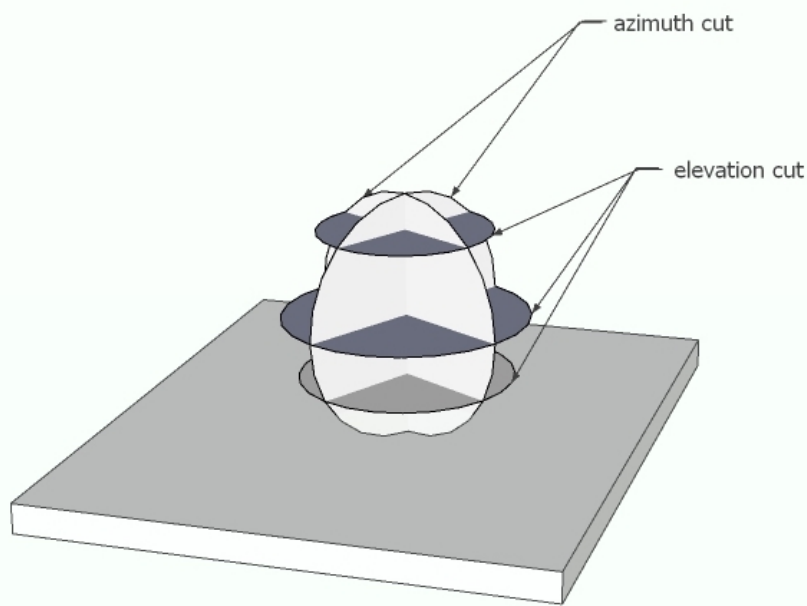


Figure 4.8: Schematic example of slices in a radiation pattern.

Thereafter, the normalized radiation pattern is supplied to the tool. The actual pattern is three dimensional. To simplify this, slices perpendicular to the az-axis are extracted. These are indicated in figure 4.8 with azimuth cuts. With an angle of  $90^\circ$  four slices are achieved, each consisting out of elevation cuts. The intersection of an elevation and azimuth plane corresponds with a certain attenuation which is fed to the tool. Figure 4.8 shows only 3 elevation planes. The radiation pattern used in the tool has an attenuation every  $10^\circ$ . In other words, a slice consists of 19 values ranging from  $0^\circ$  to  $180^\circ$  (boundaries included).

The number of required slices depends on the complexity of the radiation pattern. For symmetrical radiation patterns, like in figure 4.4 and 4.5, two azimuth cuts perpendicular to each other dividing the radiation pattern in 4 azimuth-slices are definitely sufficient. However, this might not be the case for radiation patterns with a more complex structure containing several side lobes. To tackle this issue, more azimuth-slices can be defined for increased precision. Each slice should however contain an equal amount of elevation slices. A concrete example of a configuration file can be found in appendix B.

When the attenuation of a user from a certain UABS needs to be known, the elevation and azimuth angles between the user and the antenna's direction should be calculated. Figure 4.9 represents a radiation pattern with the black dot indicating the user whose attenuation needs to be calculated. The small black lines represent azimuth and elevation planes. The tool knows the exact attenuation only at the intersection of those lines. The chance that a user is positioned at such an intersection is very small. Therefore, the attenuation for the requested point has to be estimated using bilinear interpolation. First, the attenuation is estimated at the intersection of the red and orange line using linear interpolation on the horizontal axis with the known values at the end of the red line. The same is done for the orange-green intersection using the known values at the end of the green line. Finally, linear interpolation is applied to the y-axis for the black dot on the orange line using the estimated values at the end of the orange line.

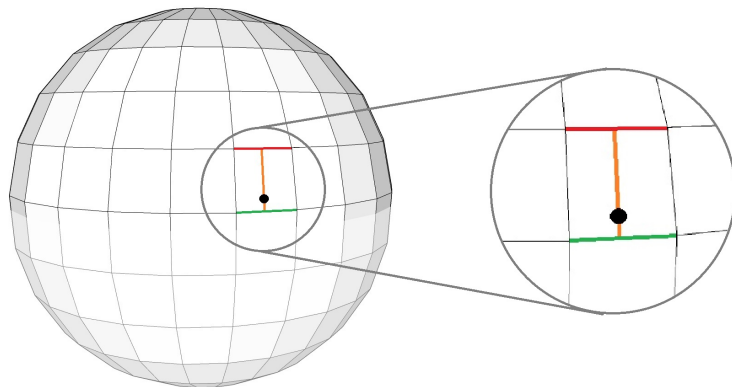


Figure 4.9: Schematic example of how bilinear interpolation works.

### 4.4.3 Performance Improvement

#### Calculating Path Loss

The path loss is required by several formulas. For instance, the formula that decides whether a UABS is feasible for a certain user makes use of this parameter but also the calculations for the downlink electromagnetic exposure require this value to be known. The formulas for the whole body  $SAR_{10g}$  require not only the path loss between the user and all UABSs but even the path loss between users themselves. These path loss calculations are based on the Walfish-Ikegami model that causes a high computational load. The calculation between two points is completely independent of any other calculation between any other points and is therefore a suitable candidate to multithread. The deployment tool creates two thread pools. The first pool creates a thread for each user where each thread calculates the path loss between the user assigned to him and all possible UABSs, causing a time complexity of  $n^2$ . Each user stores all path losses between himself and any other UABS. This results therefore in a total space complexity of  $n^2$ . When all users are finished, the thread pool is shut down and the second one is created for the same calculations but between users. The pool will, just like the previous, create threads for each user but there is an important difference. When a certain user calculates the path loss to another user, this path loss also applies for the other direction. The tool saves time by calculating the path loss only once and stores the path loss at both users. It is therefore sufficient that a given user only calculates path losses of users at his right side, since the other path losses will be calculated by the users on his left. This results in a time complexity of only  $n(\frac{n}{2})$ . When the last user finishes his thread, all users know the path loss of all other users causing a space complexity of  $n(n - 1)$ .

#### Limiting Antenna Searching

The user needs to be connected to the ‘best’ base station. To identify this best UABS, the user should be connected to each base station and the fitness value 4.18 of the network has to be evaluated. The connection that resulted in the best fitness function will be added to the solution. This process is repeated for each user but can further be improved. A user will likely be connected to either the UABS directly above him or to a UABS in the direct neighbourhood. Time complexity can thus be improved by not considering drones outside a certain radius. An ideal data structure for neighbourhood-search with geographical coordinates is a KD-tree [46, 47]. This data structure is described by Bentley in [48] and is based on a binary tree, optimal for objects consisting out of multiple keys. Each node in this tree is associated with a certain dimension and will split the hyperplane over exact one dimension. In this case, the x and y coordinate will be used in a 2D-tree ( $k=2$ ) like in figure 4.10.

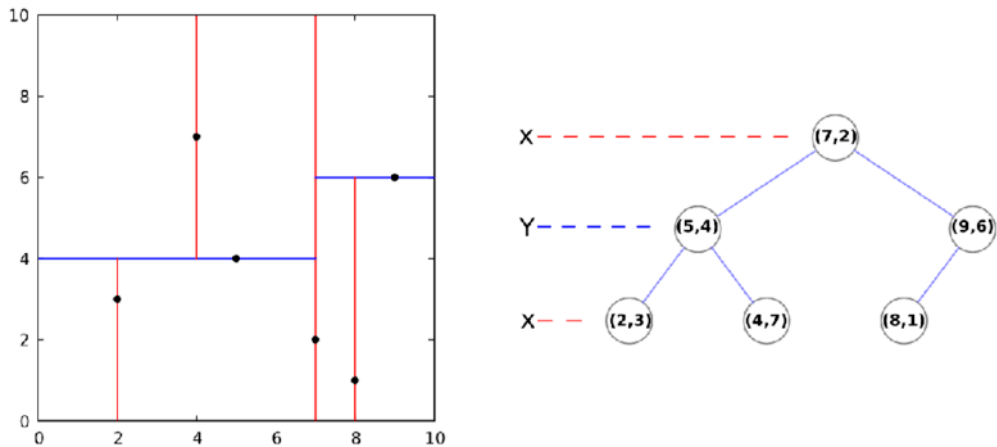


Figure 4.10: Example of a KD-tree in two dimensions.

Figure 4.11 shows that the majority of the connections are not longer than 100 metres in a power consumption optimized network. This percentage will even be higher in an exposure optimized network. In this case the choice was made to only consider UABSs within a radius of half a kilometre which is believed to have a sufficient safety margin. The rare connections that would have exceeded this radius would not contribute much to the average values.

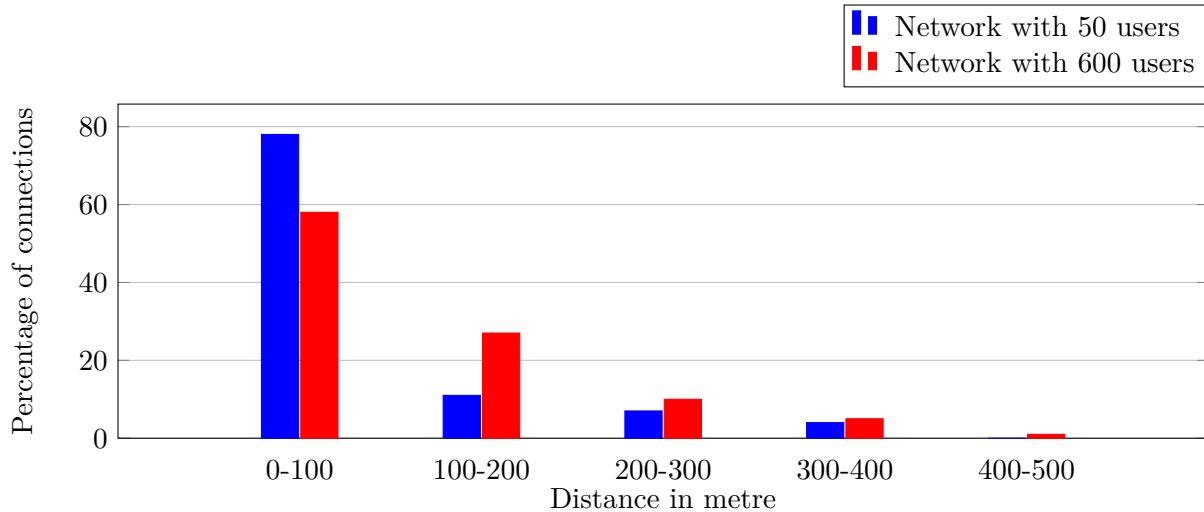


Figure 4.11: Distribution of how many connections belong to a certain interval of distance. Upper boundaries are not included.

# 5

## Results and Discussion

This chapter gives an overview of the achieved results from all considered scenarios and cases. The first section talks about a small network with only one user and one UAV. In the following section, this network is expanded for a larger population but still only one UAV is available. The network in the last section serves a large population with an unlimited number of UAVs.

### 5.1 Scenario 1: One User and One UAV

The network contains only one user in this scenario. This means that there is only one location possible for the UAV, being just above the user. This section will investigate minimal required transmission power and SAR values from different sources. Finally, also the power consumption of the entire network is measured. The “entire network” refers to all UABSSs. The entire network will for the first scenario be constructed out of a single UABS.

#### 5.1.1 The Influence of the Maximum Transmission Power

LTE makes use of power control meaning that no more power will be used than strictly necessary. The actual transmission power  $P_{tx}$  therefore ranges between zero and the maximum allowed

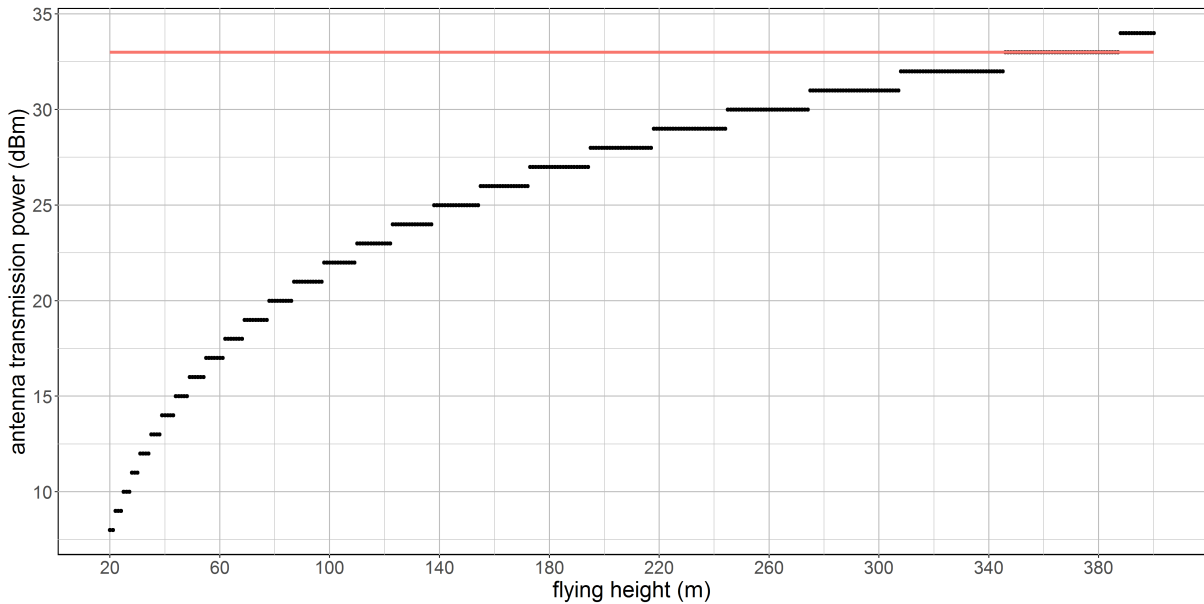


Figure 5.1: Minimal required transmission power by the antenna to reach the ground just below it. The red line shows the default maximum transmission power.

input power.  $P_{tx}$  is zero when the UABS doesn't cover anybody. For instance when the flying height is too high and therefore also the path loss that comes with it, the maximum allowed  $P_{tx}$  is not enough to cover the distance. In such case, the UABS is shut down since it cannot meet the requirements. Increasing the maximum transmission power will not influence the actual used  $P_{tx}$  or  $SAR_{10g}$  because the UABS will not use more than strictly required. It is therefore more useful to match the actual transmission power against a variable flying height.

Figure 5.1 shows a logarithmic relationship between  $P_{tx}$  and flying height. As already discussed in 3.1, the user is outdoor and just below the UABS. There is thus a free LOS between both radiators. It is clear from figure 5.1 that a discontinue step function is achieved. This is because multiple flying heights correspond to the same transmission power. When the flying height increases, so does the path loss. LTE tries to counteract this by increasing the power level. Each time the path loss becomes too high, the power level of the antenna increases with one dBm. Doing so, decreases path loss allowing the antenna to reach the user again.

After a jump in the step function, there is an overestimation meaning the input power increased more than necessary. So multiple flying heights correspond with the same  $P_{tx}$ . Further, dBm is also a logarithmic scale meaning that while 10 dBm equals 10 mW, 20 dBm equals 100 mW. This explains why the black lines become longer at higher flying altitudes. Each time the power level increases with one dBm, the overestimation becomes larger. If the tool would make use of a smaller step size, a more continuous logarithmic function would be achieved. This would however worsen the time complexity because it would take much more iterations before the

power level exceeds the path loss.

The red line in figure 5.1 indicates the default maximum transmission power used during simulations as defined in table 3.1. In a free LOS scenario with only one user, a UABS can fly up to 387 meters before losing connection.

This scenario is investigated with a microstrip patch antenna using power consumption optimization. However, the chosen optimization strategy doesn't really matter as already explained in 3.1. This is because the decision algorithm decides which user needs to be connected to which UABS. Since only one UABS is available, both optimization strategies will behave identical. Further, also the used antenna will not make any difference despite the fact that a microstrip patch antenna has attenuation while an equivalent isotropic radiator doesn't. The user is namely positioned in the perfect center of the main beam where there is no attenuation experienced in either cases. So the results are applicable for the four possible cases from figure 3.1.

### 5.1.2 Influence of the Flying Height

This section investigates how the flying height of a UABS influences  $SAR_{10g}$  and power consumption. The  $SAR_{10g}$ , which is actually induced electromagnetic radiation into our user, is represented in figure 5.2 and shows that for a low flying UAV, DL radiation is the main source of electromagnetic exposure. This changes around an altitude of 80 meters where the UL radiation from the UE exceeds the DL radiation in order to still be able to reach the high flying UABSSs.

SAR-values are caused by the transmitted power  $P_{tx}$  of the antenna. The  $P_{tx}$  in section 5.1.1 showed a discontinue behaviour that sometimes radiates more than strictly necessary. This has thus a direct influence on the DL SAR. Hence the same discontinue behaviour. The DL SAR can be simplified to a perfect constant line. This constant behaviour can once again be explained with power control. When the UABS flies lower, there is less path loss and the UABS will therefore reduce the  $P_{tx}$ . This results in formula 5.1 where the electromagnetic exposure is a constant fraction of power and distance.

$$\vec{E}(V/m) = \frac{\Delta U(V)}{\Delta x(m)} \quad (5.1)$$

Figure 5.2 doesn't show radiation from neighbours, because there are none present in this scenario. Finally, all these values are added up as explained in formula 4.1 resulting in the total SAR to which our user is exposed, represented by the black line in 5.2.

The power consumption of the entire network includes both the power required by the UAV itself and the antenna he is carrying. The power consumption of the entire network is here of

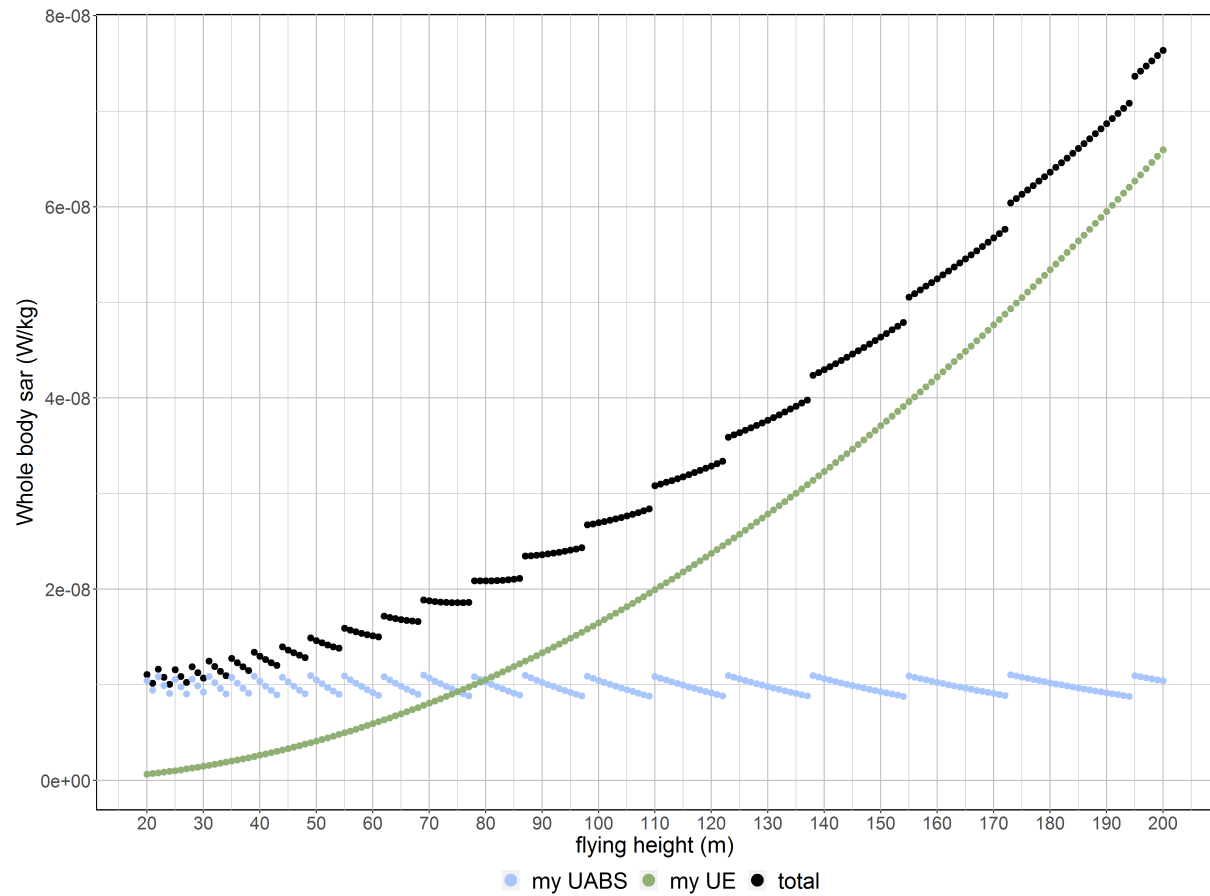


Figure 5.2: This figure shows how SAR values from different sources are influenced by different flying altitudes.

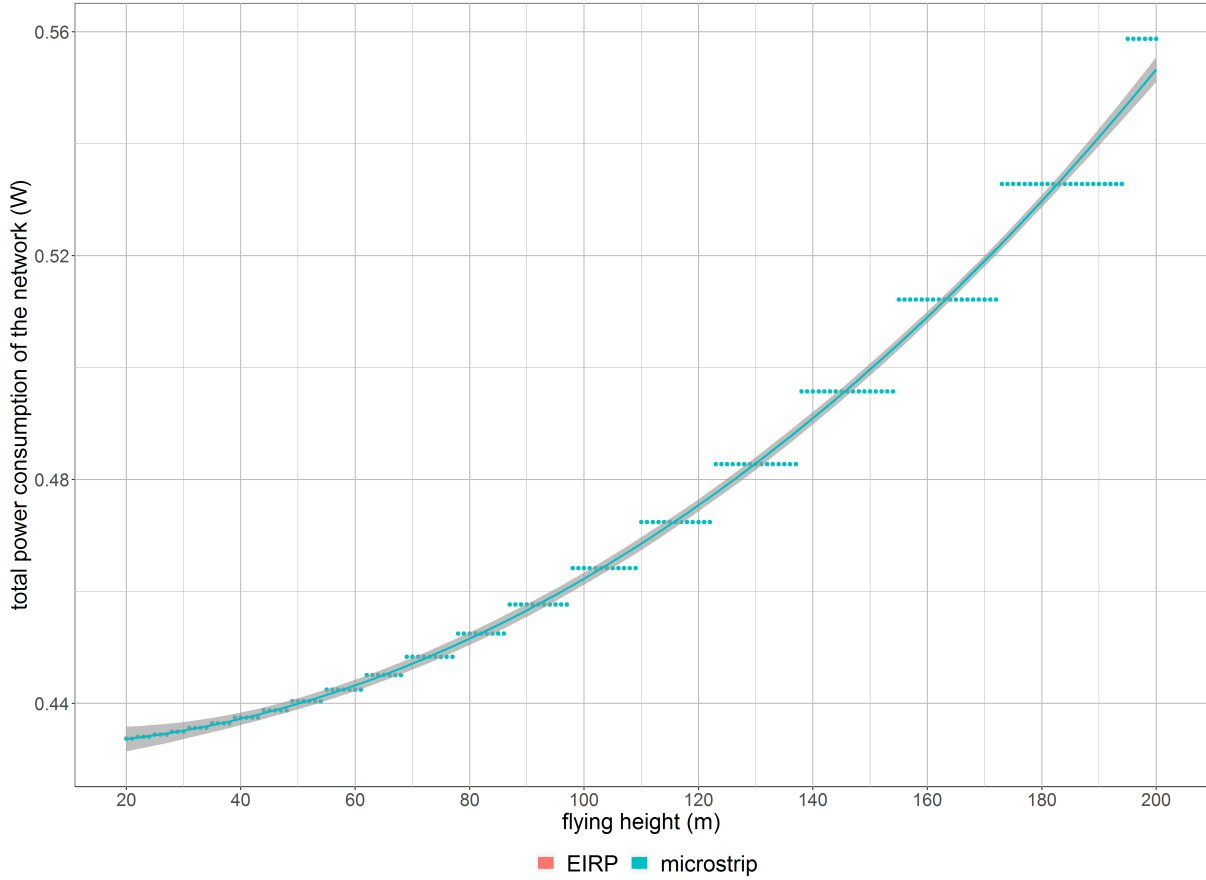


Figure 5.3: This figure shows the behaviour of the power consumption over the entire network at different flying heights. For this scenario, the power is used by only one UABS.

course for the only UABS available. Figure 5.3 shows an exponential relationship between both power consumption and flying height. This is mainly caused by the antenna attached to the UABS which will require more energy to maintain the same exposure on the ground but over a larger distance.

## 5.2 Scenario 2: Increased Traffic

This scenario has just like the previous scenario only one UAV available. However, more users will be present in the network. First, a variable flying altitude is investigated for a fixed number of 224 users. Secondly, the flying height is set to 100 meters with a variable number of users. When designing the network, there will be as much possible UAV locations as there are users in the network and the tool will consider all of them. Only when the program is finished, one UAV will remain.

### 5.2.1 Influence of the Flying Altitude

The first case investigates how the network, consisting out of one UABS, behaves when applied on an ordinary day during rush hours. Different fixed flying heights are considered while 224 active users are distributed uniformly over the city centre of Ghent.

A power consumption optimized network with an EIRP antenna (green) has the highest exposure. This is logical when comparing to an EIRP antenna in an exposure optimized network (red). However, when looking at figure 5.4 on the right, the power consumption in a power consumption optimized network is worse than in an exposure optimized network. To understand this, the behaviour of the deployment tool needs to be understood first. A power consumption optimized network will result in a few high powered UABSs because increasing the input power of an antenna costs less than activating a new UAV. Likewise, an exposure optimized network generates a lot of low powered UABSs because the lower the power of the antenna, the lower the exposure. This has the consequence that the cover radius is less and therefore requires more UAVs which costs more energy. When only a limited amount of UABSs are available, like only one in this scenario, the tool will only keep those UABSs that cover the most users. Therefore, the power consumption in a power consumption optimized network is much more higher.

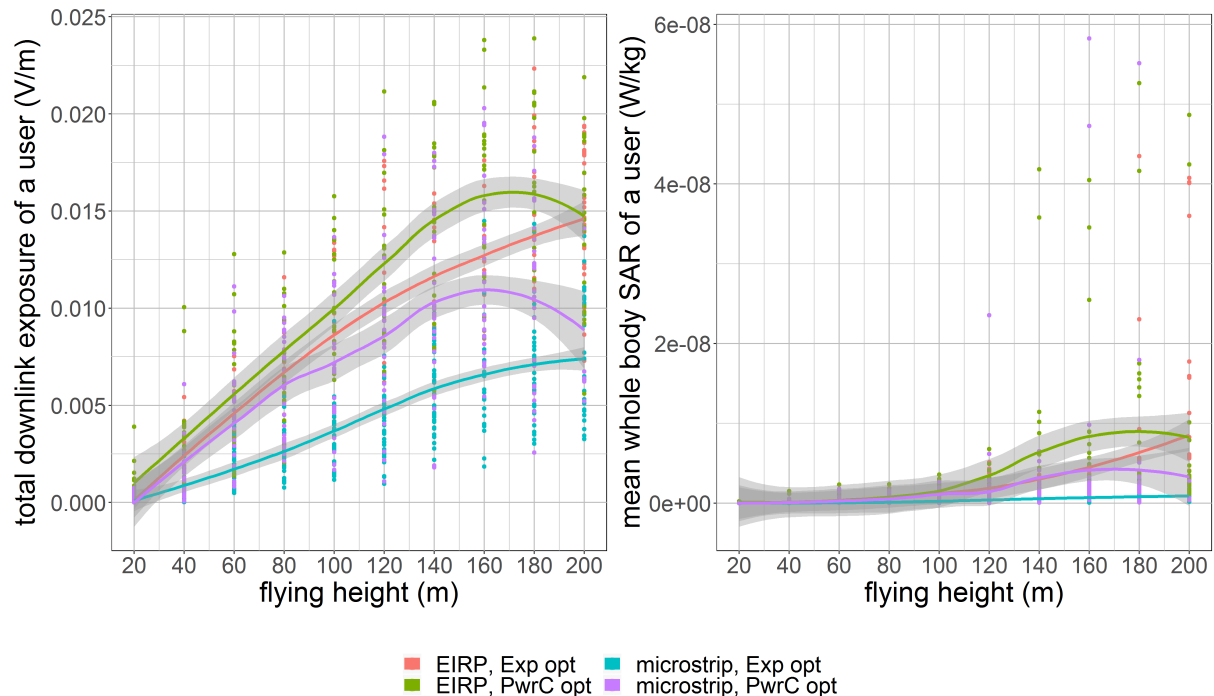


Figure 5.4: These two figures show how the flying height influences the downlink electromagnetic radiation of the average user (left) and power consumption of the entire network (right) for one UABS available in the network.

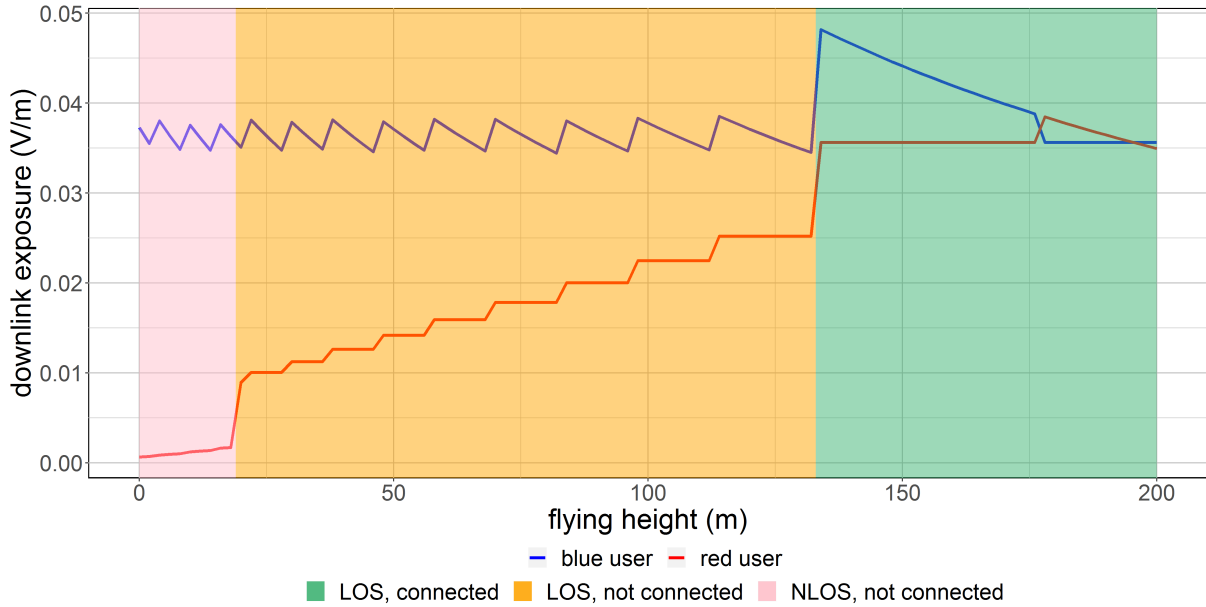


Figure 5.5: Scenario 2 with only 2 users. The coloured areas are only applicable for the red user. The blue user is connected during the entire time.

The DL exposure in figure 5.4 increases along with the flying height. One might expect a more constant behaviour like it was the case in figure 5.2 of scenario 1. To understand this, the scenario has been reduced to only two users and is illustrated in figure 5.6. The two users, who will be referred to by ‘red’ and ‘blue’, are 90 meters separated from each other with a building between them. Scenario 1 already explained that the charts can be simplified and the blue line from fig. 5.5 remains in fact constant between zero and 130 meters. The chart shows that the UABS is positioned above the blue user. The red user is in NLOS as long as the UABS remains below 20 meters.

Once the UABS increases its flying altitude, the red user comes into LOS but still remains uncovered. This is because the tool initially locates a possible UABS above each user and thereafter performs the fitness function. The applied fitness function must have decided that it is better to connect each user to the UABS above him. In a final stage, the tool checks whether the

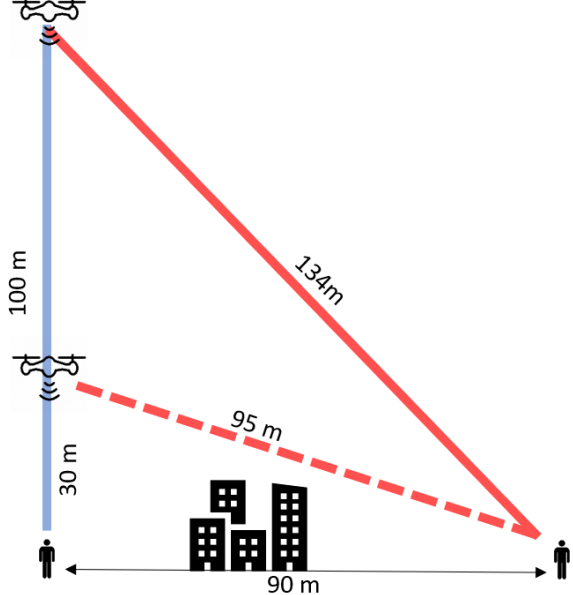


Figure 5.6: Schematic overview of scenario 2 with only 2 users.

number of online UAVs does not exceed the capacity of the facility which is here the case. The tool therefore deactivates one UABS causing the red user to be uncovered. One could argue that the red user should be connected to the online UAV who is only 90 meters away. This would however require the online UAV to increase its power consumption which would make the decisions made by the optimization strategy obsolete. When the UAV flies higher, the difference in distance between both users and the base station decreases. In other words, the Pythagorean theorem shows that when the flying height of the UABS increases, the distance to the blue user increases faster compared to the distance between that same UABS and the red user. This is also illustrated in figure 5.6. At 130 meters, the tool decides to connect both users to the same UABS. Therefore, it increases its power consumption whereby the red user would have the minimal required electromagnetic exposure. This has of course a negative influence on the blue user who is much more closer and experiences now a much higher exposure level in fig 5.5. Around 180 meters, the red and blue line switch because the UAV changes position. As explained before, the tool assigns two possible UAVs, one above each user. The tool must have decided that connecting both users to the other UAVs improves the fitness function of the entire network even though that difference might be very little.

Finally, this brings us back to the weighted average exposure from figure 5.4 where 223 users will behave like the red user and only one user behaves like the blue one. The red line therefore dominates the average exposure in figure 5.4.

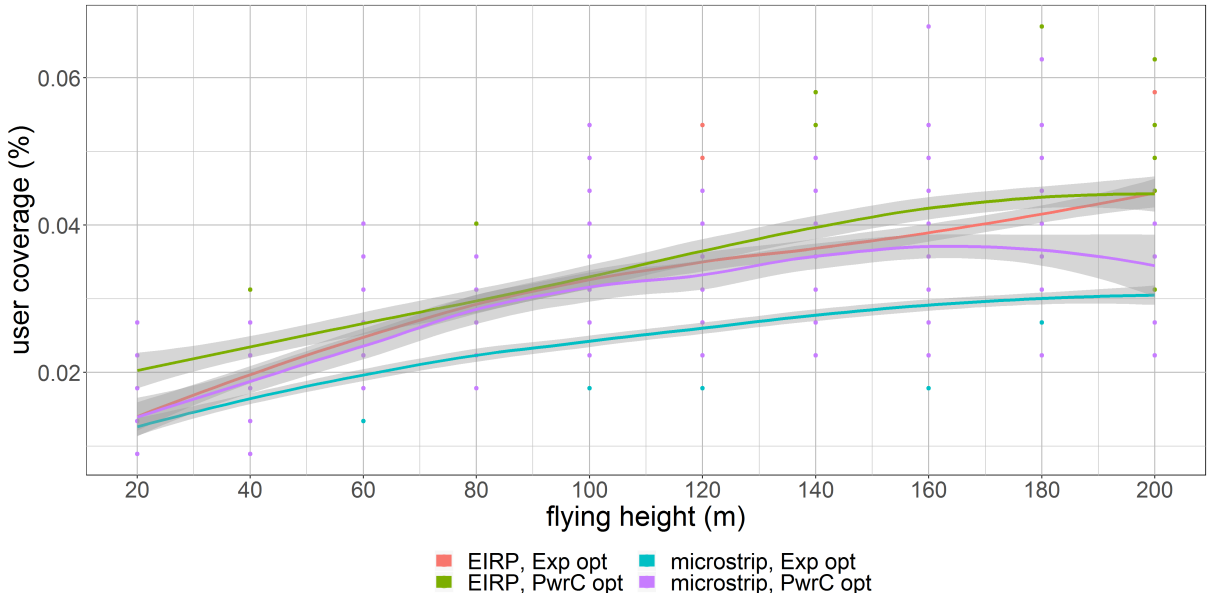


Figure 5.7: This graph shows the percentage of covered users for only one UABS at different flying heights.

Figure 5.7 shows that the flying height has a positive influence on the user coverage. When a UABS flies higher, there is less path loss between the user and the UAV caused by buildings

but also the path loss to neighbouring users decreases as explained in figure 5.5 and 5.6. Also the increasing DL exposure from figure 5.4, from earlier, indicated that the user coverage should grow. Figure 5.4 further also shows how the SAR from the UABS starts decreasing again at high altitude. This is not caused by the obstructing buildings but by the distance in general which becomes too high. When this decrease happens depends on the configuration. A power consumption optimized network tends to decrease earlier than an exposure optimized network.

When replacing the fictional EIRP antenna by a microstrip patch antenna, the percentage of covered users drops for both optimization strategies. This is because users who have a higher horizontal distance between themselves and the UABS experience a higher attenuation. When a microstrip patch antenna is positioned higher, the range of the antenna increases since the angle between the user and the UABS's main lob decreases. The user will therefore experience less attenuation.

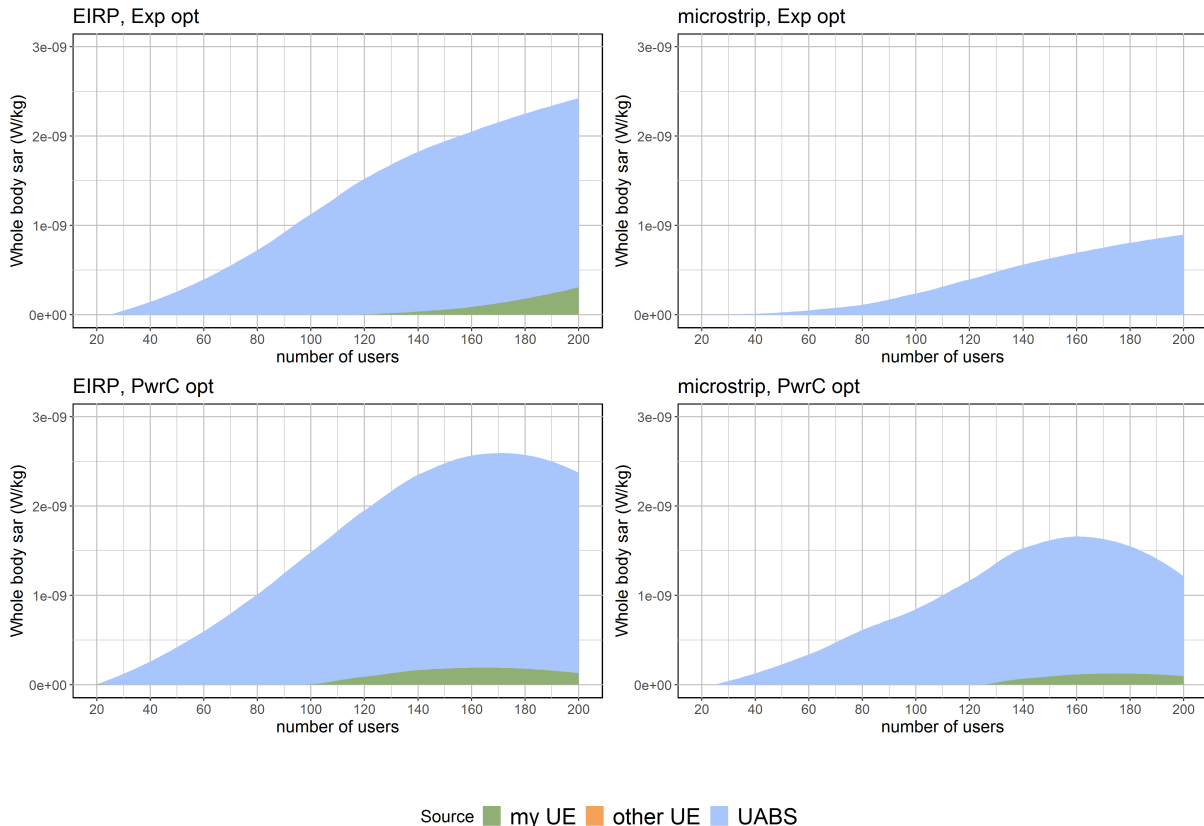


Figure 5.8: Each figure corresponds with a certain configuration and shows how the SAR from different sources are influenced by an increasing flying height.

Eventually, figure 5.8 shows the total whole body  $SAR_{10g}$  deducted from all electromagnetic sources. This combines the exposure of the only UABS available in the network, the UL exposure

from the user's own device and the exposure of the devices from all other users. Thereafter, the weighted average whole body SAR for each individual source in the network is calculated with the 50th and 95th percentile being the most important values. This is because not only the mean value is important but also users who experience higher levels of whole body  $SAR_{10g}$ .

When investigating the three different sources of which the total SAR-values are based on, we see that the radiation from the UABS is the main factor followed by the near-field radiation from the user's own device. The far-field radiation from other UE barely has influence. It looks like it is zero but it is just very low compared to the other two values and in fact increases when the flying height becomes larger.

The weighted average  $SAR_{10g}^{ul}$  from the own device is zero in an exposure optimized network with a microstrip patch antenna which is even lower than the  $SAR_{10g}^{neighbours}$ . This is because the coverage in this scenario is so low that the weighted average only consists of uncovered users and the transmission power of an uncovered user is zero.

### 5.2.2 Influence of the Number of Users

The number of covered users increases linearly compared to the number of users present in the network as shown in figure 5.9 on the right. It illustrates how an equivalent isotropic radiator is able to reach more users compared to a microstrip patch antenna. Also, power consumption optimized networks are able to reach more users compared to exposure optimized networks. This is because power consumption optimized networks will result in few high powered base stations while an exposure optimized network results in a lot of low powered base stations. This behaviour will further be explained in section 5.3

The linear regression lines from figure 5.9 can be predicted with the equations in 5.2.

$$\text{number of users} = \begin{cases} y = 0,0233x + 2,3553 & \text{if EIRP and pc} \\ y = 0,0197x + 2,6144 & \text{if EIRP and exp} \\ y = 0,0131x + 2,4371 & \text{if micro and pc} \\ y = 0,0119x + 2,4652 & \text{if micro and exp} \end{cases} \quad (5.2)$$

Figure 5.9 on the left shows the percentage of covered users that follow out of 5.9 on the right by taking the equations from 5.2 and dividing them by  $x$ . This results in a decreasing logarithmic behaviour because the regression lines from 5.9 have a slope of less than 0.5. This means that the percentage of covered users for a sparsely populated network is more compared to the percentage of users in high dense populations.

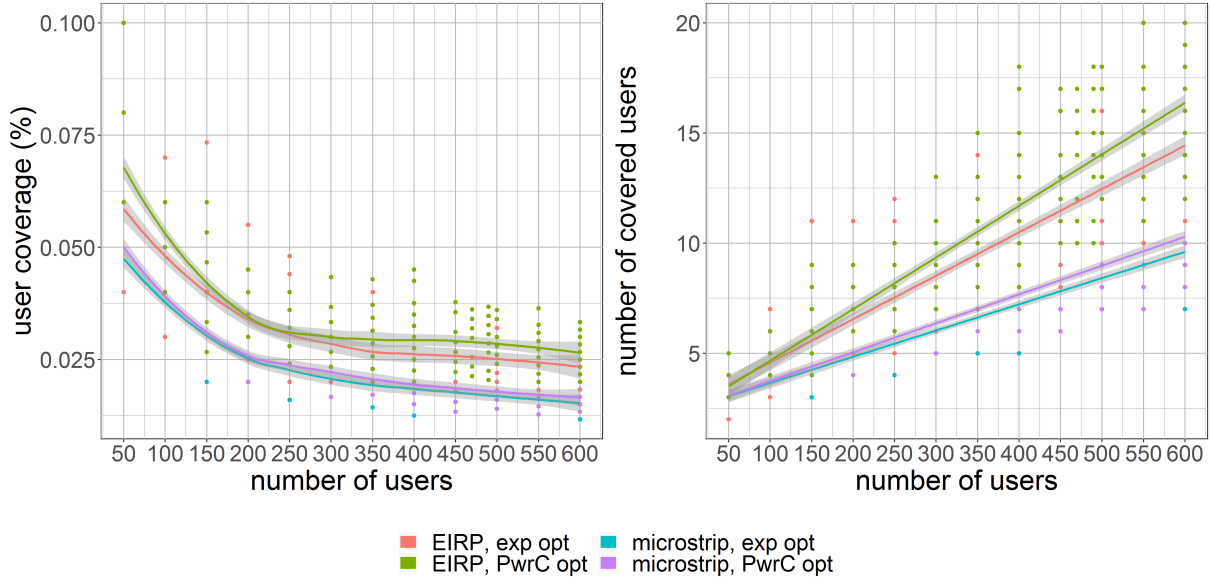


Figure 5.9: The influence of increasing traffic on the user coverage.

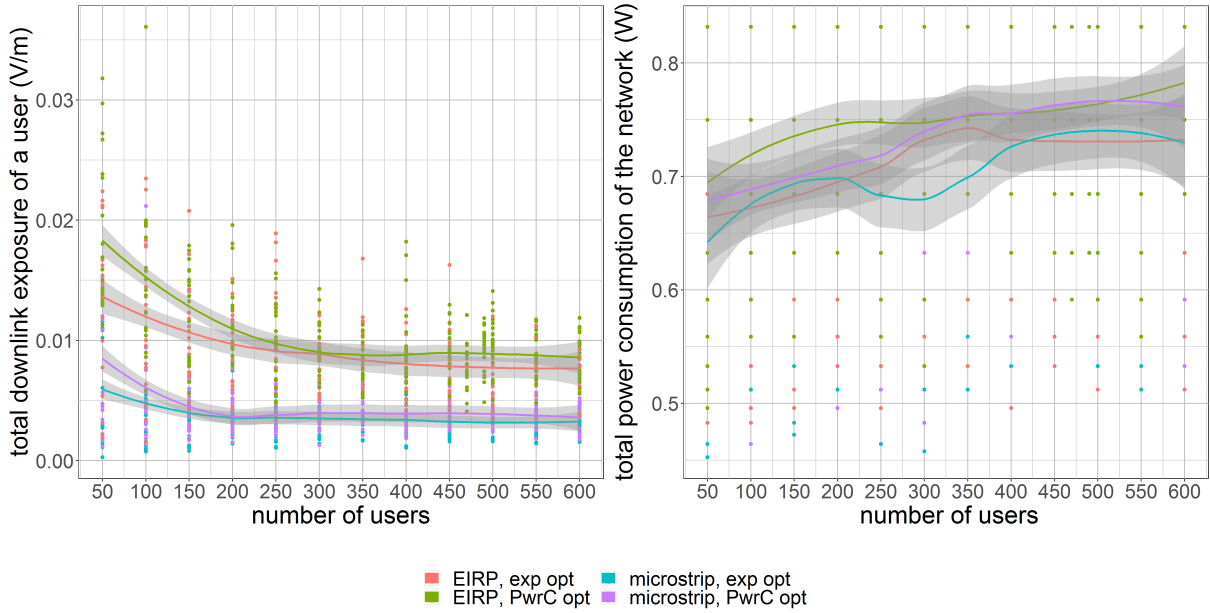


Figure 5.10: These two figures show how various sizes of population influence the downlink electromagnetic radiation of the average user (left) and power consumption of the entire network (rights) for one UABS available in the network.

The downlink exposure is shown in figure 5.10 on the left and is directly influenced by the percentage of covered users. The average electromagnetic exposure decreases when more users become uncovered. Since an equivalent isotropic radiator in a power consumption optimized

network (green) will have the highest coverage, also the DL electromagnetic radiation from UABSs will be higher compared to other configurations. Despite the fact that the percentage of covered users decreases, the effective number of covered users increases. The power consumption of the only active UABS slightly increases in order to serve those covered users.

Figure 5.11 investigates the assets of each source contributing to the total SAR. All four configurations show that base stations are the main source of electromagnetic radiation. Figure 5.9 already showed that for sparsely populated networks, a higher percentage of users is covered so the weighted average of the UL SAR will also be higher. When the population becomes more dense, more users become uncovered which decreases the weighted average of the UL SAR. The chart also proves once again that the far-field radiation from UE can be neglected. The SAR from neighbouring devices is not zero as it looks in figure 5.11 but is just really low compared to the much higher SAR-values from other sources.

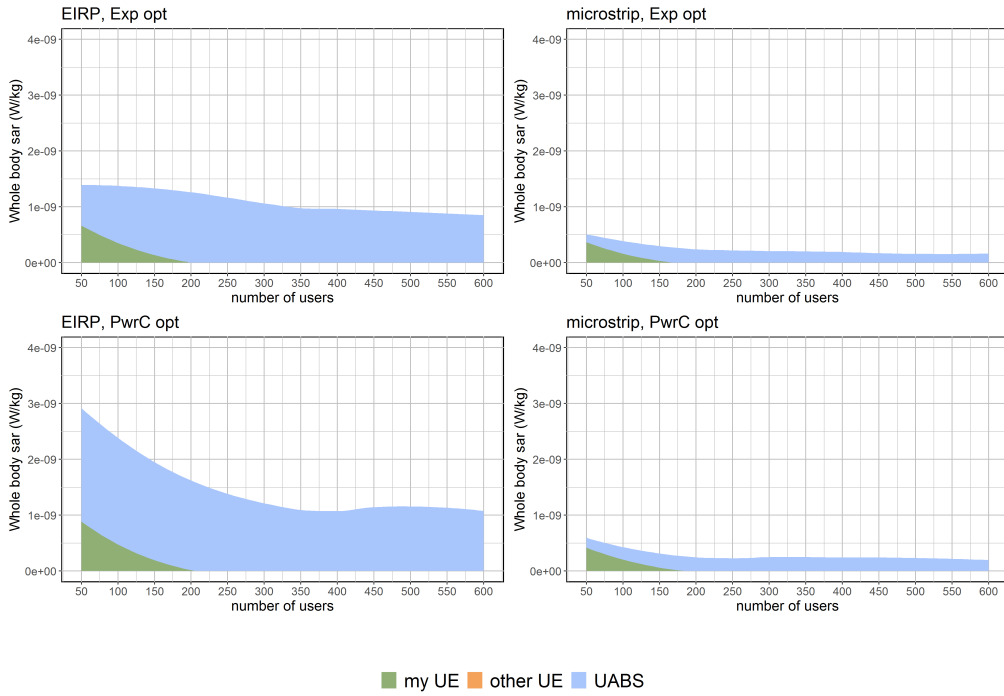


Figure 5.11: This figure shows how different sources are influenced by an increasing number of users.

While the population grows, more and more users become uncovered causing the average SAR to drop. However, this does not conclude that by increasing the population, the SAR of a user who is directly beneath a UABS would be less. To investigate this, a user is positioned in the middle of the city centre of Ghent and a UAV is positioned above him. Initially, only 49 people are active around him. The SAR of our central user is monitored while the population around him is growing. Figure 5.13 shows with the black lines which users are connected. The left map

is for only 50 users and shows that only one user is connected besides our central user. The map on the right considers 600 users and shows much more connected users.

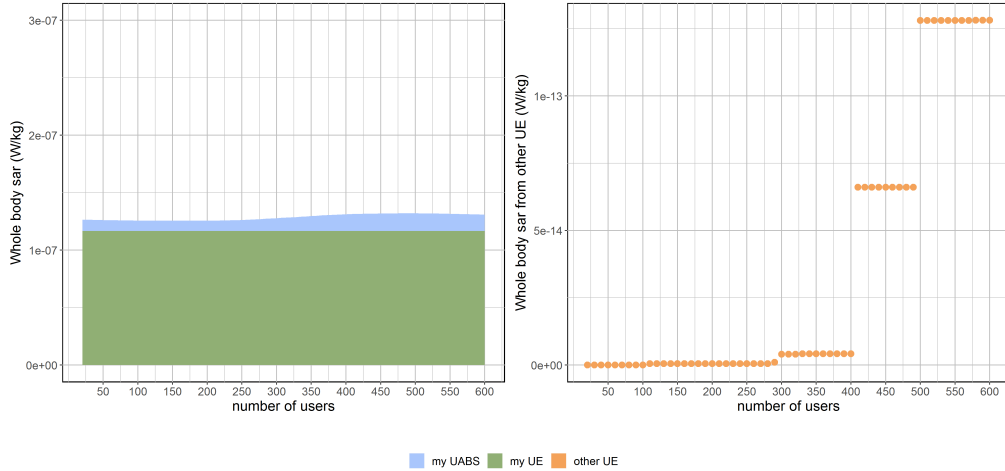


Figure 5.12: SAR-values for the user who is directly beneath the only UABS available.

Scenario 1 already showed that the SAR from the user's own device is only influenced by the flying height. The flying height for this experiment is fixed and the UL SAR from his device should therefore be also a constant. A hypothesis that is confirmed by figure 5.12. The SAR from the UABS experiences a slight increase. When the population grows, more users become available and some will spawn near the central user. The UABS will likely decide to cover these users as well as visible in figure 5.13. These users might have a slightly worse path loss because of obstructing buildings or somewhat bigger distance. The UABS reacts to this by increasing his power consumption causing an increase in the DL SAR for the central user.

The far-field radiation from UE is very low as mentioned before and is therefore not visible in figure 5.13 on the left. It is therefore illustrated in a separate chart on the right. It shows that the SAR from other UE indeed increases. This is normal behaviour considering that around the central user more and more people become available of which some will be connected to the UABS and therefore also emitting radiation.

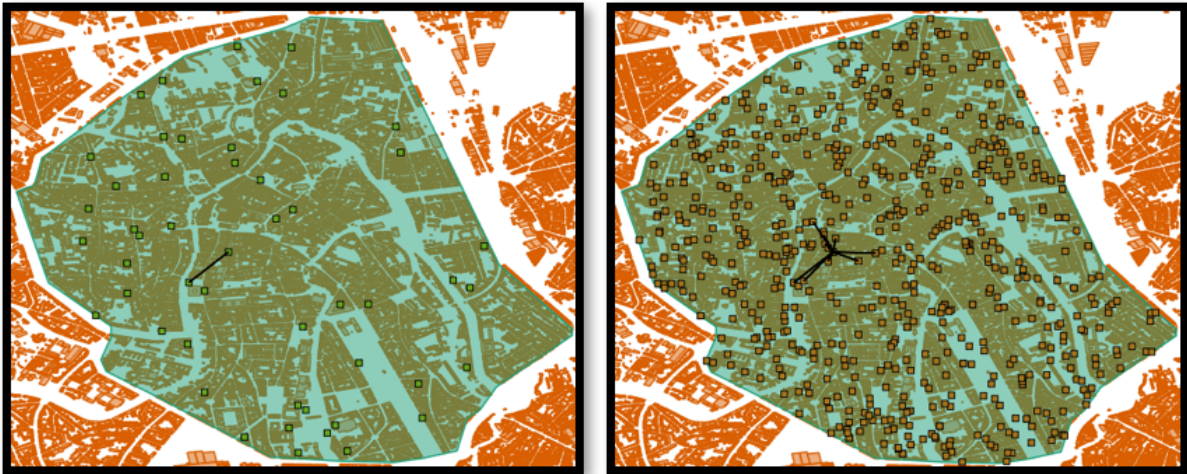


Figure 5.13: Overview of which users are connected to the UABS. The map on the left is for 50 active users while the map on the right has 600 active users.

### 5.3 Scenario 3: Unlimited UAVs

This scenario has just like the previous scenario much more users in the network and investigates the same cases which include the variable flying height and the variable number of users. The only difference is that the restriction of only one UABS is dropped.

#### 5.3.1 Influence of the Flying Altitude

The first case of this scenario examines how the network behaves for various flying heights and a fixed number of 224 users. Scenario 2 already explained that when only one UAV is available, a power consumption optimized network won't result in a low powered network. In this scenario, there is no limitation on the number of UAVs and the network remains thus unaltered after the decision algorithm is done. Figure 5.14 clearly proves that the different optimization strategies work as intended. Power consumption optimized networks have indeed a lower power consumption but therefore result in higher electromagnetic radiation. On the other hand, an exposure optimized network will reduce the electromagnetic exposure by using more UAVs and thence also increase the network's power consumption. This conclusion was already made in [11] and is supported by these results.

Figure 5.14 shows that the number of required UAVs decreases when the flying altitude becomes higher; a behaviour which was also determined in [19]. The exposure in an exposure optimized network increases logarithmically while in a power consumption optimized network the exposure has a concave relationship with the flying height, and has its lowest point at around 70 metres.

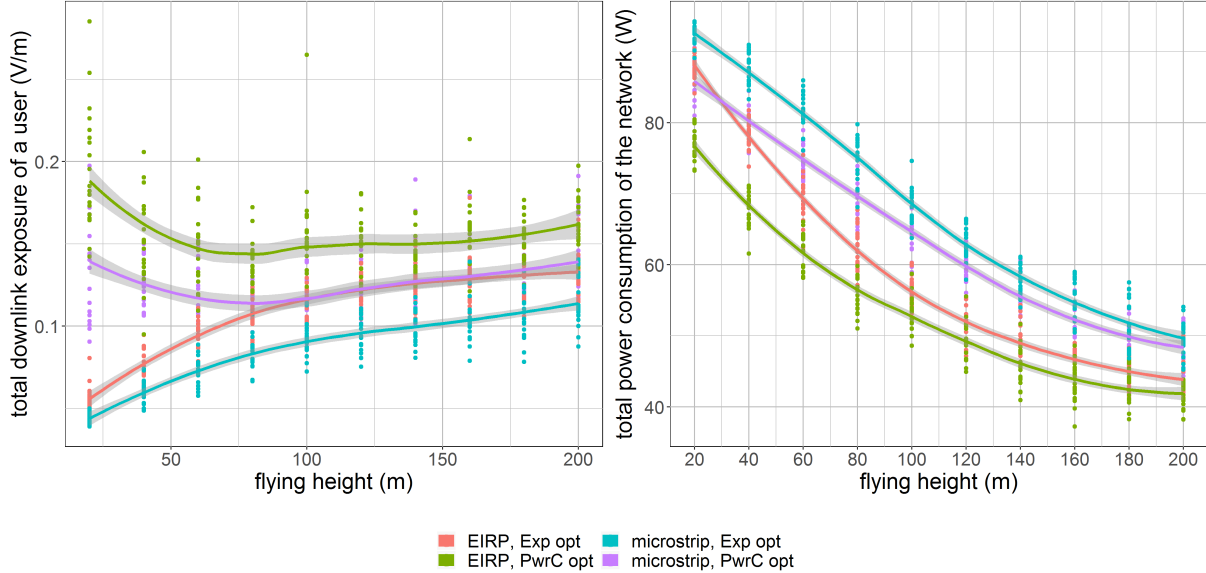


Figure 5.14: These two figures show how the flying height influences the downlink electromagnetic radiation of the average user (left) and power consumption of the entire network (right) for an unlimited number of drones.

This can be explained when looking at figure 5.15. At a flying height of 20 meters, the exposure optimized network has on average 220 to 224 UABSs. That is (almost) one UABS for each user so it's logical that the electromagnetic exposure is very low. The number of UAVs in a power consumption optimized network is much less in order to save energy but figure 5.15 shows on the left the same percentage of coverage for this flying altitude. So these UAVs will try to cover users much further away and some of these connections will even be more worsened by obstructing buildings. Because of this, users who are close and in LOS will experience much higher electromagnetic radiation. This path loss reduces when the UABSs start to fly higher than the average building and therefore exposure decreases. Not only the power consumption optimized networks profit from higher flying altitudes, also the exposure optimized networks do. For only a little bit more electromagnetic exposure, much less UAVs are required.

Both 5.14 and 5.15 show that the network profits from increasing the flying altitude. Not only less UAVs are needed but also the power consumption is lower. Both can be explained by the lower path loss when UABSs fly higher.

Scenario 1 already proved that with low flying UAVs, the main source of electromagnetic radiation are UABSs. This changed around 80 meters where UL electromagnetic radiation of the UE exceeds DL radiation in order to still be able to reach the high flying UABSs. When looking at the different individual sources in 5.16, we notice the same behaviour where the UL SAR indeed increases. However, a more logarithmic increase is shown despite the fact that figure 5.2

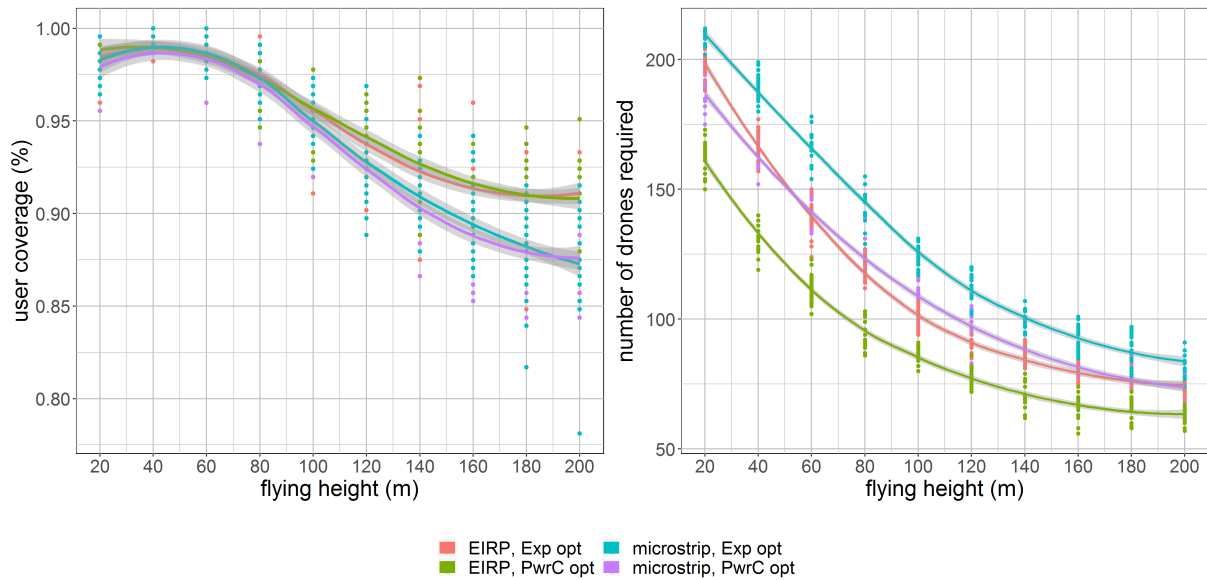


Figure 5.15: This graph shows how much UAVs are required at different flying heights while trying to achieve a 100% coverage.

Showed that the UL SAR increases exponentially. This was however deducted with only one user present in the network as opposed to this scenario where 224 users are present. The covered users will still behave like in scenario 1 but much more users are uncovered (fig. 5.15) which decreases the average SAR. In conclusion, the average UL SAR will not increase as fast as the UL SAR of an individual that is covered.

We can see from 5.16 that once out of the buildings level (around 70 to 80 meters), the SAR from the serving UABS remains more or less constant; a behaviour that was already determined in ‘scenario 1’ and ‘scenario 2: experiment 5.12’.

When looking at the exposure from ‘other UABSs’, we see an increase in electromagnetic radiation at higher flying altitudes. Also here the lower path loss from less obstructing buildings will be the reason. The figures from 5.16 further also clearly show that this increase in electromagnetic radiation will be less for a microstrip patch antenna. The reason behind this is that energy will be more focused towards the ground and there is less sideways radiation because of attenuation.

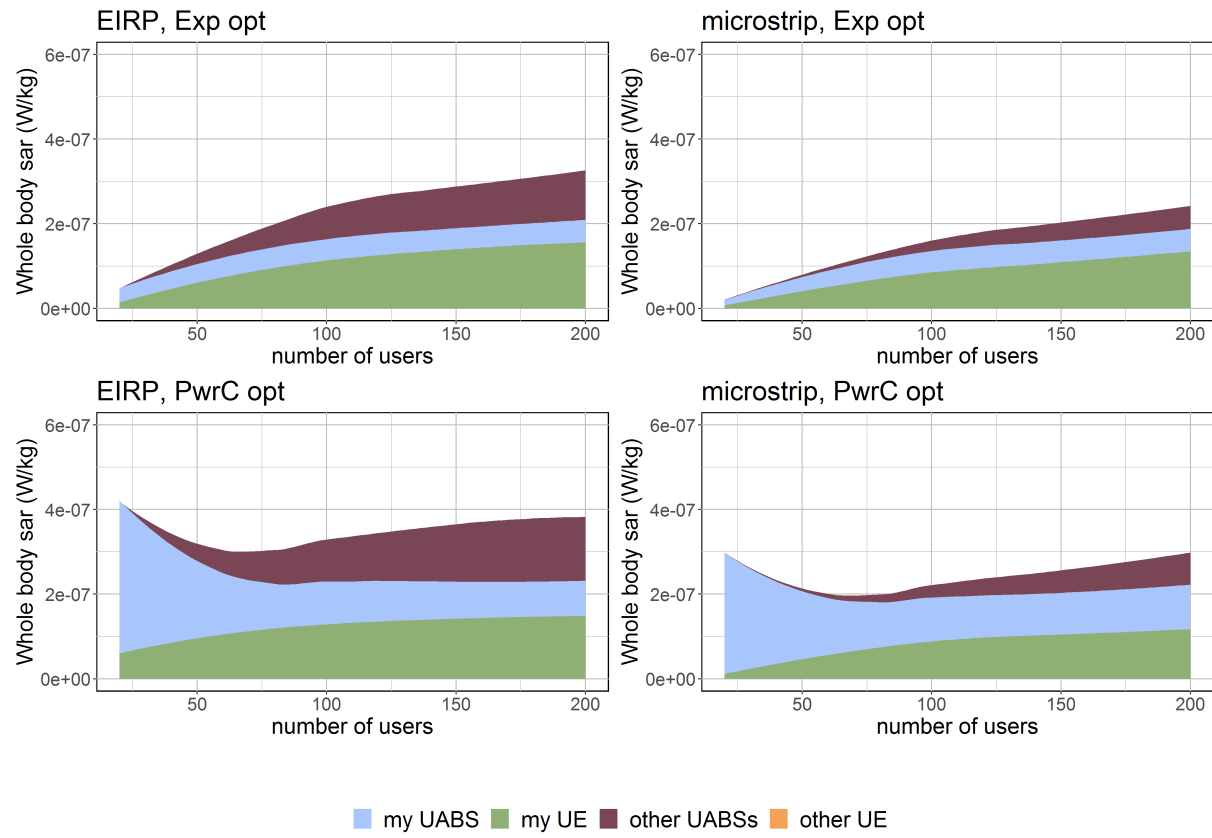


Figure 5.16: Each figure corresponds with a certain configuration and shows how the SAR from different sources are influenced by an increasing flying height.

### 5.3.2 Influence of the Number of Users

The last case of scenario 3 investigates a variable number of users for a fixed flying height of 100 meters. There is no restriction on the number of available UAVs just like in the previous case meaning that there are at most as much UAVs as users in the network. The correct behaviour of the decision algorithm became already clear in the previous subsection 5.3.1 but is also confirmed by this case. Figure 5.17 shows on the left how the tool tries to reach a 100% coverage. The tool reaches this goal better for larger populations. The difference remains however very little. The tool also requires more UAVs for these large populations. An expected behaviour when looking at scenario 5.2.2 where, with only one UABS available, the percentage of covered users decreases for these larger populations. The difference in optimization strategy is very little for small amounts of people but increases very quickly. Further, 5.18 shows an increase in exposure for larger populations because more UAVs come with these larger populations and more exposure comes with more UAVs as visible in 5.17.

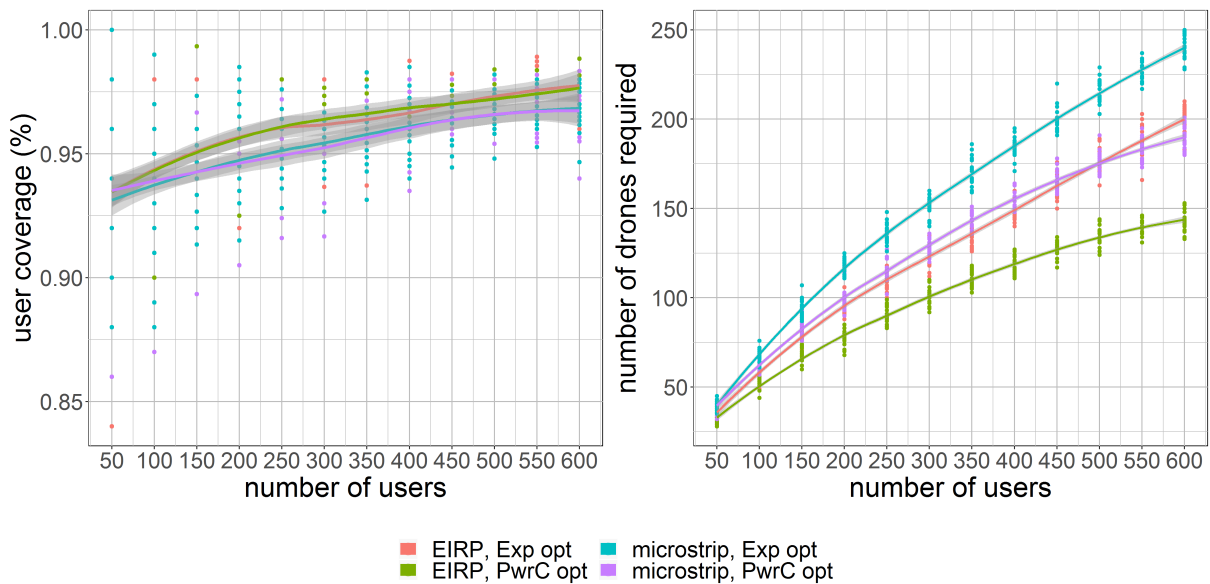


Figure 5.17: This graph shows how much UAVs are required for different flying heights while trying to achieve a 100% coverage.

In a scenario with 600 active users, a clear difference is noticeable between the four configurations. For instance, an EIRP power consumption optimized network requires the least amount of UAVs (fig. 5.17 on the right). This is logical when looking at figure 5.18 where UAVs in such a configuration cause the highest amount of electromagnetic radiation. This behaviour was already discussed in subsection 5.2.2.

On the complete opposite, we have a microstrip patch antenna in an exposure optimized network. This strategy prioritizes the minimization of electromagnetic exposure. In addition, a microstrip

antenna has a much more limited range. Therefore, much more UAVs are required in order to reach 100% coverage (fig. 5.17) and therefore require much more energy to power all the UAVs (fig. 5.17 on the right).

This means that scenario 3 learns that a power consumption optimized network indeed results in less UAVs and less power consumption of the entire network. At the same time, scenario 2 showed that the active UABSs have a higher individual power consumption. We can therefore state that a power consumption optimized network will reduce its total power consumption by using a few high powered UAVs.

Likewise for an exposure optimized network, we can conclude that the network has indeed a lower electromagnetic exposure but the power consumption of the entire network is much higher. In scenario 2 became already clear that the active UABSs have a low power consumption in order to guarantee a low electromagnetic exposure towards the users. We can conclude that an exposure optimized network will reduce the exposure of an individual by using a lot of low powered UAVs.

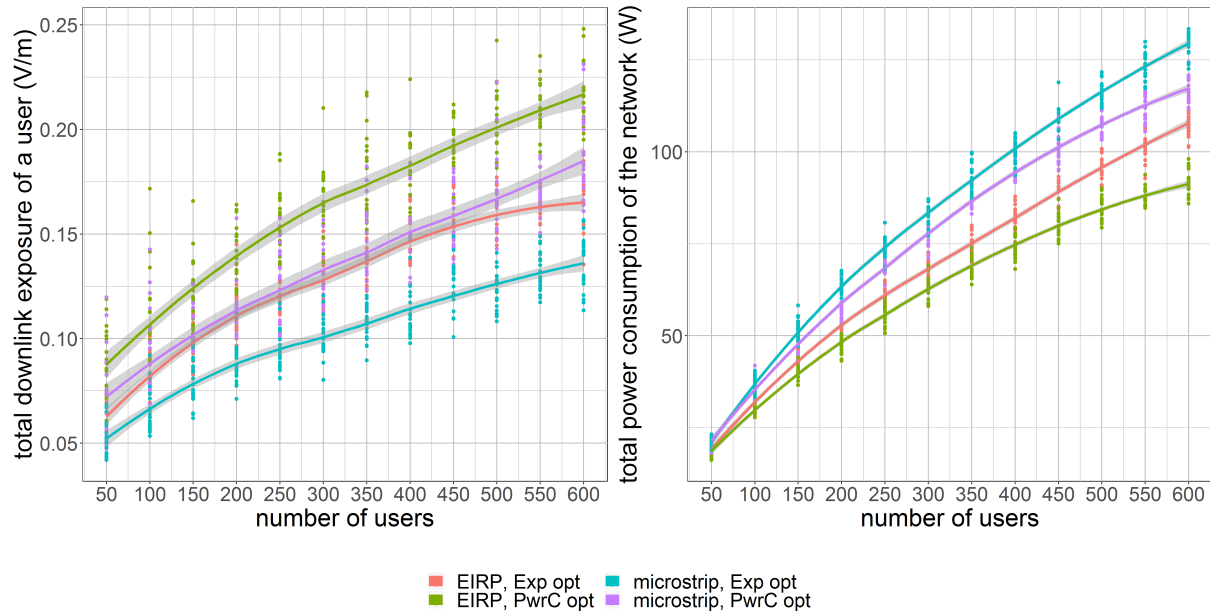


Figure 5.18: The influence of the population density on the downlink electromagnetic radiation (left) and power consumption (right).

When looking at the different contributions to the total SAR in figure 5.19, we see that the weighted average SAR from the user's own device and from the serving UABS remains constant. The flying altitude is always the same so also the required energy to cover that distance will remain the same. The only SAR values that increase are the DL SAR from other UABSs and the UL SAR from other UE. When more users come online, also more UAVs will be radiating. Moreover, there is very little path loss because the flying height is higher than the average

building.

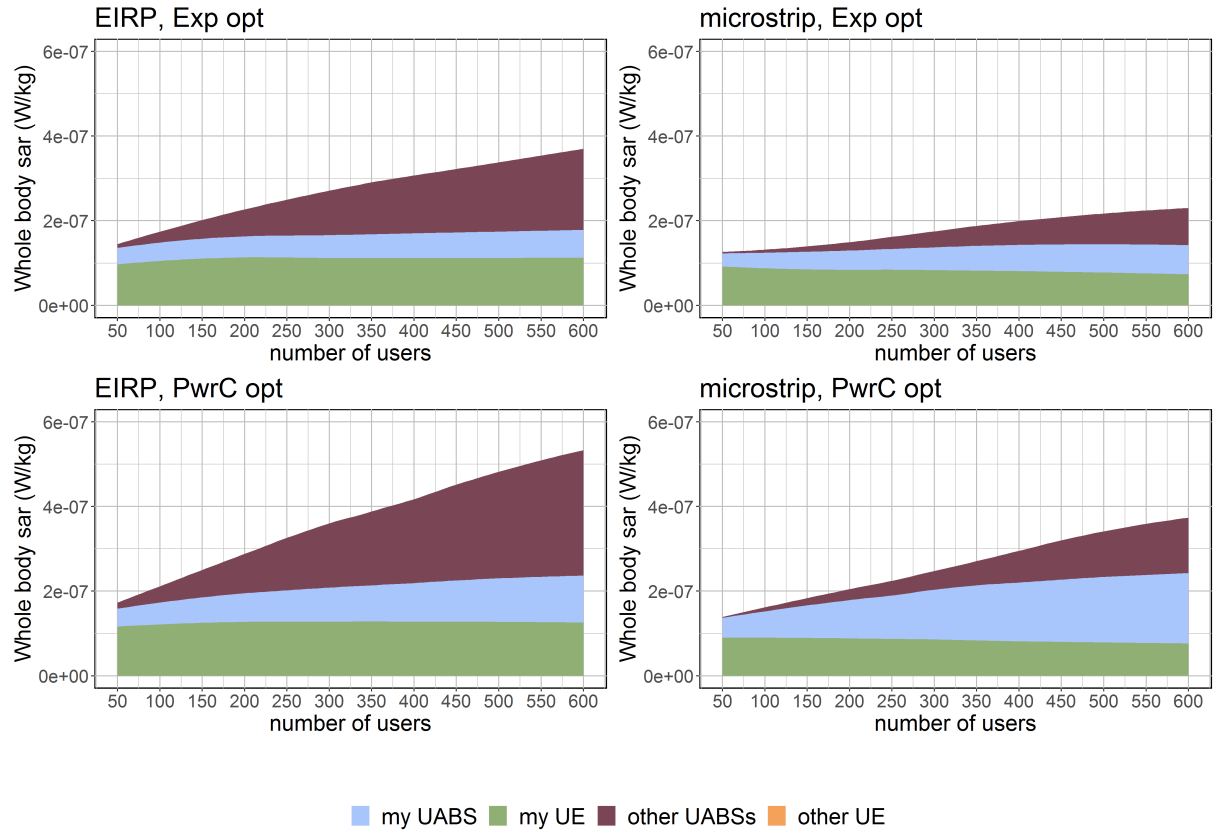


Figure 5.19: Each figure corresponds with a certain configuration and shows how the SAR from different sources are influenced by an increasing population density. An unlimited number of UABSSs is available.

# 6

## Conclusions

### 6.1 Conclusion

All conclusions are based on the default configuration as described in table 3.1 unless mentioned otherwise. Literature showed that a network can be optimized towards either the power consumption of the entire network or the electromagnetic exposure of the average user using a fitness function. This is because the power required to activate a new base station is much higher than for expanding its range [11]. The fitness function was originally applied for fixed transmission towers but can also be used for UABSs as this research shows. However, the fitness function should be used with care considering that UABSs can be placed anywhere as opposed to the transmission towers from [11] who have a predetermined position. In an exposure optimized network, this causes a lot of users to get a UABS all by themselves because this is the best approach to minimize exposure. A power consumption optimized network on the other hand will try to limit the number of drones in order to save energy. So as a rule of thumb: an exposure optimized network will result in a lot of low powered devices (increasing the overall power consumption) while a power consumption optimized network results in a few high powered devices (increasing the exposure of the average user). If the goal is to remain in the air for a longer period of time, an exposure optimized network is recommended because the power consumption of an individual UABS is lower. On the other hand, a power consumption optimized network is cheaper because less drones are involved. Moreover, the results show that the electromagnetic

radiation in a power consumption optimized network (with high powered UABSSs) is far below the thresholds enforced by the Flemish government.

The user's main sources of exposure are the user's own device and the UABS who is serving him, followed by all other UABSSs in the network. When the population increases, also the exposure from other people's UE increases. However, the electromagnetic exposure from these devices can be ignored compared to the much higher electromagnetic exposure from the other sources. A bigger population also causes an increase in number of drones. So when the population grows, the exposure of the user increases mainly because of a growing exposure from other UABSSs that are not serving the user. An exposure optimized network will limit the total exposure mainly by trying to reduce the exposure from other UABSSs.

A directional microstrip patch antenna is introduced because it gives several advantages compared to omnidirectional antennae. Directional antennae are able to focus their energy there where it is needed, namely towards the ground. Microstrip patch antennae further benefit from their thin and lightweight design. The performance of this directional microstrip patch antenna has been compared to a fictional equivalent isotropic radiator. This equivalent isotropic radiator has higher exposure and coverage for less power compared to realistic antennae like microstrip patch antennae because of the absence of attenuation and can hypothetically be compared to an antenna with a very big aperture angle. This type of antenna can achieve the same coverage with less resources like power and number of drones. A microstrip patch antenna with a more limited aperture angle of 90° requires more resources but causes less sideways radiation. So the exposure from other UABSSs will be way less.

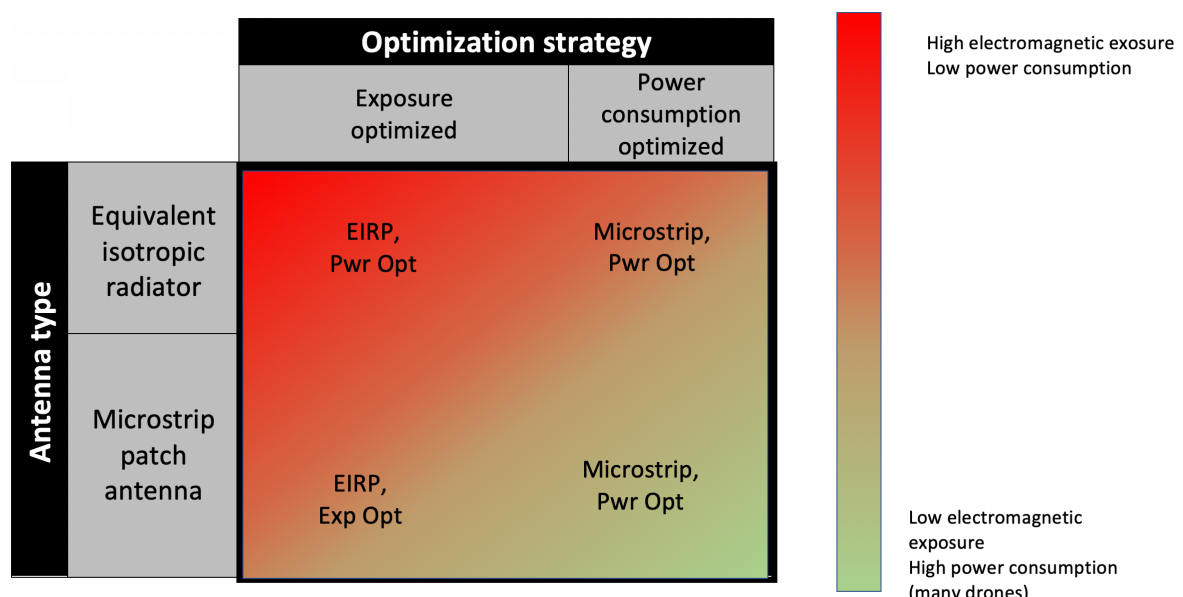


Figure 6.1: Matrix with the four possible configurations, colour-coded based on the results.

Remarkable is that an EIRP exposure optimized network behaves very similar to a microstrip power consumption optimized network as shown in figure 6.1. This results in the best of both worlds. The microstrip patch antenna will generate less electromagnetic radiation by design and the power consumption optimization reduces the number of required drones and power. A microstrip patch antenna with an aperture angle of  $90^\circ$  is considered as a good solution but if budget is more limited, an antenna with a larger aperture angle would further reduce cost without interfering with the Flemish legislation regarding electromagnetic exposure.

The electromagnetic radiation of an exposure optimized network increases with higher flying altitudes. This increase is mainly caused by the user's own device and UABSs who are serving other users. Around 80 metres, the exposure from the user's device surpasses the exposure from the serving UABS. On the other hand, a power consumption optimized network shows a more concave relationship with the lowest exposure measured around 70 to 80 metres. Further, the results also show that the number of required drones decreases when the flying height becomes larger; a conclusion that was also made in [19]. When also considering the results from [20] where a flying altitude of 80 metres is suggested for an optimal access and backhaul connectivity, a flying height of 80 metres is also here proposed for the city centre of Ghent.

In short, a power consumption optimized network is proposed with a fixed flying height of 80 metres. A microstrip patch antenna with a sufficiently large aperture angle is a good starting point. However, different antenna array configurations still have to be investigated.

## 6.2 Future work

The chosen microstrip patch antenna is solely based on literature and performing an excessive research to various types of radiation patterns is outside the scope of this master dissertation. It is expected that the radiation can further be improved by using microstrip patch antennae in more complex array-configurations.

Also, the tool makes use of an exact algorithm. Despite the fact that several tactics have been introduced to improve performance, large populations still cause long runtimes. It might be useful to reduce the quality of the result in order to improve performance. Mozafari et al. discusses in [21] several other approaches besides exact algorithms like heuristic methods, machine learning and so on.

## Bibliography

- [1] “kaart van mobiel netwerkbereik.” <https://www.test-aankoop.be/hightech/gsms-en-smartphones/module/kaart-van-mobiel-netwerkbereik>. Accessed: 03-03-2020.
- [2] “Vijf jaar geleden sloeg het noodlot toe op pukkelpop,” *Het nieuwsblad*, 2016.
- [3] “Base overschreed stralingsnormen na aanslagen,” *De standaard*, 2019.
- [4] L. Hardell and C. Sage, “Biological effects from electromagnetic field exposure and public exposure standards,” *Biomedicine and Pharmacotherapy*, vol. 62, no. 2, pp. 104 – 109, 2008.
- [5] “What are electromagnetic fields.” <https://www.who.int/peh-emf/about/WhatisEMF/en/index1.html>. Accessed: 15-10-2019.
- [6] “Elektromagnetische velden en gezondheid: Uw wegwijzer in het elektromagnetische landschap,” *Federale overheidsdienst: volksgezondheid, veiligheid van de voedselketen en leefmilieu*, vol. 5, 2014.
- [7] “Normen zendantennes.” <https://omgeving.vlaanderen.be/normen-zendantennes>. Accessed: 19-03-2020.
- [8] A. Ahlbom, U. Bergqvist, J. Bernhardt, J. Cesarini, M. Grandolfo, M. Hietanen, A. McKinlay, M. Repacholi, D. H. Sliney, J. A. Stolwijk, *et al.*, “Guidelines for limiting exposure to time-varying electric, magnetic, and electromagnetic fields (up to 300 ghz),” *Health physics*, vol. 74, no. 4, pp. 494–521, 1998.
- [9] E. Commission, “Council recommendation of 12 july 1999 on the limitation of exposure of the general public to electromagnetic fields (0 hz to 300 ghz),” *Official Journal of the European Communities*, vol. 59, 1999.
- [10] D. Plets, W. Joseph, K. Vanhecke, and L. Martens, “Exposure optimization in indoor wireless networks by heuristic network planning,” *Progress In Electromagnetics Research*, vol. 139, pp. 445–478, 01 2013.

- [11] M. Deruyck, E. Tanghe, D. Plets, L. Martens, and W. Joseph, “Optimizing lte wireless access networks towards power consumption and electromagnetic exposure of human beings,” *Computer Networks*, vol. 94, 12 2015.
- [12] D. Plets, W. Joseph, S. Aerts, K. Vanhecke, G. Vermeeren, and L. Martens, “Prediction and comparison of downlink electric-field and uplink localised sar values for realistic indoor wireless planning,” *Radiation Protection Dosimetry*, vol. 162, no. 4, pp. 487–498, 2014.
- [13] D. Plets, W. Joseph, K. Vanhecke, and L. Martens, “Downlink electric-field and uplink sar prediction algorithm in indoor wireless network planner,” in *The 8th European Conference on Antennas and Propagation (EuCAP 2014)*, pp. 2457–2461, IEEE, 2014.
- [14] S. Kuehn, S. Pfeifer, B. Kochali, and N. Kuster, “Modelling of total exposure in hypothetical 5g mobile networks for varied topologies and user scenarios,” *Final Report of Project CRR-816, Available on line at: <https://tinyurl.com/r6z2gqn>*, 2019.
- [15] D. Plets, W. Joseph, K. Vanhecke, G. Vermeeren, J. Wiart, S. Aerts, N. Varsier, and L. Martens, “Joint minimization of uplink and downlink whole-body exposure dose in indoor wireless networks,” *BioMed research international*, vol. 2015, 2015.
- [16] Y. Zeng, Q. Wu, and R. Zhang, “Accessing from the sky: A tutorial on uav communications for 5g and beyond,” *Proceedings of the IEEE*, vol. 107, no. 12, pp. 2327–2375, 2019.
- [17] Y. Kawamoto, H. Nishiyama, N. Kato, F. Ono, and R. Miura, “Toward future unmanned aerial vehicle networks: Architecture, resource allocation and field experiments,” *IEEE Wireless Communications*, vol. 26, no. 1, pp. 94–99, 2018.
- [18] R. Gangula, O. Esrafilian, D. Gesbert, C. Roux, F. Kaltenberger, and R. Knopp, “Flying rebots: First results on an autonomous uav-based lte relay using open airinterface,” in *2018 IEEE 19th International Workshop on Signal Processing Advances in Wireless Communications (SPAWC)*, pp. 1–5, IEEE, 2018.
- [19] M. Deruyck, J. Wyckmans, W. Joseph, and L. Martens, “Designing uav-aided emergency networks for large-scale disaster scenarios,” *EURASIP Journal on Wireless Communications and Networking*, vol. 2018, 12 2018.
- [20] G. Castellanos, M. Deruyck, L. Martens, and W. Joseph, “Performance evaluation of direct-link backhaul for uav-aided emergency networks,” *Sensors*, vol. 19, no. 15, p. 3342, 2019.
- [21] M. Mozaffari, W. Saad, M. Bennis, Y.-H. Nam, and M. Debbah, “A tutorial on uavs for wireless networks: Applications, challenges, and open problems,” *IEEE communications surveys & tutorials*, vol. 21, no. 3, pp. 2334–2360, 2019.

- [22] M. Mozaffari, A. T. Z. Kasgari, W. Saad, M. Bennis, and M. Debbah, "Beyond 5g with uavs: Foundations of a 3d wireless cellular network," *IEEE Transactions on Wireless Communications*, vol. 18, no. 1, pp. 357–372, 2018.
- [23] M. Deruyck, A. Marri, S. Mignardi, L. Martens, W. Joseph, and R. Verdone, "Performance evaluation of the dynamic trajectory design for an unmanned aerial base station in a single frequency network," in *2017 IEEE 28th Annual International Symposium on Personal, Indoor, and Mobile Radio Communications (PIMRC)*, pp. 1–7, IEEE, 2017.
- [24] H. Huang and A. V. Savkin, "A method for optimized deployment of unmanned aerial vehicles for maximum coverage and minimum interference in cellular networks," *IEEE Transactions on Industrial Informatics*, vol. 15, no. 5, pp. 2638–2647, 2018.
- [25] A. V. Savkin and H. Huang, "Deployment of unmanned aerial vehicle base stations for optimal quality of coverage," *IEEE Wireless Communications Letters*, vol. 8, no. 1, pp. 321–324, 2018.
- [26] Q. Wu, L. Liu, and R. Zhang, "Fundamental trade-offs in communication and trajectory design for uav-enabled wireless network," *IEEE Wireless Communications*, vol. 26, no. 1, pp. 36–44, 2019.
- [27] C. T. Cicek, H. Gultekin, B. Tavli, and H. Yanikomeroglu, "Uav base station location optimization for next generation wireless networks: Overview and future research directions," in *2019 1st International Conference on Unmanned Vehicle Systems-Oman (UVS)*, pp. 1–6, IEEE, 2019.
- [28] A. Rizwan, D. Biswas, and V. Ramachandra, "Impact of uav structure on antenna radiation patterns at different frequencies," in *2017 IEEE International Conference on Antenna Innovations & Modern Technologies for Ground, Aircraft and Satellite Applications (iAIM)*, pp. 1–5, IEEE, 2017.
- [29] Y. Zheng, J. Zhou, W. Wang, and M. Chen, "A low-profile broadband circularly polarized antenna array for uav ground-to-air communication," in *2018 IEEE Asia-Pacific Conference on Antennas and Propagation (APCAP)*, pp. 219–220, IEEE, 2018.
- [30] C. Sairam, T. Khumanthem, S. Ahirwar, and S. Singh, "Broadband blade antenna for airborne applications," in *2011 Annual IEEE India Conference*, pp. 1–4, IEEE, 2011.
- [31] B. A. Arand, R. Shamsaei, and B. Yektakhah, "Design and fabrication of a broadband blade monopole antenna operating in 30 mhz–600 mhz frequency band," in *2013 21st Iranian Conference on Electrical Engineering (ICEE)*, pp. 1–3, IEEE, 2013.
- [32] M. Nosrati, A. Jafargholi, R. Pazoki, and N. Tavassolian, "Broadband slotted blade dipole antenna for airborne uav applications," *IEEE Transactions on Antennas and Propagation*, vol. 66, no. 8, pp. 3857–3864, 2018.

- [33] M. Nosrati, A. Jafargholi, and N. Tavassolian, “A broadband blade dipole antenna for uav applications,” in *2016 IEEE International Symposium on Antennas and Propagation (APSURSI)*, pp. 1777–1778, IEEE, 2016.
- [34] L. Akhoondzadeh-Asl, J. Hill, J.-J. Laurin, and M. Riel, “Novel low profile wideband monopole antenna for avionics applications,” *IEEE transactions on antennas and propagation*, vol. 61, no. 11, pp. 5766–5770, 2013.
- [35] M. Park and J. Jung, “An analysis of communication performance according to antenna directionality in uav operation environment,” in *2010 2nd IEEE International Conference on Network Infrastructure and Digital Content*, pp. 854–857, IEEE, 2010.
- [36] I. Singh and V. Tripathi, “Micro strip patch antenna and its applications: a survey,” *Int. J. Comp. Tech. Appl.*, vol. 2, no. 5, pp. 1595–1599, 2011.
- [37] K. Kashwan, V. Rajeshkumar, T. Gunasekaran, and K. S. Kumar, “Design and characterization of pin fed microstrip patch antennae,” in *2011 Eighth International Conference on Fuzzy Systems and Knowledge Discovery (FSKD)*, vol. 4, pp. 2258–2262, IEEE, 2011.
- [38] S. S. Siddiq, G. Karthikeya, T. Tanjavur, and N. Agnihotri, “Microstrip dual band millimeter-wave antenna array for uav applications,” in *2016 21st International Conference on Microwave, Radar and Wireless Communications (MIKON)*, pp. 1–4, IEEE, 2016.
- [39] X. Sun, R. Blázquez-García, A. García-Tejero, J. M. Fernández-González, M. Burgos-García, and M. Sierra-Castañer, “Circular array antenna tor uav-uav communications,” in *2017 11th European Conference on Antennas and Propagation (EUCAP)*, pp. 2025–2028, IEEE, 2017.
- [40] A. Sudarsan and A. Prabhu, “Design and development of microstrip patch antenna,” *International Journal of Antennas (JANT) Vol*, vol. 3, 2017.
- [41] “Specific absorption rate (sar) for cellular telephones.” <https://www.fcc.gov/general/specific-absorption-rate-sar-cellular-telephones>. Accessed: 27-03-2020.
- [42] A. Christ, M.-C. Gosselin, M. Christopoulou, S. Kühn, and N. Kuster, “Age-dependent tissue-specific exposure of cell phone users,” *Physics in Medicine & Biology*, vol. 55, no. 7, p. 1767, 2010.
- [43] P. Joshi, D. Colombi, B. Thors, L.-E. Larsson, and C. Törnevik, “Output power levels of 4g user equipment and implications on realistic rf emf exposure assessments,” *IEEE Access*, vol. 5, pp. 4545–4550, 2017.
- [44] “Bundesamt für strahlenschutz.” [http://www.bfs.de/SiteGlobals/Forms/Suche/BfS/EN/SARsuche\\_Formular.html](http://www.bfs.de/SiteGlobals/Forms/Suche/BfS/EN/SARsuche_Formular.html). Accessed: 14-10-2019.

- [45] A. Gati, E. Conil, M.-F. Wong, and J. Wiart, “Duality between uplink local and down-link whole-body exposures in operating networks,” *IEEE transactions on electromagnetic compatibility*, vol. 52, no. 4, pp. 829–836, 2010.
- [46] N. Bhatia *et al.*, “Survey of nearest neighbor techniques,” *arXiv preprint arXiv:1007.0085*, 2010.
- [47] S. Dhanabal and S. Chandramathi, “A review of various k-nearest neighbor query processing techniques,” *International Journal of Computer Applications*, vol. 31, no. 7, pp. 14–22, 2011.
- [48] J. L. Bentley, “Multidimensional binary search trees used for associative searching,” *Communications of the ACM*, vol. 18, no. 9, pp. 509–517, 1975.

# Appendices

# A

## Radiation Patterns: Datasheet

Table A.1 gives an overview of the attenuation in the E and H plane. The first radiation pattern has a square groundplane with an edge of 0.060 meter while the second pattern is more of a rectangular shape with a width of 0.0524m and a length of 0.0438m. All other settings are equal as defined in 4.2.1

Table A.1: Overview of attenuation in dBm.

angle	pattern 1		pattern 2	
	E	H	E	H
0	0	0	0	0
10	-0,17	-0,14	-0.1561	-0.158
20	-0,67	-0,57	-0.5797	-0.6257
30	-1,48	-1,27	-1.263	-1.386
40	-2,57	-2,22	-2.193	-2.412
50	-3,90	-3,39	-3.357	-3.665
60	-5,40	-4,73	-4.741	-5.099
70	-7,09	-6,23	-6.337	-6.658
80	-8,82	-7,87	-8.136	-8.278
90	-10,54	-9,70	-10.11	-9.88
100	-12,20	-11,84	-12.14	-11.34
110	-13,73	-14,37	-13.81	-12.47
120	-15,04	-17,65	-14.42	-13.00
130	-16,01	-21,83	-13.72	-12.82
140	-16,47	-23,63	-12.41	-12.08
150	-16,42	-20,37	-11.15	-11.15
160	-16,05	-17,49	-10.21	-10.33
170	-15,69	-15,93	-9.683	-9.786
180	-15,54	-15,54	-9.596	-9.596
190	-15,69	-16,30	-9.963	-9.784
200	-16,05	-18,44	-10.79	-10.33
210	-16,42	-22,85	-12.07	-11.15
220	-16,47	-31,23	-13.71	-12.07
230	-16,00	-24,07	-15.25	-12.80
240	-15,03	-18,05	-15.65	-12.99
250	-13,72	-14,42	-14.3	-12.45
260	-12,20	-11,81	-12.11	-11.33
270	-10,54	-9,70	-9.882	-9.866
280	-8,82	-7,87	-7.859	-8.267
290	-7,09	-6,23	-6.069	-6.649
300	-5,40	-4,73	-4.502	-5.093
310	-3,90	-3,39	-3.154	-3.661
320	-2,57	-2,22	-2.029	-2.409
330	-1,48	-1,27	-1.138	-1.384
340	-0,67	-0,57	-0.4963	-0.6246
350	-0,17	-0,14	-1143	-0.1575

# B

## Radiation patterns: Example Configuration

In listing 2, a possible configuration for a radiation pattern is described. It is important to notice that this example configuration does not represent the used configuration in this master dissertation. The `radiationPattern`-tag consists of a `slices`-tag. This tag can contain as much slices as desired. In this example, 3 slices are defined indicated with the `attenuation`-tag. This tag contains a mandatory attribute `az` which defines the azimuth angle to which all underlying attenuation values belong. Inside the `attenuation`-tag, all attenuation values are written in a `value`-tag. Each `attenuation`-tag must contain an equal amount of `value`-tags.

The tool distributes all values equally over the  $180^\circ$  of that slice. In the example below, each `attenuation`-tag contains 10 values meaning that the exact attenuation is known every  $20^\circ$ .

The highlighted value of  $-14, 42$  is therefore measured at an azimuth angle of  $0^\circ$  and an elevation angle of  $120^\circ$  (counterclockwise).

```

1 <radiationPattern>
2   <slices>
3     <attenuation az="0">
4       <value>0</value>
5       <value>-0.5797</value>
6       <value>-2.193</value>
7       <value>-4.741</value>
8       <value>-8.136</value>
9       <value>-12.14</value>
10      <value>-14.42</value>
11      <value>-12.41</value>
12      <value>-10.21</value>
13      <value>-9.596</value>
14    </attenuation>
15    <attenuation az="90">
16      <value>0</value>
17      <value>-0.6257</value>
18      <value>-2.412</value>
19      <value>-5.099</value>
20      <value>-8.278</value>
21      <value>-11.34</value>
22      <value>-13.00</value>
23      <value>-12.08</value>
24      <value>-10.33</value>
25      <value>-9.596</value>
26    </attenuation>
27    <attenuation az="180">
28      <value>0</value>
29      <value>-0.4963</value>
30      <value>-2.029</value>
31      <value>-4.502</value>
32      <value>-7.859</value>
33      <value>-12.11</value>
34      <value>-15.65</value>
35      <value>-13.71</value>
36      <value>-10.79</value>
37      <value>-9.596</value>
38    </attenuation>
39  </slices>
40 </radiationPattern>

```

Listing 2: Example configuration of a radiation pattern.